

CHARACTERIZATION OF TITANIUM
ALUMINIDE ALLOYS SYNTHESIZED
BY MECHANICAL ALLOYING

TECHNIQUE



ROZMAN MOHD TAHAR

UMP

MASTER OF SCIENCE
(ADVANCED MATERIALS)
UNIVERSITI MALAYSIA PAHANG

CHARACTERIZATION OF TITANIUM ALUMINIDE ALLOYS SYNTHESIZED
BY MECHANICAL ALLOYING TECHNIQUE

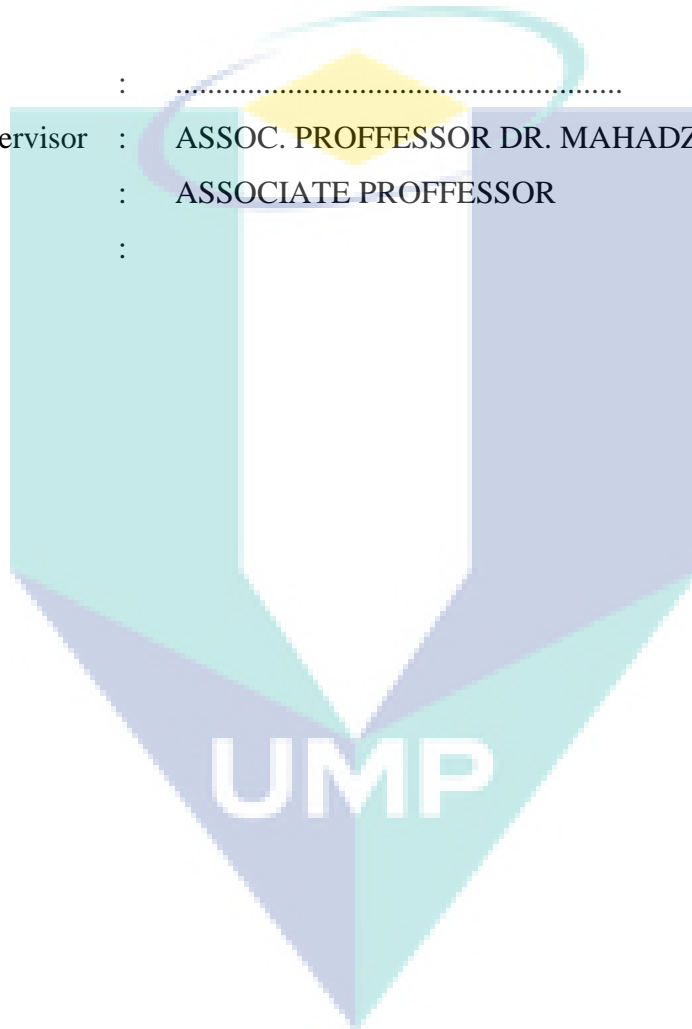


AUGUST 2015

SUPERVISOR'S DECLARATION

I hereby declare that I have checked this thesis and in my opinion, this thesis is adequate in terms of scope and quality for the award of the degree of Master of Science in Advanced Materials.

Signature :
Name of Supervisor : ASSOC. PROFESSOR DR. MAHADZIR BIN ISHAK
Position : ASSOCIATE PROFESSOR
Date :



STUDENT'S DECLARATION

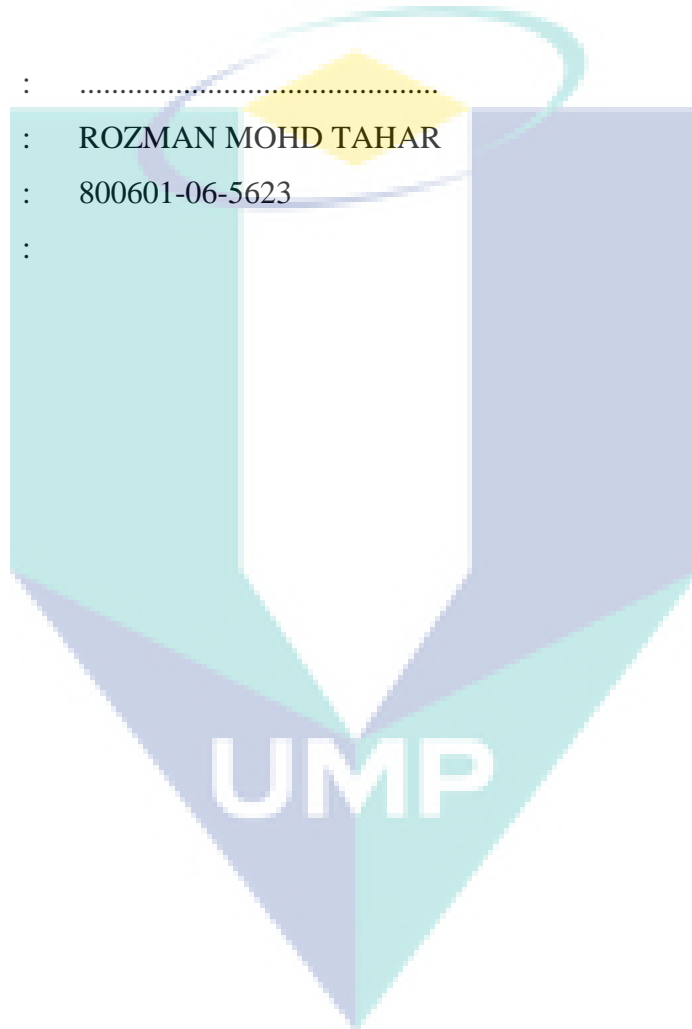
I hereby declare that the work in this thesis is my own except for quotations and summaries which have been duly acknowledged. The thesis has not been accepted for any degree and is not concurrently submitted for award of other degree.

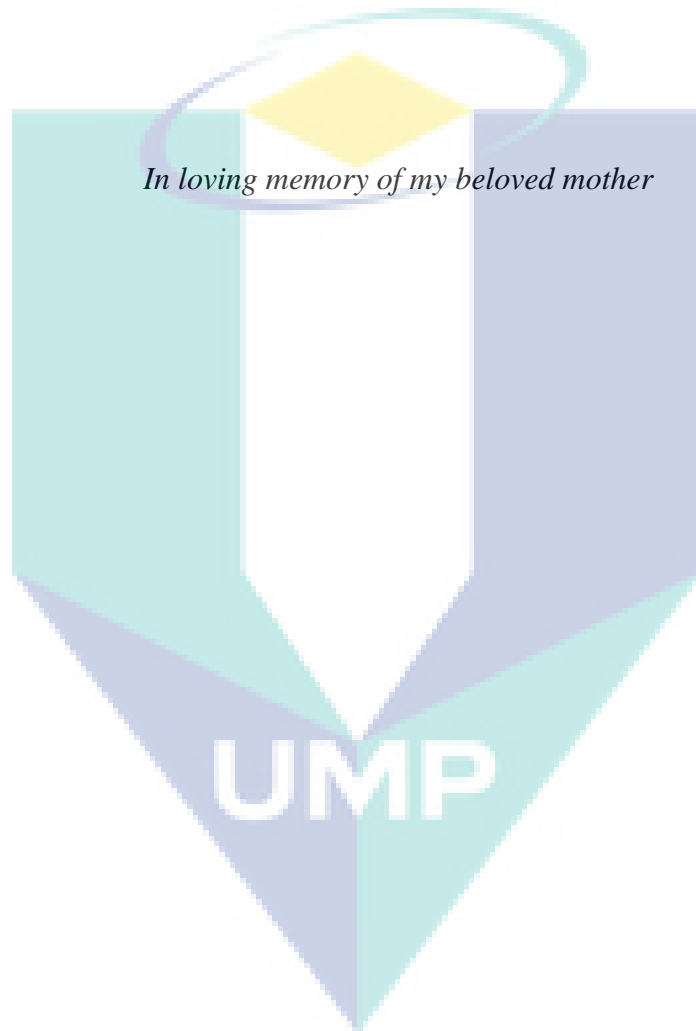
Signature :

Name : ROZMAN MOHD TAHAR

ID Number : 800601-06-5623

Date :





In loving memory of my beloved mother

UMP

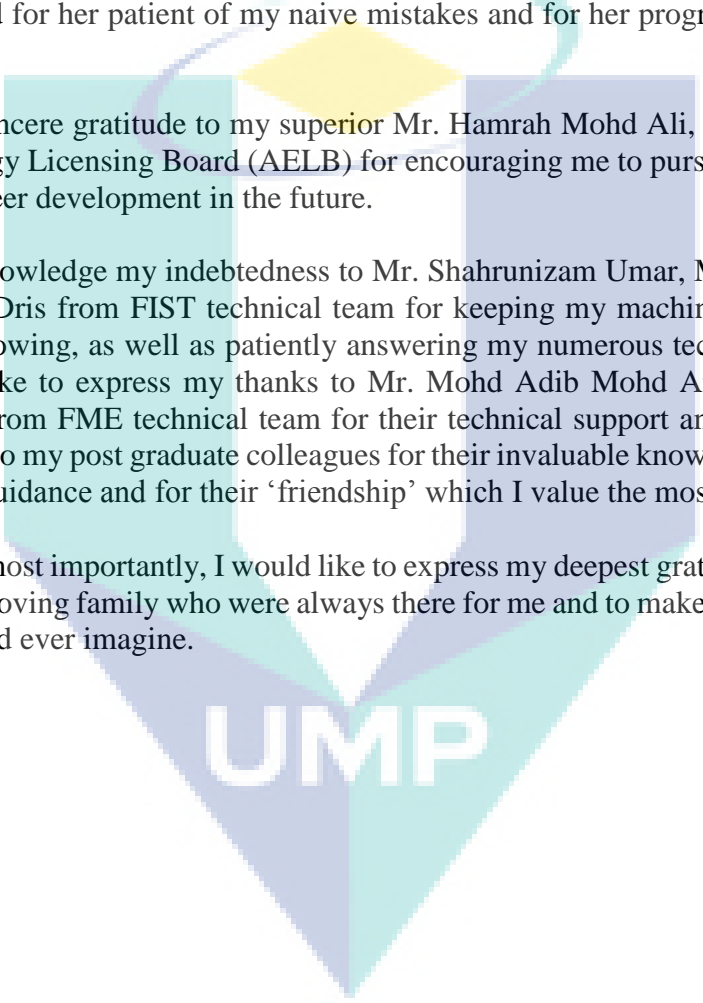
ACKNOWLEDGEMENTS

There are many people I would like to thank and acknowledge for their support and motivation throughout this course of research. My appreciation specially dedicated to my supervisor Associate Professor Dr. Mahadzir Ishak for giving me the opportunity to work on this project as a part of my MSc. study, for his enthusiastic guidance, continuous encouragement and constant support in making this research possible. I am truly grateful for his generous effort to enlighten and assist me in all aspects of the work. My special thanks to Associate Professor Dr. Jinan Basheer Ahmed Al-Dabbagh for her valuable suggestions, insightful ideas and support which I got from her time to time. I am truly indebted for her patient of my naive mistakes and for her progressive vision to my future career.

My sincere gratitude to my superior Mr. Hamrah Mohd Ali, Director General of Atomic Energy Licensing Board (AELB) for encouraging me to pursue my further study for better career development in the future.

I acknowledge my indebtedness to Mr. Shahrizam Umar, Mr. Farid Jaafar and Mr. Latip Hj Dris from FIST technical team for keeping my machines running and my specimens glowing, as well as patiently answering my numerous technical questions. I would also like to express my thanks to Mr. Mohd Adib Mohd Amin and Mr. Aziha Abdul Aziz from FME technical team for their technical support and assistance. I owe many thanks to my post graduate colleagues for their invaluable knowledge sharing, time, suggestion, guidance and for their 'friendship' which I value the most.

And most importantly, I would like to express my deepest gratitude to my beloved wife and my loving family who were always there for me and to make my life worth more than one could ever imagine.

The logo of Universiti Malaysia Perlis (UMP) is a large, stylized shield shape. It is composed of several overlapping triangles in shades of teal, light blue, and yellow. The letters 'UMP' are prominently displayed in white, bold, sans-serif font across the center of the shield.

UMP

ABSTRACT

One of the methods in powder metallurgy namely as mechanical alloying is not only a simple and inexpensive process, but also a promising technique in improving material's properties. However, the final product is highly dependent on the milling parameters and conditions and very sensitive to environmental factors. In this present study, processing of Ti-Al powders by mechanical alloying technique and subsequent heat treatment was performed with the purpose to gain better understanding of their effect on structural and phase formation of the titanium aluminide alloys, and its relationships to physical, thermal and mechanical properties. It was found that, dry milling at an intermediate speed of 300 rpm is the most optimum condition to produce Ti-Al with crystallite size in nano range. Solid state reaction during mechanical alloying resulted in the formation of Ti(Al) solid solution and remarkable reduction of crystallite size as low as 20 nm. In the initial stage of milling, the thermal stability was influenced by the crystallite size refinement, but after prolonged milling, the stability was regulated by alloying degree of powder constituent. The density and micro-hardness value tag along with the crystallite refinement with gradual decreased of densities from 4.1 g/cm³ down to 3.51 g/cm³, while the hardness increased systematically from 43 to 117 HV by milling duration. After the secondary processing step by subsequent heat treatment up to 850 °C, the powder constituent were transformed into a new inter-metallic phase of a dominant TiAl₃. When the heating temperature was raised to 1000 °C, it transformed into an inter-metallic mixtures varying from TiAl₃, γ -TiAl and α 2-Ti₃Al. The dual phase γ -TiAl + α 2-Ti₃Al were obtained in powder milled for 80 and 100 h. A remarkable increase in hardness as high as 622 HV were obtained, while the density values were around 3.7 – 3.9 g/cm³. Mechanical alloying technique was proven as an effective method for producing nano-structured Ti-Al powder, where the parameter need to be selected carefully and thoroughly to obtain the optimum crystallite size. The results conclude that physical, thermal and mechanical properties of powder product has high dependency on crystallite size and alloying degree of the powder constituent produce from mechanical alloying technique. However, after heat treatment, the properties of the alloys were influenced by new phases of the powder constituent in turn governs their performance. In order to get a broader picture on the effect of mechanical alloying process on the formation of Ti-Al alloys, optimal heat-treatment conditions to produce a desired microstructure, and the influence of grain growth need to be further studied. In addition, selection of consolidation process should be reconsidered in other to performed additional mechanical test and analysis.

ABSTRAK

Salah satu kaedah yang dalam metalurgi serbuk yang dikenali sebagai pengalioan mekanikal bukan sahaja proses yang mudah dan murah, tetapi juga sebagai satu teknik berkesan dalam meningkatkan sifat bahan. Walau bagaimanapun, produk akhir hasil daripada proses ini adalah sangat bergantung kepada parameter pengalioan mekanikal dan sangat sensitif kepada faktor-faktor persekitaran. Dalam kajian ini, pemprosesan serbuk Ti-Al menggunakan teknik pengalioan mekanikal diikuti rawatan haba di lakukan bagi mendapatkan pemahaman yang lebih jelas mengenai kesannya terhadap struktur dan perubahan fasa aloi titanium alumida, dan hubungkaitnya kepada sifat fizikal, termal dan mekanikal. Hasil kajian mendapati bahawa pemprosesan kering pada kelajuan pertengahan 300 rpm adalah keadaan yang paling optimum untuk menghasilkan Ti-Al dengan saiz kumin hablur dalam skala nano meter. Tindak balas pepejal-pepejal semasa pengalioan mekanikal menyebabkan pembentukan larutan pepejal Ti(Al) dan pengurangan saiz kumin hablur yang sangat ketara serendah 20 nm. Pada peringkat awal pemprosesan, kestabilan terma serbuk logam Ti-Al adalah dipengaruhi oleh pengurangan saiz kumin, tetapi selepas proses dipanjangkan, kestabilannya adalah dipengaruhi oleh tahap pengalioan dan jujuk serbuk Ti-Al. Nilai ketumpatan pula berkadar terus dengan pengurangan saiz kumin dengan beransur-ansur menurun daripada 4.1 g/cm^3 kepada 3.51 g/cm^3 , manakala nilai kekerasan mikro Vickers berkadar songsang dengan pengurangan saiz kumin dengan peningkatan secara sistematik daripada 43 HV kepada 117 HV. Selepas pemprosesan sekunder melalui rawatan haba pada suhu sehingga $850 \text{ }^\circ\text{C}$ dilakukan, jujuk serbuk Ti-Al telah berubah menjadi fasa logam baru di mana TiAl_3 terbentuk sebagai fasa dominan. Apabila suhu pemanasan dinaikkan kepada $1000 \text{ }^\circ\text{C}$ diikuti oleh penuaan, jujuk serbuk Ti-Al berubah menjadi fasa baru dengan campuran fasa yang berbeza-beza dari TiAl_3 , $\gamma\text{-TiAl}$ dan $\alpha\text{-Ti}_3\text{Al}$. Fasa dwi $\gamma\text{-TiAl} + \alpha\text{-Ti}_3\text{Al}$ telah diperolehi pada serbuk yang diproses pengalioan mekanikal selama 80 dan 100 jam. Nilai kekerasan mikro didapati meningkat dengan sangat ketara setinggi 622 HV, manakala nilai ketumpatan yang diperolehi adalah sekitar $3.7 - 3.9 \text{ g/cm}^3$. Melalui kajian ini, teknik pengalioan mekanikal terbukti sebagai kaedah yang berkesan untuk menghasilkan serbuk logam Ti -Al berstruktur nano, dimana parameter pengalioan perlu dipilih dengan berhati-hati dan teliti untuk mendapatkan saiz kumin hablur yang optimum. Kajian ini menyimpulkan bahawa sifat fizikal, termal dan mekanikal produk serbuk mempunyai kebergantungan yang tinggi terhadap saiz kumin hablur dan kadar pengalioan jujuk serbuk Ti-Al yang dihasilkan melalui teknik pengalioan mekanikal. Selepas proses rawatan haba pula, sifat-sifat aloi ditentukan oleh fasa baru jujuk aloi yang seterusnya mengawal prestasi aloi yang terbentuk. Walau bagaimanapun, untuk mendapatkan gambaran yang lebih jelas tentang kesan proses pengalioan mekanikal pada pembentukan Ti -Al aloi, keadaan haba rawatan yang optimum untuk menghasilkan mikrostruktur yang dikehendaki, dan pengaruh pertumbuhan kumin hablur memerlukan kajian lanjut. Di samping itu, pemilihan proses penyatuan juga perlu dipertimbangkan semula bagi membolehkan ujian mekanikal dan analisis tambahan dijalankan.

TABLE OF CONTENTS

	Page
SUPERVISOR'S DECLARATION	ii
STUDENT'S DECLARATION	iii
DEDICATION	iv
ACKNOWLEDGEMENTS	v
ABSTRACT	vi
ABSTRAK	vii
TABLE OF CONTENTS	viii
LIST OF TABLES	ix
LIST OF FIGURES	x
LIST OF SYMBOLS	xi
LIST OF ABBREVIATIONS	xii
CHAPTER 1 INTRODUCTION	
1.1 Background	1
1.2 Problem Statement	3
1.3 Objective of the Study	4
1.4 Scope of the Study	5
1.5 Overview of the thesis	5
CHAPTER 2 LITERATURE REVIEW	
2.1 Introduction	7
2.2 Nano-crystalline Materials	7
2.3 Titanium Aluminide Base Alloys	10
2.3.1 Development of Titanium Aluminide Base Alloys	10
2.3.2 Properties of Titanium Aluminide	12
2.3.3 Phases of Titanium Aluminide	15
2.4 Mechanical Alloying	17
2.5 Mechanical Alloying of Titanium Aluminide	19
2.5.1 Effect of MA on Crystallite Size	19

2.5.2	Effect of MA on Phase Transformation	20
2.5.3	Effect of Process Control Agent	21
2.5.4	Effect of Heat Treatment Temperature	22
2.6	Summary	23

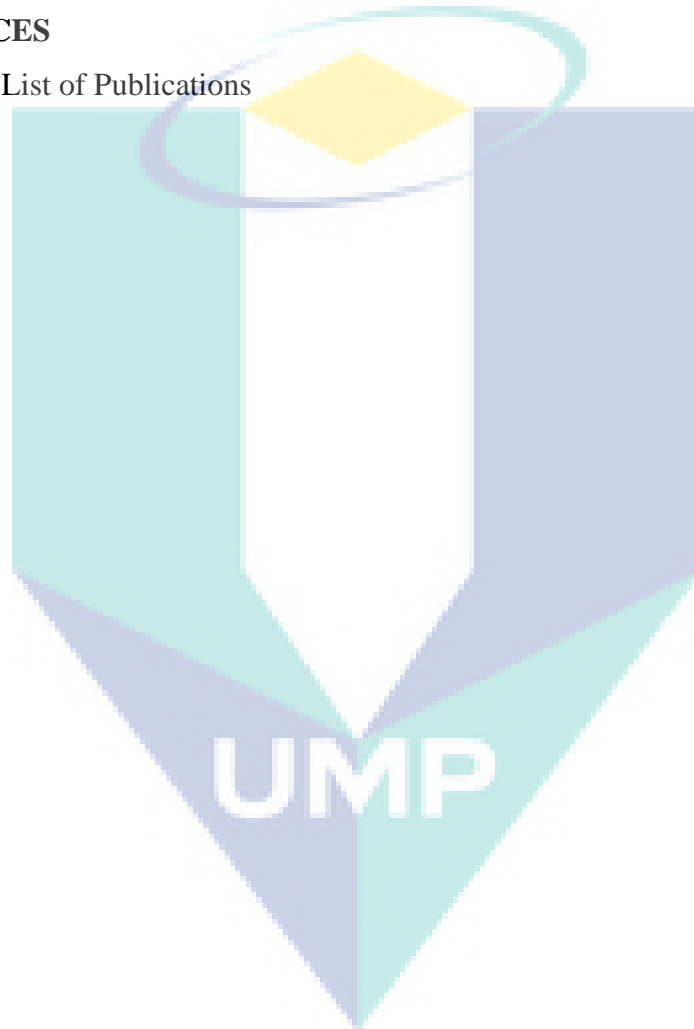
CHAPTER 3 EXPERIMENTAL PROCEDURES

3.1	Introduction	24
3.1.1	Flowchart of Study	25
3.2	Sample Preparation	26
3.2.1	Materials	26
3.2.2	Mechanical Alloying	27
3.2.3	Powder Consolidation	28
3.2.4	Heat Treatment	29
3.3	Test and Analysis	30
3.3.1	X-ray diffraction Analysis	30
3.3.2	Scanning Electron Microscopy and Field Emission Scanning Electron Microscopy	31
3.3.3	Energy Dispersion X-ray Spectroscopy	32
3.3.4	High Resolution Transmission Electron Microscopy	33
3.3.5	Thermal Analysis	34
3.3.6	Density Measurement	35
3.3.7	Micro-Hardness Measurement	36
3.4	Summary	38

CHAPTER 4 RESULTS AND DISCUSSION

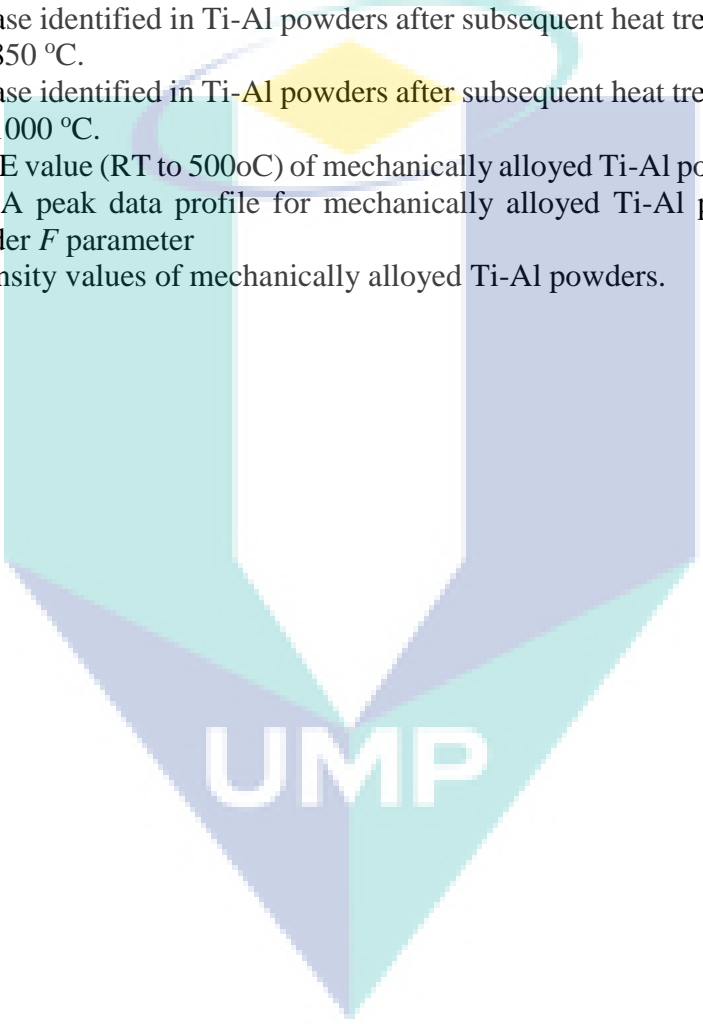
4.1	Introduction	39
4.2	Morphological Observation	39
4.3	Characterization of Mechanically Alloyed Powders	45
4.3.1	Effect of MA on Phase Formation	45
4.3.2	Effect of Heat Treatment On Phase Formation	54
4.3.3	Effect of MA on Crystallite Size	62
4.3.4	Effect of Heat Treatment On Crystallite Size	65
4.3.5	Effect of MA on Thermal Stability	67
4.4	Physical and Mechanical Analyses	70
4.4.1	Effect of MA and Heat Treatment On Density	70
4.4.2	Effect of MA on Micro Hardness	73
4.4.3	Effect of Heat Treatment On Micro Hardness	75

4.5	Summary	77
CHAPTER 5	CONCLUSIONS AND RECOMMENDATIONS	78
5.1	Conclusions	78
5.2	Contribution of the Study	79
5.3	Recommendations for Future Work	79
REFERENCES		81
APPENDICES		88
A	List of Publications	88



LIST OF TABLES

Table No.	Title	Page
2.1	Comparison of gamma titanium aluminide properties to super alloys.	13
2.2	Comparison on alloys properties base on γ -TiAl, α_2 -Ti ₃ Al, and TiAl ₃ .	17
3.1	MA parameters and conditions.	28
3.2	MA experimental set.	28
4.1	Phase identified in Ti-Al powders after subsequent heat treatment at 850 °C.	56
4.2	Phase identified in Ti-Al powders after subsequent heat treatment at 1000 °C.	59
4.3	CTE value (RT to 500oC) of mechanically alloyed Ti-Al powders.	68
4.4	DTA peak data profile for mechanically alloyed Ti-Al powder under <i>F</i> parameter	71
4.5	Density values of mechanically alloyed Ti-Al powders.	72

A large, semi-transparent watermark logo for UMP (Universitas Muhammadiyah Purwokerto) is centered on the page. The logo consists of a shield-like shape with a white background and a blue border. Inside the shield, the letters 'UMP' are written in a bold, white, sans-serif font. The shield is divided into four quadrants by a vertical and a horizontal line, with the top-left and bottom-right quadrants being light blue and the top-right and bottom-left quadrants being a slightly darker shade of blue.

UMP

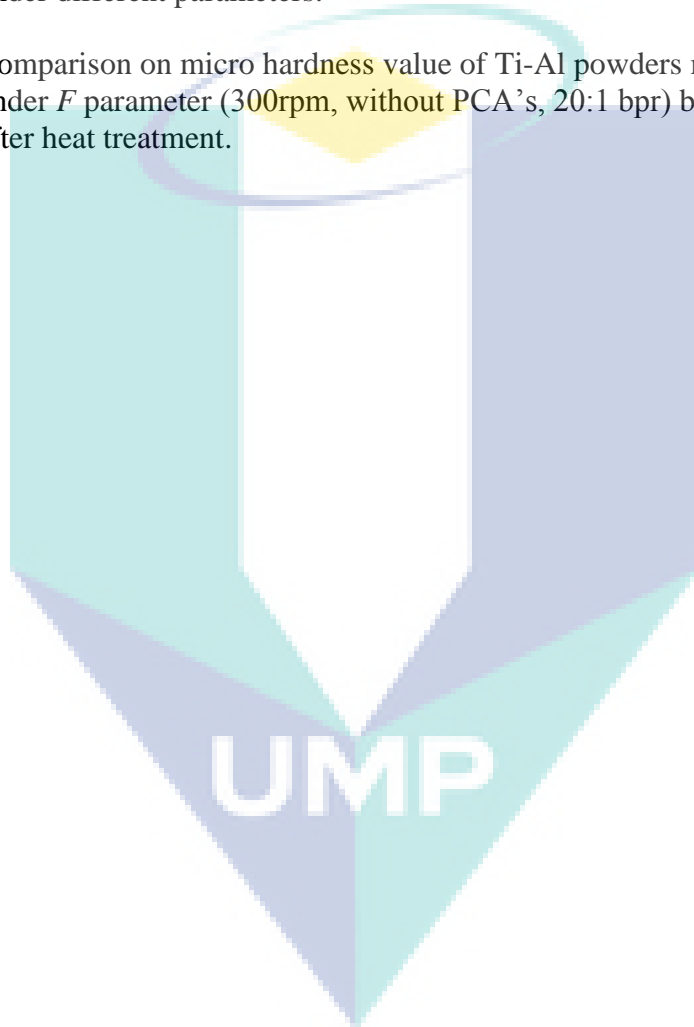
LIST OF FIGURES

Figure No.	Title	Page
2.1	Variation of hardness with reciprocal of the square root of crystallite size in γ -TiAl alloys produced by different methods.	9
2.2	General Electric GEnx-1B engine for Boeing 787 Dreamliner with low pressure turbine (LPT) blade made from cast TiAl.	11
2.3	High performance automotive component made from titanium aluminide base alloys for special type of cars. a) Exhaust valves, and b) turbochargers wheel.	12
2.4.	Comparison of titanium aluminide base alloys with alloy steel and Ni-based super alloys. (a) Specific strength as a function of temperature, and (b) Specific modulus as a function of temperature.	13
2.5	Ti-Al binary phase diagram.	15
2.6	Crystal structures of the (a) L1 ₀ and (b) D0 ₁₉ in TiAl phases	16
3.1	Research framework of this study.	25
3.2	Elemental titanium and aluminum powder used as a feed materials.	26
3.3	Restch PM 100 planetary ball milling machine.	27
3.4	(a) Consolidated powder product. (b) custom made tool die used for the powder compaction processes	29
3.5	Rigaku Miniflex X-ray diffraction equipment.	31
3.6	(a) Zeiss Evo 50 SEM. (b) Joel JSM 7800F FESEM.	32
3.7	Oxford X-Max EDX device coupled with FESEM.	33
3.8	Linseis P75 Platinum Series dilatometer.	35
3.9	Experimental set up for the density measurement by using Archimedes method.	36
3.10	Tukon 1200 Wilson Hardness testing machine.	37

Figure No.	Title	Page
4.1	(a) SEM micrographs of the initial Ti-Al powder mixture (b) Optical microscopy pictograph of Ti powder (c) Optical microscopy pictograph of Al powder.	40
4.2	FESEM micrographs and visual observation of Ti-Al powders milled under <i>D</i> parameter (300rpm, 2.5%wt Hexane, 20:1 bpr). 10 h milled (a), (b), (c) and (d). 50 h milled (e), (f), (g) and (h).	41
4.3	SEM micrographs and visual observation of Ti-Al powders milled under <i>E</i> parameter (200rpm, without PCA's, 10:1 bpr). 2 h milled (a) and (b). 4 h milled (c) and (d). 6 h milled (e) and (f).	43
4.4	SEM/FESEM micrographs and visual observation of Ti-Al milled powders. <i>F</i> parameter – 40 h milled (a) and (b). <i>G</i> parameter – 40 h milled (c) and (d). <i>F</i> parameter – 100 h milled (e) and (f).	44
4.5	HRTEM images of high density of dislocation on Ti-Al powders powder milled under <i>F</i> parameter (300rpm, without PCA's, 20:1 bpr) for 100h.	45
4.6	X-ray diffractogram for Ti, Al and initial Ti-Al powder mixture.	46
4.7	X-ray diffractogram for Ti-Al powders milled under <i>A</i> parameter (300rpm, 5.0%wt Hexane, 10:1 bpr).	47
4.8	X-ray diffractogram for Ti-Al powders milled under <i>B</i> parameter (400rpm, 5% wt Hexane, 10:1 bpr).	47
4.9	X-ray diffractogram for Ti-Al powders milled under <i>C</i> parameter (300rpm, 5% wt Hexane, 20:1 bpr).	48
4.10	X-ray diffractogram for Ti-Al powders milled under <i>D</i> parameter (300rpm, 2.5%wt Hexane, 20:1 bpr).	48
4.11	X-ray diffractogram for Ti-Al powders milled under <i>E</i> parameter (200rpm, without PCA's, 10:1 bpr)	49
4.12	X-ray diffractogram for Ti-Al powders milled under <i>F</i> parameter (300rpm, without PCA's, 20:1 bpr).	49
4.13	X-ray diffractogram for Ti-Al powders milled under <i>G</i> parameter (400rpm, without PCA's, 20:1 bpr).	50
4.14	FESEM images and EDX spectrums for Ti-Al powders milled under <i>D</i> parameter (300rpm, 2.5%wt Hexane, 20:1 bpr) and <i>F</i> parameter (300rpm, without PCA's, 20:1 bpr). (a) <i>D</i> -10 h, (b) <i>D</i> – 50, (c) <i>F</i> - 40 h, and (d) <i>F</i> - 100 h of milling.	52

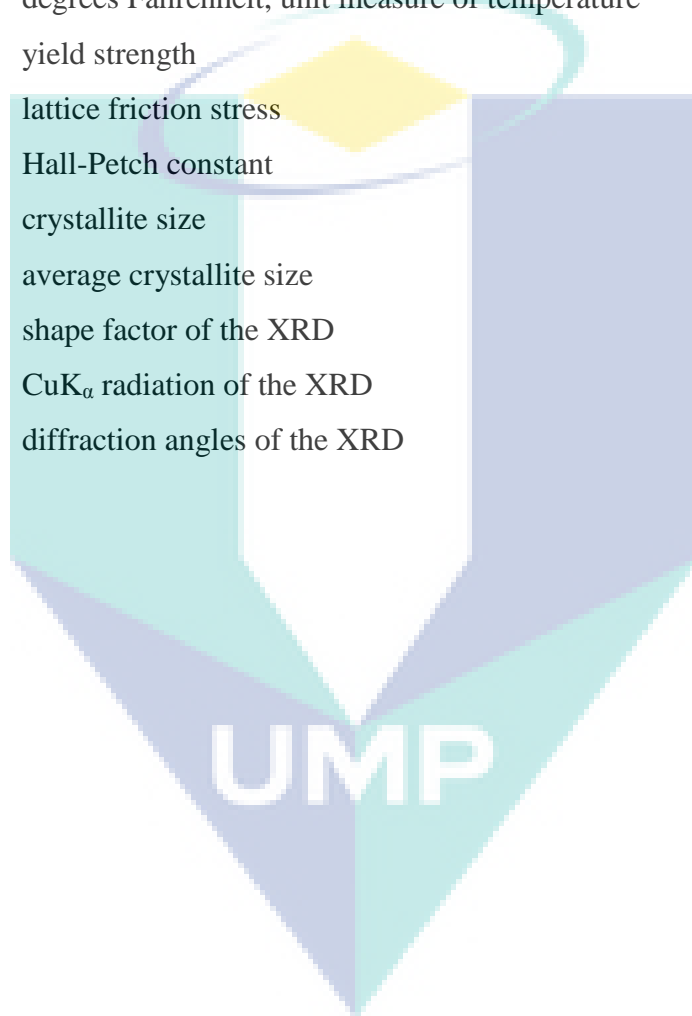
Figure No.	Title	Page
4.15	FESEM images and EDX spectrums of Ti--Al powder milled under <i>G</i> parameter (400rpm, without PCA's, 20:1 bpr) after 40 h with a likely phase of (a) Ti ₃ Al and (b) TiAl phase.	53
4.16	SAED pattern from TEM analysis of Ti-Al powders powder milled under <i>F</i> parameter (300rpm, without PCA's, 20:1 bpr) for 100 h with TiAl ₃ phase.	53
4.17	X-ray diffractogram of Ti-Al powders milled under <i>A</i> parameter (300rpm, 5% wt Hexane, 10:1 bpr) after heating up to 850 °C.	54
4.18	X-ray diffractogram for Ti-Al powders milled under <i>B</i> (400rpm, 5% wt Hexane, 10:1 bpr) parameter after heating up to 850 °C.	55
4.19	X-ray diffractogram for Ti-Al powders milled under <i>D</i> parameter (300rpm, 2.5% wt Hexane, 20:1 bpr) after heating up to 850°C.	55
4.20	X-ray diffractogram for Ti-Al powders milled under <i>E</i> parameter (200rpm, without PCA's, 10:1 bpr) after heating up to 850°C.	56
4.21	X-ray diffractogram for Ti-Al powders milled under <i>F</i> parameter (300rpm, without PCA's, 20:1 bpr) after heating up to 1000°C for 2 h.	58
4.22	X-ray diffractogram for Ti-Al powders milled under <i>G</i> parameter (400rpm, without PCA's, 20:1 bpr) after heating up to 1000°C for 3 h.	59
4.23	FESEM images and EDX spectrums of Ti-Al powder milled under <i>F</i> parameter after 100 h of milling.	60
4.24	SAED pattern from TEM analysis of Ti-Al powders powder milled under <i>F</i> parameter for 100 h.	61
4.25	Crystallite size evolution of Ti-Al powder milled under different parameters.	63
4.26	HRTEM images of TiAl powder milled under <i>F</i> parameter (300rpm, without PCA's, 20:1 bpr) for 100 h.	64
4.27	Crystallite size evolution after subsequent heat treatment of Ti-Al powder milled under different parameters.	67
4.28	Calculated DTA peak thermogram of Ti-Al powders milled under <i>F</i> parameters (300rpm, without PCA's, 20:1 bpr).	69

Figure No.	Title	Page
4.29	Comparison between density value and crystallite size of Ti-Al powders milled under <i>F</i> parameter.	72
4.30	Density value for Ti-Al of powders milled under <i>F</i> parameter (300rpm, without PCA's, 20:1 bpr) before and after subsequent heat treatment.	73
4.31	Micro-hardness values by milling duration of Ti-Al powders milled under different parameters.	75
4.32	Comparison on micro hardness value of Ti-Al powders milled under <i>F</i> parameter (300rpm, without PCA's, 20:1 bpr) before and after heat treatment.	76



LIST OF SYMBOLS

at.%	atomic percent
°C	degrees Celsius, unit measure of temperature
β	full width at half maximum (FWHM) of the XRD peaks
β_M	full width at half maximum (FWHM) obtained
β_I	correction factor for instrumental broadening
°F	degrees Fahrenheit, unit measure of temperature
σ_y	yield strength
σ_o	lattice friction stress
K_y	Hall-Petch constant
d	crystallite size
D	average crystallite size
K	shape factor of the XRD
λ	CuK $_{\alpha}$ radiation of the XRD
θ	diffraction angles of the XRD



LIST OF ABBREVIATIONS

Al	Aluminium
ASTM	American Society for Testing and Materials
cm	centi meters, unit measure of length - 10^{-2} meters
CTE	coefficient of thermal expansion
DP	duplex microstructure
EDX	electron dispersive x-ray
FESEM	field emission scanning electron microscope
g	gram, unit measure of mass
GPa	giga pascal, unit measure of stress – 10^9 Pascals
h	hour, unit measure of time – 3600 second
HRTEM	high resolution transmission electron microscope
HV	Vickers hardness, unit measure of micro hardness - kg/mm^2
HIP	hot isostatic pressing
kg	kilogram, unit measure of mass – 10^3 grams
LVDT	linear variable differential transformer
MA	mechanical alloying
MPa	mega pascal, unit measure of stress – 10^6 Pascals
N	Newton, unit measure of force
NASA	National Aeronautics and Space Administration
NL	near lamellar microstructure
nm	nano meter, unit measure of length – 10^{-12} meters
PM	powder metallurgy
Psi	pound per square inch - unit measure of stress
SPS	spark plasma sintering
SEM	scanning electron microscope
Ti	Titanium
TiAl	Titanium aluminide
XRD	X-ray diffraction
YS	yield strength

CHAPTER 1

INTRODUCTION

1.1 BACKGROUND

Advanced technology such as aerospace, chemical, nuclear, medical and even weaponry sectors has high dependency towards great quality of alloys in ensuring its reliability and durability in hostile environment and extreme operational conditions. Hasty development in the industrial sectors and advancement in the technology application demanded for materials that are lighter, stronger, stiffer, and useful at higher temperatures. Reducing structural weight is one of the major ways to reduce carbon emissions and improve aircraft performance. Lighter and stronger materials allow greater range and speed, and may also contribute to reducing operational costs. Tri-aluminide, especially titanium aluminide base alloys, are regarded as one of the most promising candidates for high temperature structural materials in the 21st century. This is due to their low density combined with good mechanical properties and corrosion resistance at medium high temperature range. Titanium aluminide is a group of intermetallics created by alloying of titanium and aluminum along with minor addition ternary elements. The combination of their low density ($3.7 - 4.1\text{g/cm}^3$), high specific strength and relatively good properties at an elevated temperature, good creep characteristics at temperatures up to $900\text{ }^\circ\text{C}$ (Xiao et al., 2009) and, excellent oxidation and corrosion resistance makes them very attractive as high-temperature structural materials for aerospace, automotive and other applications (Lagos and Agote, 2013).

Titanium aluminide base alloys have been prototyped and tested for use in aircraft turbines engine, automotive and hypersonic airplanes. In particular, titanium aluminide base alloys offer a great reduction in weight and acceptable mechanical performance

characteristics compared to nickel base super-alloys, which can help attain weight-savings and cost reduction goals. Hence, replacement of nickel base super-alloys parts and component with titanium aluminide base alloys in high performance aircraft's gas turbine engines is expected to reduce the structural weight by 20–30% and will produce leaner and efficient structural systems (Voice et al., 2005) which also contribute to fuel savings and the reduction of CO₂ emissions. In automotive industries, the high stability of titanium aluminide exhaust valve in hot environment has resulted in a significant improvement in engine performance from the reduced inertia and friction loss in normal engines (Froes and Suryanarayana, 1996). Eventually, this will increase the fuel efficiency and contribute in reduction of the pollutant emissions, along with noise reduction during operation.

Nevertheless, the attractive properties of titanium aluminide-based alloys were outweighed by poor ductility at ambient temperature below 700°C, low strength at elevated temperature, and insufficient oxidation resistance above 850°C (Al-Dabbagh et al., 2013). The low ductility of titanium aluminide further caused difficulties in processing and machining at room temperature, and resulted in high manufacturing cost. In order to overcome this problem, many efforts have been devoted to fabricate nano-structured titanium aluminide alloys, which have an additional advantage of giving rise to a good combination of strength and ductility (Farhang et al., 2010). The initial processing route for fabrication of titanium aluminide base alloys components was investment casting and wrought processing of ingot metallurgy materials. This method have received the most attention because of their potential for low cost and high volume production. However, Clemens and Kestler (2000) reported that this processing route can lead to fluctuations in the Al content of more than ± 2 at.%, leading to a non-uniform microstructure. These microstructures have a significant variation in the mechanical properties leading to the deterioration of the properties of the alloys. On the other hand, powder metallurgy (PM) technologies offers for more precise control of composition and microstructure, as well as reducing the fabrication costs of producing complex, near net shape components (Moll and McTiernan, 2000).

An innovative development of PM method has enable a viable commercial practice for cost effective materials to be produce with controlled, uniformly refined structures and optimum mechanical properties (Zhao et al., 1997). Amongst the wide

options of PM method, the MA technique has been considered the most powerful tool for the fabrication of nano-structured materials because of its simplicity and relatively inexpensive equipment (Koch, 1993). MA has attracted the attention of a large numbers of researchers because of its ability for the production of fine dispersion of second phase (usually oxide) particles, extension of solid solubility limits, refinement of grain sizes down to nano meter range, synthesis of novel crystalline and quasi-crystalline phases, development of amorphous (glassy) phases and disordering of ordered intermetallics (Cahn et al., 1991). Courtney and Maurice (1989), praised MA technique as the “Aladdin’s lamp of powder metallurgy” because of the capability of this technique to produce alloys and compounds that are difficult or impossible to be obtained by conventional melting and casting techniques. In addition, this method has opened the possibility for producing materials with unique physical and mechanical properties at room temperature, which can be scaled up in large quantities up to several tons (Koch, 1997).

1.2 PROBLEM STATEMENT

The properties of titanium aluminide alloys are depend on their phases and strongly influenced by their microstructures, which is controlled by processing methods and composition modifications. Mechanical alloying (MA) is one of the techniques in PM route which employs a reputation that offers not only a refinement of crystallite size to nano-structure, but also for obtaining materials of high structural homogeneity (Farhang et al., 2010). Unlike ingot metallurgy and investment cast, materials produced from MA have a fine and homogeneous starting microstructure which can be an important advantage to achieve desired microstructure. However, the properties of specific materials obtained by MA are very sensitive to experimental conditions such as; milling type, rotation speed, type and amount of process control agents (PCA) and atmosphere (Suryanarayana, 2001). Recent publication by El-Eskandarany (2013) imply that the selection of these parameters, are vital in obtaining alloys in nano range crystallite size with specific phase and desired properties. Even then, all these process variables are not completely independent.

The possibility of producing Ti-Al intermetallics phase by using MA technique has only been explored recently in powder metallurgy (PM) materials. Many researchers have devoted their work to understand the formation of titanium aluminide through MA from elemental Ti-Al powders. However, there is still no general consensus on the precise mechanism behind the phase formation of these alloys by mechanical alloying technique. In addition, most of the results and findings implicate a significant difference and are in contradiction with the existing understanding and viewpoint regarding the mechanism of titanium aluminide phase formation (Guo et al., 1990, Suryanarayana et al., 1992, Oehring et al., 1993, Itsukaichi et al., 1993, Bhattacharya et al., 2004 and Forouzanmehr et al., 2009, Gonzalez et al., 2009 and Farhang et al., 2010). The main reason is because of the parameters selection for MA involves a large degree of uncertainty in obtaining desired phases and microstructures. For example, the optimum milling time depends on the type of mill, size of the grinding medium, temperature of milling, ball-to-powder ratio, etc. Such inter dependent effect of these variables make this simple process, become more complicated to obtain desirable microstructure and properties for specific materials (El-Eskandarany, 2013).

In this research project, the production factor of MA processes were investigated thoroughly under specific and controlled parameters in order to synthesize nano-structured Ti-Al alloys. Elemental titanium and aluminium powder were used which has been proven useful than pre-alloyed intermetallic powder because they are cheaper and due to their ability to generate exothermic heat from their reaction. In turn, the reaction taking place for the synthesis of the Ti-Al intermetallic compound often results in temperatures lower than the melting point of aluminium. Combined with increased inter-diffusion reaction between Ti and Al by mechanical activation during ball milling, the reaction energy is utilized, making it more energy efficient. Furthermore, the optimum composition of Al were used as starting materials for the synthesis of dual phase γ -TiAl + α 2-Ti₃Al alloys making it more economic.

1.3 OBJECTIVES OF THE STUDY

This work is intended to gain a better understanding on the effect MA processes and subsequent heat treatment on the phase formation and its relationships to physical,

thermal and mechanical properties of the titanium aluminide alloys. The specific goals of this work include;

- i. To investigate the effect of MA parameters on the production of nano-structured Ti-Al powders.
- ii. To study the effect of MA and heat treatment parameters on the phase formation of titanium aluminide alloys.
- iii. To assess the relationship of titanium aluminide alloys characteristics on the densities and mechanical properties.

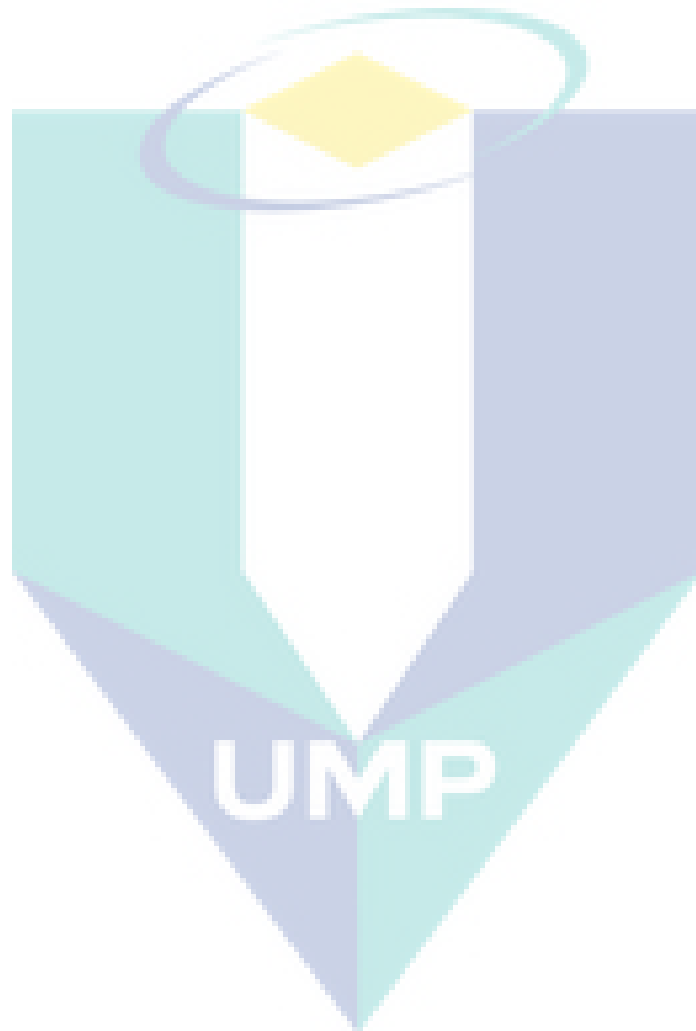
1.4 SCOPE OF THE STUDY

The scope of this work is to produce nano crystalline titanium aluminide alloys from blended elemental Ti and Al powders with a composition of 50% of Ti and 50% of Al. It is aimed to explore the feasibility of MA processes by planetary ball mill and subsequent heat treatment (annealing) with interest to produce nanostructured dual phase γ -TiAl + α -Ti₃Al alloys. The evaluations on the phase transformation, structure (crystallite size), physical (density), mechanical (Vickers micro hardness) and thermal (DTA) properties were essentials in order to determine whether MA can alter the phase formation of Ti-Al intermetallics and improve the critical properties of titanium aluminide alloys.

1.5 OVERVIEW OF THE THESIS

The layout of the thesis report is divided into five chapters. Chapter 1 is an introduction of the research. Chapter 2 provides a literature review covering relevant background research conducted in the area. Chapter 3 describes the experimental procedures. Results and discussions are presented in Chapter 4 and finalized with a conclusion and recommendations for future work in Chapter 5. This research work can be validate by numbers of papers published in international journals and presented at

international conferences. Appendix A provides a list of all publications and proceedings related to this research work.



CHAPTER 2

LITERATURE REVIEW

2.1 INTRODUCTION

This chapter provides a literature review covering relevant background research conducted in the area including the introduction to nano-crystalline materials, titanium aluminide base alloys and the processing route to be explored in this course of research. The review on nano-crystalline materials discussed on the theoretical background, classification, processing route and it's potential over conventional materials. The review on titanium aluminide discussed on the development and current status of titanium aluminide base alloys with emphasis on its properties with comparison to superalloys. Emphasized were also given to both mechanical alloying processes and heat treatment in the production of titanium aluminide base alloys.

2.2 NANO-CRYSTALLINE MATERIALS

Materials scientists have been continuously research towards improving the properties and performance of materials for significant enhancements in mechanical and physical properties. Advancement in nanotechnology has enable for the creation of systematic synthesis techniques to control the structure of the materials in order to provide a precisely tailored set of properties for designated applications. One of the promising strategies in improving material's properties is by reducing the crystallite size. The driving force behind this effort was the possibility of synthesizing materials with strengths approaching the theoretical value by reducing the crystallite size to nano scale (Meyers et al., 2006). Furthermore, nano-crystalline materials may exhibit increased strength and hardness, improved toughness, reduced elastic modulus and ductility,

enhanced diffusivity, higher specific heat, enhanced thermal expansion coefficient (CTE), and superior soft magnetic properties in comparison with conventional polycrystalline materials (Kadkhodapour et al., 2009). Nano-crystalline materials is a distinctive class of advanced engineering materials have now become a major identifiable activity in materials science and engineering with vast prospect for applications in a wide range of fields. These materials are expected to play a key role in the next generation of human civilization because of their superior properties when compared with their coarse grained counterparts (Meyers et al., 2006). Nano-crystalline materials are single or multi-phase polycrystalline solids with a crystallite size of a few nano meters and typically less than 100 nm. Attention in nano-crystalline materials arises from the realization that by controlling the sizes of the crystallite size, one begins to alter a variety of the physical, mechanical, and chemical properties of bulk materials (Roco, 2011). There has been shown that, by decreasing the crystallite size by 2 - 3 orders of magnitude, nanostructured materials are at least 4 - 5 times stronger than their conventional coarse-grained counterparts.

The properties of nano-crystalline materials could be tailored or engineered through the modification of micro-structural features, more precisely by controlling the crystallite size, morphology, and composition specifically. All of those are made possible by controlling the process parameters by a numbers of different techniques including inert gas condensation, rapid solidification from the liquid state, mechanical alloying, electro-deposition, crystallization from amorphous materials, severe plastic deformation, cryo-milling, plasma synthesis, chemical vapour deposition, pulse electron deposition, sputtering, physical vapour deposition and spark erosion (Meyers et al., 2006). Amongst many such processes which are in commercial use, rapid solidification from the liquid state, mechanical alloying, plasma processing, and vapour electro-deposition have been receiving serious attention from researchers. It has been shown that materials processed this way possess improved physical and mechanical characteristics in comparison with materials processed by conventional ingot solidification (Murty et al., 2003). Gleiter (1989) proposed the basic idea of nano-crystalline materials in which 50% or more of the atoms are situated in the grain boundaries. Since the grain sizes are too small, a significant volume of the microstructure in nano-crystalline materials is composed of interfaces, mainly grain boundaries. The large volume fraction of the atoms resides in grain

boundaries consequently yielded in nano-crystalline materials exhibit properties that are significantly different from, and often improved over their conventional coarse-grained counterparts (Suryanarayana, 1995). In addition, comparison to the coarse-grained materials, nano-crystalline materials are also notable in enhanced diffusivity, and superior soft and hard magnetic properties. Even a cooperative phenomenon such as melting point and melting thermodynamic functions such as enthalpy and entropy of melting point could be affected in nano-crystalline materials.

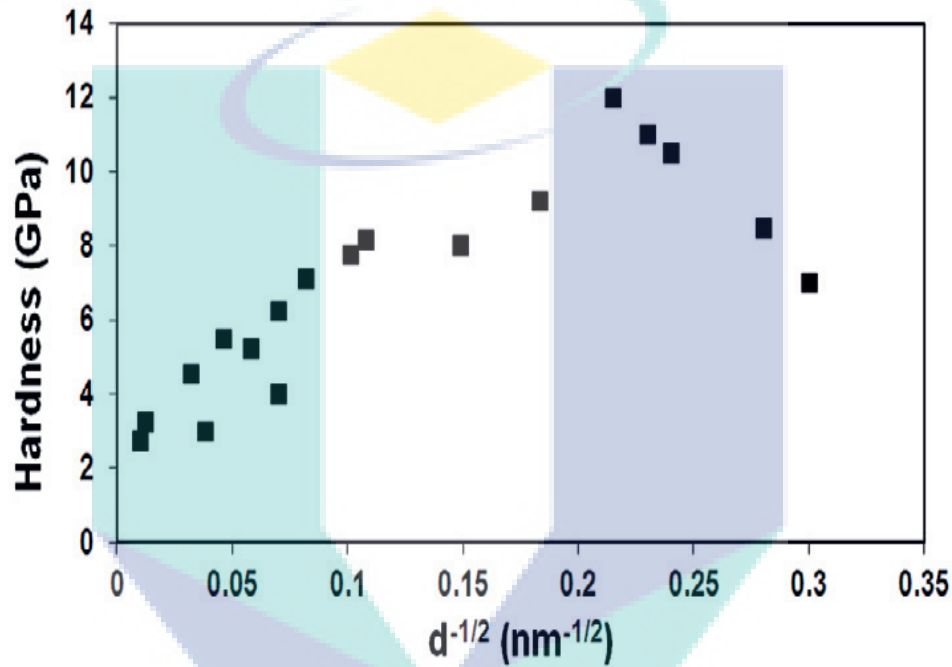


Figure 2.1: Variation of hardness with reciprocal of the square root of crystallite size in γ -TiAl alloys produced by different methods.

Hall (1951) and Petch (1953) proposed that, nano-crystalline materials are harder and stronger than one that is coarse grained material because of it has greater total grain boundary area to impede dislocation motion. For most materials, the yield strength increases with a decrease in crystallite size according to the Hall-Petch (Hall, 1951 and Petch 1953) equation:

$$\sigma_y = \sigma_o + K_y d^{1/2} \quad (2.1)$$

where, σ_y is the yield strength, σ_0 is the lattice friction stress, K_y is the Hall-Petch constant, and d is the crystallite size. However, experiments on many nano-crystalline materials demonstrated that when the crystallite reached the critical size which is typically less than about 30 nm, the strength has been found to decrease gradually with decreasing in crystallite size as shown in Figure 2.1 (Suryanarayana, 2012). This phenomenon has been referred as the inverse Hall–Petch effect. Figure 2.1 shows the hardness of γ -TiAl alloys plotted as a function of crystallite size from materials produced by conventional casting methods to novel mechanical alloying and deposition methods which demonstrate the inverse Hall–Petch effect when the crystallite size reached criticality below a size of 30 nm.

2.3 TITANIUM ALUMINIDE BASE ALLOYS

2.3.1 Development of Titanium Aluminide Base Alloys

The earliest major work on titanium aluminide base alloys was initiated by the U.S. Air Force Materials Laboratory between periods of 1975 to 1983 (Kim, 1994). This collaboration with Pratt and Whitney recommended “first generation” Ti-48Al-1V-(0.1C) as the best alloy composition based on ductility and creep resistance. The second major development program between the Air Force and General Electric (GE) during a periods of 1986-1991, identified a “second generation” Ti-48Al₂(Cr or Mn)-2Nb as the best alloy composition (Kim, 1994). Improved and relatively high ductility, modest strength, but combined with good environmental resistance and manufacturability, this alloys make suitable for low pressure turbine (LPT) blade applications (Kim, 1995a). GE conducted successful engine tests on a full-set wheel of gamma blades, which improved overall confidence in the material in 1993. But it is more than a decade later GE announced its commercialization of titanium aluminide-based alloy for its low-pressure turbine (LPT) blades to be utilized in GENx type engines (Figure 2.2) to power the Boeing 787 Dreamliner passenger craft. This is the first mass commercial production of titanium aluminide base alloys (Norris, 2006). In addition, titanium aluminide were also extensively studied for use in High Speed Civil Transport (HSCT) aircraft which is designed to fly at Mach 2.4. This programme is designated to meet environmental goals of reduced exhaust and noise pollutions while take-off and landing at conventional

airports (Bartolotta and Krause, 1999). In order to meet these stringent requirements, several critical components of the large exhaust nozzle of HSTC propulsion system are fabricated from γ -titanium aluminide. This is including the divergent flap and hybrid type of nozzle sidewall made from a fabrication of both wrought gamma and cast gamma substructure, proposed for noise attenuation and exhaust reduction (Kim, 1995a). In automotive industries, the first commercial use of titanium aluminide base alloys is for turbochargers and exhaust valves (Figure 2.3) for Formula One and sports cars to replace the existing conventional Ti-base alloys (Beschliesser et al., 2003). Parts and component made out of titanium aluminide have also been prototyped and tested to replace Ni-based super-alloys but the limiting factor is to match the mechanical performance and significantly in production costs of titanium metal and its processing (Tetsui, 1999). Through deeper understanding of titanium aluminide's microstructure, deformation mechanisms, advances in micro-alloying, and development in advance processing technologies initiated by NASA Glenn Research Center (USA), Plansee (Austria), and GKSS Research Center (Germany) has led to the production of titanium aluminide sheet material namely, Gamma Met PX (GMPX) which is commercially available (Appel et al., 2000). This sheet alloys are manufactured by using Advanced Sheet Rolling Process (ASRP) is homogenous thin titanium aluminide sheet with high Nb-content based on the TNB alloys developed by GKSS has resulted in cost reduction to \$150/lb (NASA, 2003).

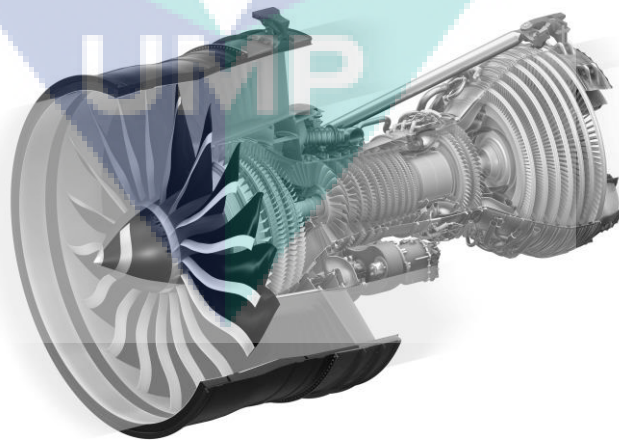


Figure 2.2: General Electric GEnx-1B engine for Boeing 787 Dreamliner with low pressure turbine blade made from cast TiAl (Appel et al., 2011).

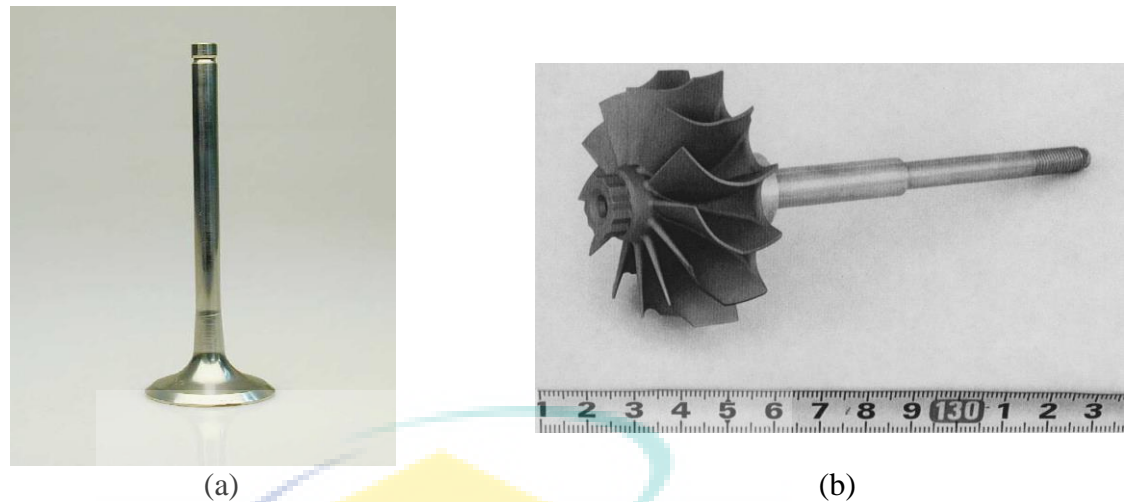


Figure 2.3: High performance automotive component made from titanium aluminide base alloys. a) Exhaust valves (Klaus, 2006) and b) turbochargers wheel (Yamaguchi et al., 2000).

2.3.2 Properties of Titanium Aluminide

Over the past 20 years, due to their superior properties, titanium aluminide have received an increased attention for titanium base alloys beyond than conventional titanium alloys. This group of alloys has an excellent combination of properties including low density, high Young's modulus, good high temperature oxidation, and high specific stiffness (Appel et al., 2011). Titanium aluminide also display high specific yield strength and favorable creep properties at elevated temperatures as well as excellent high temperature strength and modulus retention (Yamaguchi et al., 2000). Due to their special attribute of physical and mechanical properties, titanium aluminide base alloys hold a great potential for applications as a high temperature structural material in the aerospace and automotive industries as well as in other high temperature applications (Clemens and Kestler, 2000). As shown in Figure 2.4, specific strength and specific modulus of titanium aluminide alloys are remarkably higher than alloy steel and nickel based super alloys especially at high temperatures (Kim, 1995a). Compared to Ni-based super-alloys, these alloys offer opportunities for substantial weight reductions with a density half that of nickel-based super-alloys, and compared to titanium alloys they offer a better creep, oxidation and burn resistance, and increased strength at elevated temperatures (Lipsitt, 1985). Properties of γ -titanium aluminide base alloys in comparison with super-alloys are listed in Table 2.1 (Kim, 1989).

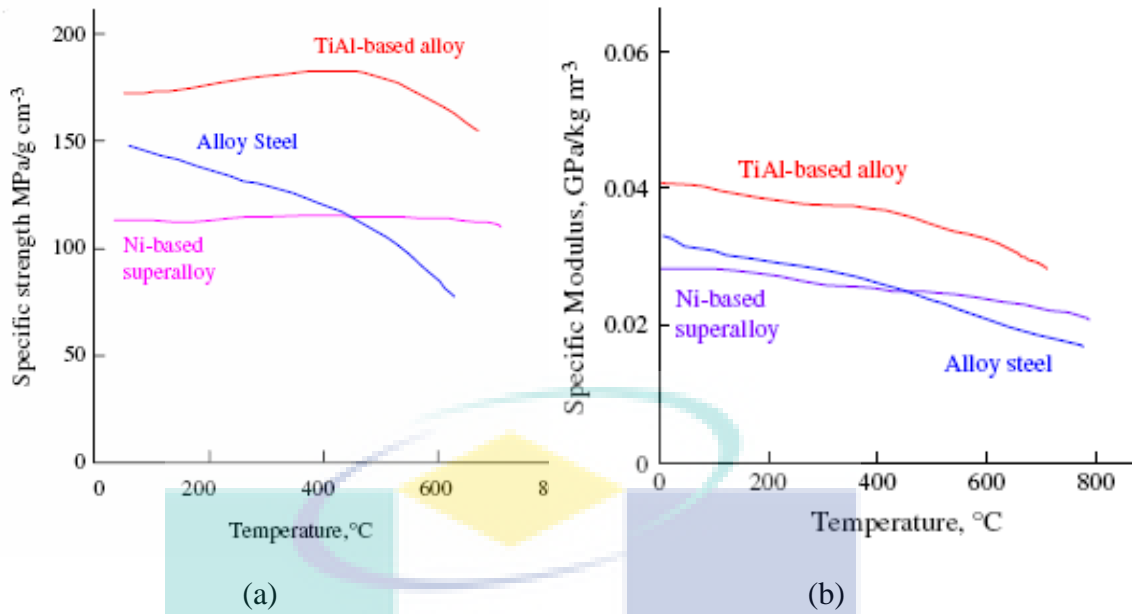


Figure 2.4: Comparison of titanium aluminide base alloys with alloy steel and Ni-based super alloys as a function of temperature. (a) Specific strength and (b) Specific modulus.

Table 2.1: Comparison of gamma titanium aluminide properties to super alloys.

Properties	γ -TiAl base alloys	Ni-base super alloys
Density (gm/cm ³)	3.7–3.9	8.3
Room temperature modulus (GPa)	160–176	206
Yield strength (MPa)	400–630	1000
Tensile strength (MPa)	450–700	1200
Ductility at room temperature (%)	1–3	15
Creep limit (°C)	1000	1090
Oxidation (°C)	900–1000	1090
Cost (\$/lb) , Gamma Met PX-Plansee, Austria	1300	20

However, due to the long range order of intermetallics, the superior properties of titanium aluminide are outweighed by poor room temperature ductility and fracture toughness which resulted in difficulties for processing and machining at room temperature (Maki et al., 1996). In addition, its development has been further held back by a lack of engineering design practices for low ductility materials (Wu, 2006). As shown in Table 2.1, mechanical properties such as room temperature ductility, and yield strength are less favorable than super-alloys. Along with this, at \$1300/lb, titanium aluminide are 65 times more costly to fabricate compared to super-alloys.

The oxidation resistance of titanium aluminide base alloys is based on the addition of an element which will oxidize selectively and produce a protective surface oxide such as Al_2O_3 and TiO_2 layer. Oxide layer is advantageous for corrosion resistance as it act as a barrier from external atom access to metal lattice and higher oxygen content can make titanium stronger (Wendler and Kaczmarek, 2005). However, the oxidation resistance of these alloys is insufficient at high temperatures for prolonged high performance applications. When the service temperature greater than $800\text{ }^\circ\text{C}$, diffusion rate of oxygen into the alloys as an interstitial atom become aggressive, creates embrittlement within the alloys that leading to the deterioration of their properties. Another reason for the reduced oxidation resistance is due to the fact that, at elevated temperature the less-protective TiO_2 is more prone to form than protective Al_2O_3 (Liu and Stiegler, 2002). Even though the oxidation resistance of titanium aluminide base alloys is greater than that of Ti-alloys, it is still lag behind super-alloys.

In a context of thermal stability, the thermal properties of titanium aluminide are a combination of low thermal expansion and high thermal conductivity (Recina, 2000). At a temperature of $538\text{ }^\circ\text{C}$, the thermal expansion of titanium aluminide is around $11.8 \times 10^{-6}/\text{K}$ (Donachie and Donachie, 2002). This value is lower than Ni-based super-alloys of around $14.2 \times 10^{-6} /\text{K}$ (Leyens and Peters, 2003) that gives titanium aluminide some advantages compared to traditionally used super-alloys. The low thermal expansion coefficient of titanium aluminide can be sustained at high temperature which is due to high bonding strength between the atoms and long-range order. Another important material property for used in high-temperature applications is the thermal conductivity which is a value of the heat transport properties. The thermal conductivity varies between $22\text{ W/m} \times \text{K}$ to $12.3\text{ W/m} \times \text{K}$ have been reported for different TiAl base alloys, and microstructures. The γ -titanium aluminide alloys have a thermal conductivity about three times higher than α_2 -titanium aluminide alloys with both of them have up to five times higher conductivity than off-stoichiometric alloys and higher than nickel-based super-alloys which has a values around $11.4\text{ W/m} \times \text{K}$ at room temperature (Recina, 2000).

2.3.3 Phases of Titanium Aluminide

There are several intermetallics compounds of titanium aluminide namely as TiAl, Ti₃Al, TiAl₃, TiAl₂, Ti₅Al₁₁ and etc as shown in Figure 2.5 (Voice et al., 2005). However, among these inter-metallic compounds, titanium aluminide are found to exist in three main phases, namely as γ -TiAl phase, α 2-Ti₃Al phase and TiAl₃ (Hao et al., 2000). Although three different main phases of titanium aluminide, most literature has been focused on the α 2 and γ phases as it has been found to have futuristic engineering significance.

γ -TiAl phase has a composition of aluminium content between 48.5% - 66%. At a composition of aluminium greater than 50%, titanium aluminide exist in the pure γ -phase. This γ -phase exist in a crystal structure of L1₀ ordered face-centered tetragonal as shown in Figure 2.6 (a), which can be retained up to melting point. The structure of the γ -phase of titanium aluminide displays a very attractive properties of that high melting point about 1460 °C, low density at 3.9 - 4.2 kg/cm³, high elastic modulus, high diffusion co-efficient, good resistance to oxidation and corrosion, and lower tendencies to combust in comparison to titanium (Liu et al., 1990). The γ -TiAl phase also exhibits an excellent oxidation resistance and has very low hydrogen absorption. However, the ductility of this

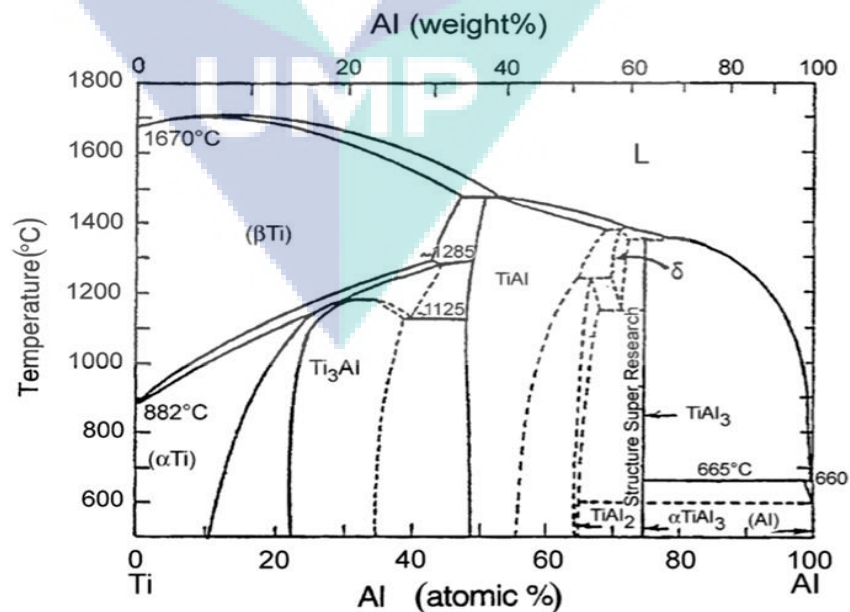


Figure 2.5: Ti-Al binary phase diagram.

phase in room temperature is close to none which further cause difficulties in machining and additional post-machining treatment. Micro-structural refinement and small alloy additions to this alloy composition somehow shows little improvement in ductility, but still unacceptable from an engineering standpoint (Appel et al., 2004). In normal air condition, γ -TiAl intermetallics are known to be highly resistant to atmospheric corrosion at room temperature. However, they have a tendency to oxidize to form Al_2O_3 preferentially to TiO_2 exists only up to 850 °C, which is known as high temperature corrosion (Bird et al., 2004).

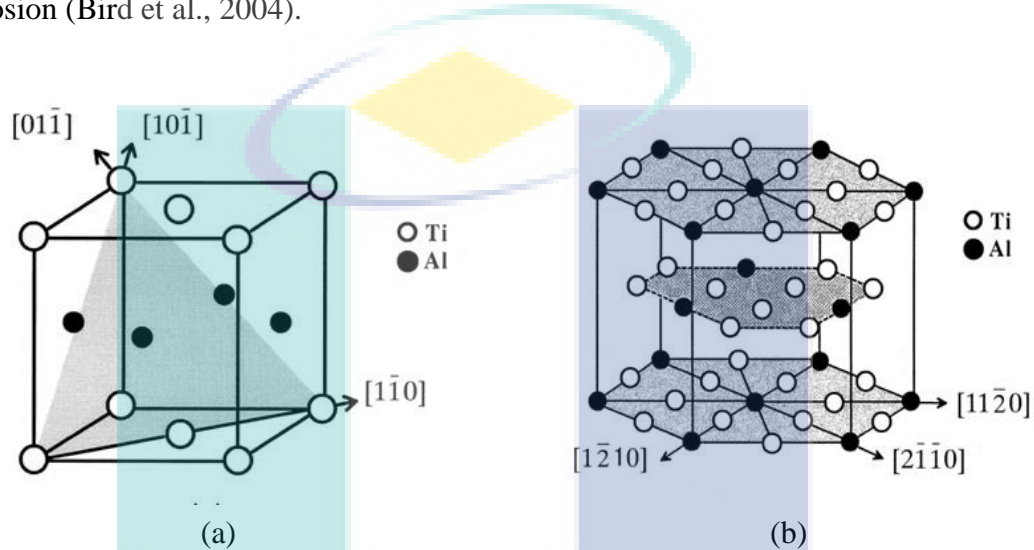


Figure 2.6: Crystal structures of the (a) $L1_0$ and (b) $D0_{19}$ in Titanium aluminide phases (Yamaguchi et al., 2000).

On the other hand, with aluminium composition less between 22% - 39%, the alloy yield in the formation of α_2 - Ti_3Al phase with the hexagonal $D0_{19}$ structure, Figure 2.6(b). This α_2 phase exhibits a very high melting point at about 1600 °C, but slightly higher in density around 4.1 – 4.7 kg/cm³. This phase displays a good high temperature strength and better room temperature ductility compared to γ phase, yet the ductility is still behind of any engineering significance. In addition, it also has a high rate of Oxygen and Hydrogen absorption, which in turn leads to further embrittlement at high temperatures (Sarkar et al., 2009). Comparisons on the properties of alloys base on different phases of titanium aluminide are listed in Table 2.2 (Liu et al., 1990).

Hence individually, these γ -TiAl and α_2 - Ti_3Al does not have much conducive properties for a range of commercial engineering applications, but a dual phases ($\gamma+\alpha_2$) of these two has been found to be very viable for several structural applications which

exists in the composition of aluminium content between 40% - 48.5% (Chraponski et al., 2003). This dual phase exhibited strengths equivalent to that of super-alloys at room and high temperature and have the ability to retain its creep and oxidation resistance at temperatures up to 850 °C which is suitable for an operation in a car and aircraft engines (Draper et al., 2007). But dual phases ($\gamma+\alpha_2$) have been found to be very sensitive to its microstructure, crystallite size, and micro-alloying. Some findings of researcher have shown that ductility of $\gamma+\alpha_2$ phase alloys can be improved by increasing the aluminium content up to 48%, and then decreases beyond 50% of aluminium concentration in the composition. Ramanujan (2000) found that, refinement of the dual phase $\gamma+\alpha_2$ phase microstructure along with micro-alloying additions remarkably increased the ductility as high as 6%.

Table 2.2: Comparison on alloys properties base on γ -TiAl, α_2 -Ti₃Al, and TiAl₃.

Properties	γ -TiAl	α_2 -Ti ₃ Al	TiAl ₃
Critical ordering temperature (°C)	1460	1100	1350
Melting point (°C)	1460	1600	1350
Density (g/cm ³)	3.7- 3.9	4.1- 4.7	3.4
Young's modulus (GPa)	160 – 176	120 – 145	192
Microhardness, Vickers (kg/mm ²)	180-450	180-350	465-670
Oxidation Resistance (°C)	800	650	1000

2.4 MECHANICAL ALLOYING

The mechanical alloying (MA) process was first developed in 1966 at the International Nickel Company (INCO) as part of a program to produce a material combining oxide dispersion strengthening with precipitation hardening in a nickel-based super-alloy. Attention was turned to the ball-milling process when it has successfully used for preparing fine, uniform dispersions of oxide particles in nickel-base super-alloys which cannot be obtained by the conventional powder metallurgy method (Benjamin et al., 1992). Since then, MA has attracted the attention of a large numbers of researchers for the production of fine dispersion of second phase (usually oxide) particles, extension of solid solubility limits, refinement of grain sizes down to nano meter range, synthesis of novel crystalline and quasi-crystalline phases, development of amorphous (glassy) phases and disordering of ordered intermetallics. (Koch, 1993). This method has opened

the possibility of producing homogenous nano-crystalline materials with unique physical and mechanical properties at room temperature, which can be scaled up in large quantities up to several tons (Koch, 1997).

MA can be successfully performed in high-energy mills such as attritor-type ball mill, planetary-type ball mill, centrifugal-type ball mill, and vibratory-type ball mill which allows production of homogeneous materials from blended elemental powder mixtures (Gaffet et al., 1995). The unique solid state reaction process takes place between the fresh powder surfaces of the precursor materials at room temperature. It requires at least one fairly ductile metal to act as a host or binder and the other components can consist of other ductile metals, brittle metals, and inter-metallic compounds or non-metals and refractory compounds (Fecht, 1995). The technique produces nano-structured materials by structural disintegration as a result of severe repeated deformation of powder particles in a high-energy ball mill. In this technique, the powder particles were subjected to welding, fracturing, re-welding and re-fracturing until the desired microstructure and composition is achieved (Oehring et al., 1993). In addition, intense cold working during milling leads to a dramatic increase in the number of point and lattice defects which leads to decreasing the thermodynamic stability of the starting materials. Based on the type of defects applied, different kinds of nano-crystalline materials, with different physical and mechanical properties, can be obtained (Froes and Suryanarayana, 1989). As a result, a materials with well-controlled microstructure and morphology, and enhanced physical and mechanical properties, new phases or new engineering advanced materials can be obtained at room temperature. In addition, MA also has the ability of alloying elements that is difficult to be alloyed, inducement of chemical (displacement) reactions at low temperatures and has the advantage as a scalable process (Benjamin, 1990).

However, the MA process is affected by several factors that are playing very important roles in the fabrication of homogeneous materials. The properties of the milled powders of the final product, such as the particle size distribution, the degree of disorder, amorphization and the final stoichiometry depend on the milling parameters and conditions (Fecht et al., 1990). More precise the control and monitoring of milling conditions, the better end product can be obtained. Factors such as the type of mills (e.g., high-energy mills and low-energy mills), the materials of milling tool (e.g., ceramics, stainless steel or tungsten carbide), types of milling media (e.g., balls or rods), milling

atmosphere (e.g., air, nitrogen or inert gas), environment (e.g., dry milling or wet milling), milling media-to-powder weight ratio, milling temperature and milling duration, are the key factors that affected the final product (Suryanarayana, 2001). Even then, all these process variables are not completely independent. For example, the optimum milling time depends on the type of mill, size of the grinding medium, temperature of milling, ball-to-powder ratio, etc. Such inter dependent effect of these variables make this simple process, become more complicated to obtain desirable microstructure and properties for specific materials (Froes and Suryanarayana, 1989).

2.5 MECHANICAL ALLOYING OF TITANIUM ALUMINIDE

Mechanical alloying is highly praised as the easiest and simplest method for the fabrication of titanium aluminide intermetallics in nano-crystalline size at room temperature. However, because of the process variable, many researchers have found variable results in MA of Ti-Al powder. But most of them conclude that the milling parameter plays a vital role in obtaining desired structure or phases (Guo et al. 1990, Suryanarayana et al. 1992, Oehring et al., 1993, Itsukaichi et al., 1993, Bhattacharya et al., 2004 and Forouzanmehr et al., 2009, Gonzalez et al., 2009 and Farhang et al., 2010).

2.5.1 Effect of MA to Crystallite Size

Refinement of crystallite size is one of the main advantages of processing materials using mechanical alloying technique as smaller size improved physical and mechanical characteristics of materials. Besides from that, producing a nano size of crystallite are beneficial in order to offset the effect of crystal growth during consolidation process of Ti-Al powder materials. However, finding from previous research indicated a variable results regarding the time consumed for crystallite refinement of Ti-Al powders. Benhaddad et al. (1997) studied the effect of ball milling time on Ti-Al powders. They found that during the first 5 – 20 h of milling, the crystallite size was increased over the starting materials at around 80 nm. On continuous milling, the size only decreased to around 70 nm after 40 h. The increased of size at the initial stage of milling were not observed by Forouzanmehr et al. (2009). They performed a milling by using Fritch pulverisette 5 planetary ball mill, with hardened chromium steel balls and vial, and ball-

to-powder weight ratio at 10:1 nominally at room temperature. After 60 h of milling, the crystallite size of Ti(Al) solid solution was measured to be at 13 nm and on continuous milling up to 80 h, the size was reduced to 8 nm. On the other hand, it takes Gonzalez et al. (2009) a shorter duration to obtain smaller crystallite size. By using SPEX 8000 mill with hardened steel balls and vial, and ball-to-powder weight ratio at 8:1, they produced a crystallite with a size of 8 nm just after 5 h of milling. Prolonged milling to 50 h, a crystallite size of 5 nm were observed. Farhang et al. (2010) were using Fritsch P6 planetary ball mill at a speed of 300 rpm with an addition of Hexane as PCA. They observed a peak broadening and decreasing intensity of their XRD results which was due to the decreased in crystallite size from 26 nm after 10 h to about 13 nm after 40 h milling. Taking everything into account, the equipment employed and milling durations play a vital role in obtaining desired structure of powder constituent. However, other factors such as the size of the starting materials, atmosphere, PCA addition, milling speed, milling media, ball to powder weight ratio and etc were also contribute to significant influence to the mechanically alloyed powders.

2.5.2 Effect of MA on Phase Transformation

Even though MA could lead to the formation of extended solid solutions or metastable phases, the behavior during MA is highly dependent on the equipment used and milling condition. For example, even after 100 h of milling, Oehring et al. (1993) reported that amorphous states could not be obtained in an argon atmosphere. However, in the same atmosphere, by continuous milling up to 1000 h, Itsukaichi et al. (1993) indicated a formation of an amorphous-like phase, while Takasaki and Furuya (1999) indicate the same amorphous phase just after 15 h of milling in H₂ atmosphere. Khosroshahi et al. (2008) studied on formation kinetic of nanostructured γ -TiAl via mechanical alloying method. They found that a solid solution occurs as early as 10 h followed by amorphous phase after 20 h milling. On the other hand, formation of Ti(Al) solid solution was reported Gonzalez et al. (2009) earlier at 5 h of milling. On further milling up to 10 h, amorphisation takes place and followed by a transformation to a f.c.c. solid solution Ti(Al) after further milling of 50 h. A similar sequence was reported by Forouzanmehr et al. (2009) whose conduct a study on solid-state reactions of nanocrystalline TiAl synthesized by MA. It was found that a Ti(Al) solid solution was formed

at the early stage of milling, followed by the formation of an amorphous phase at longer milling duration of 40 h. On further milling up to 80 h, the amorphous structure transformed to a supersaturated Ti(Al) solid solution. However, in spite of variables in findings of past work, the sequence of Ti-Al phase formation during MA can be summarized as; $Ti+Al \rightarrow Ti(Al) \text{ solid solution} \rightarrow \text{Amorphous phase} \rightarrow \text{f.c.c. / hcp Ti(Al) phase}$ as proposed by Suryanarayana et al. (1992). Somehow, Farhang et al. (2010) and Yu et al. (2009) has successfully produced Ti–Al intermetallics by mechanical alloying. With a nominal composition of Ti50%Al, Farhang et al. (2010) obtained a trace amounts of γ -TiAl phase after 80 h of milling, which was completely transformed to γ -TiAl, α -Ti₃Al and TiAl₃ intermetallic compounds after additional milling up to 100 h.

2.5.3 Effect of Process Control Agent

Contamination is one of the main problem in mechanical alloying of Ti-Al powders. As milling always result in the product to forms a compact coating on the balls and vial walls, process control agent (PCA) such as hydrocarbons or alcohols, for instance methanol, hexane, ethanol or even stearic acid, are used to facilitate sampling. These agents somehow may react chemically with the products of the MA, changing the phase constitution of the product (Suzuki and Nagumo 1992). Bhattacharya et al., (2004) studied the effects of milling parameters on yield and contamination. By using different type of PCA such as cyclohexane and stearic acid, they found that the phase obtained in the presence of a PCA differs from the disordered h.c.p. phase formed which was milled in the absence of PCA. In additions, PCA's not only restricted the sticking problem but also greatly delayed the alloying process. Besides from that, the final product of MA always resulted in the formation of unusual phase composition that may often be explained as a result of contamination mainly by interstitial oxygen, nitrogen and hydrogen. Guo et al., (1990) reported a high concentrations of oxygen (20.7 wt%) and nitrogen (32.6 wt.%) were obtained in powders constituent of mechanically alloyed of titanium and aluminium powder mixture. A high concentration of nitrogen (3.34 wt%) were also noticed by Suryanarayana et al. (1992) in the sample after milling. According to Benjamin (1992), Source of impurities may also originate from the elements of the milling tools. Contamination of the powder produced by MA increases by increasing the ball to powder weight ratio, speed of milling, milling energy and by use of a process

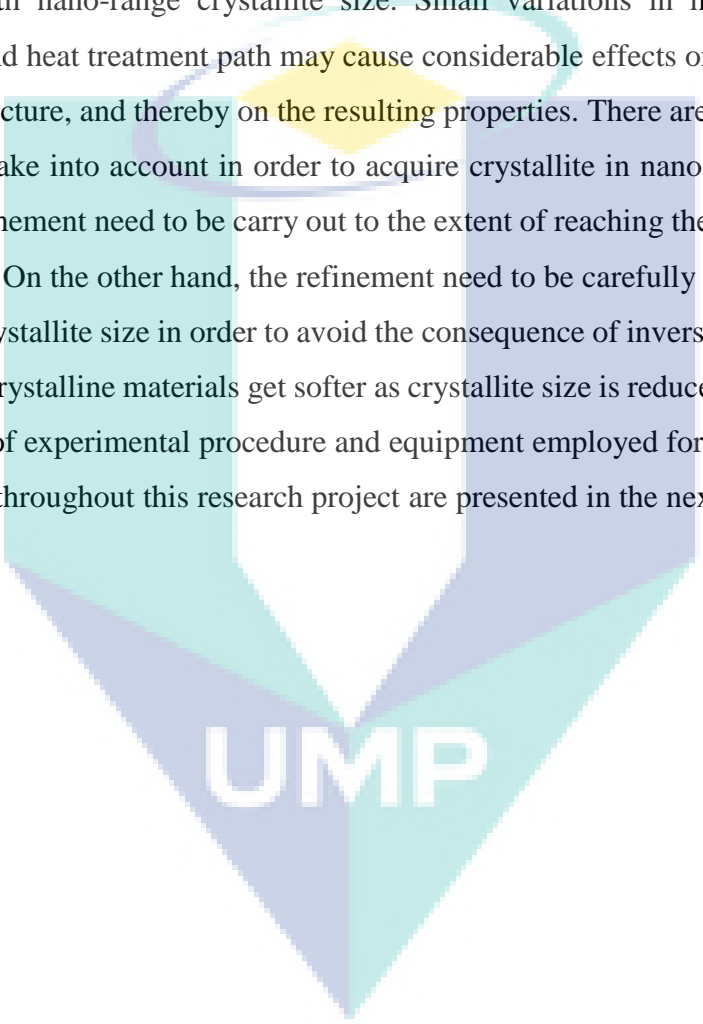
control agents (PCA). Even if MA is carried out under high purity Argon, contaminants are likely to occur which appear from the surface of powders or from contamination of the gas atmosphere caused by periodic sampling (Gerasimov and Pavlov, 1996).

2.5.4 Effect of Heat Treatment Temperature

Proper heat treating requires precise control over temperature, holding time, cooling rate and medium in order to obtain desired phases and microstructures. Since a smaller crystallites size usually enhances mechanical properties, the heat treatment are often performed at a temperature that prevent the grains of solution from growing too large, which will risk in the loss of desirable properties. It has been well established that the formation of $TiAl_3$ depending on the scale of the Ti-Al diffusion couples and is attributed by the first reaction between Ti and Al in Ti-Al powders. On continuous heating, formation of γ -TiAl occurs from the reaction developed between $TiAl_3$ and residual Ti. If on continuous heating, Ti is still not fully consumed, γ -TiAl will react with remaining Ti to form α_2 - Ti_3Al (Kim et al., 1991). As reported by Gerasimov and Pavlov (1996), Takasaki and Furuya (1999), Khosroshahi et al. (2008) and Forouzanmehr et al. (2009), annealing of mechanically alloyed Ti-Al powders at 900 °C resulted in the formation identical phase of initial composition as predicted in Ti-Al binary phase diagram. All of them reported a formation of single phase γ -TiAl after annealing. On the other hand, Gabbitas et al. (2012) reported that, even milling at short duration has significant effect on phase formation of Ti-Al powders into Ti-Al intermetallics. According to them, when heated to 1000 °C, powders milled for 12 h turn into a dominant γ -TiAl, while powders milled for 8 and 4 h exhibit a formation of dominant $TiAl_3$ phase. Formation of multiple Ti-Al phase after annealing, were also reported by Yu et al. (2009). At a temperature of 400 °C, they observed a formation of $TiAl_3$. When the treatment temperature were increased to 600 °C they obtained a multiple Ti-Al phase of γ -TiAl + α_2 - Ti_3Al + $TiAl_3$ and at 800 °C and 1000 °C, they produce a dual phase γ -TiAl and α_2 - Ti_3Al . In general, results of mechanical treatment in the Ti-Al system do not depend on the initial state of powder mixture, but determined by treatment temperature and MA condition.

2.9 SUMMARY

Apparently, recent progress in the development of TiAl base alloys has been achieved. However, there is still no general consensus on the precise mechanism behind the phase formation of these alloys by mechanical alloying technique. Besides of investigating the effect of MA by ball milling route on the phase formation of Ti-Al phases from elemental Ti and Al powders, the focal point of this research is to produce an alloys with nano-range crystallite size. Small variations in mechanical alloying parameters and heat treatment path may cause considerable effects on the phase changes and microstructure, and thereby on the resulting properties. There are two considerations that need to take into account in order to acquire crystallite in nano-size range. On one hand, the refinement need to be carry out to the extent of reaching the smallest crystallite size possible. On the other hand, the refinement need to be carefully executed just above the critical crystallite size in order to avoid the consequence of inverse Hall–Petch effect, where nano-crystalline materials get softer as crystallite size is reduced below the critical size. Details of experimental procedure and equipment employed for sample preparation and analyses throughout this research project are presented in the next chapter.

The logo of UMP (Universitas Muhammadiyah Purwokerto) is a large, downward-pointing triangle composed of several smaller triangles in shades of teal, light blue, and yellow. The letters "UMP" are printed in white, bold, sans-serif font across the center of the triangle.

UMP

CHAPTER 3

EXPERIMENTAL PROCEDURES

3.1 INTRODUCTION

This chapter describes the experimental procedure and equipment employed for sample preparation throughout this research project. This chapter comprises of the materials used and processes involved in sample preparations including the mechanical alloying process, consolidation techniques and heat treatment process under specific conditions. The latter section described both the specifications and capabilities of the laboratory equipment used and test procedures for analyzing the samples including XRD, EDX, SEM/FESEM, HRTEM, thermal analysis, densities and micro hardness measurement. These analyses are important in order to investigate the production factors to synthesized Ti-Al nano powders, the effect of MA process and heat treatment on the phase formation of Ti-Al intermetallics and its influence on the densities and mechanical properties of the alloys product.

3.1.1 Flowchart of Study

The flowchart of this research study are presented in figure 3.1. The process starts with mixing of Ti and Al elemental powder before milling in a ball milling equipment. Selected powder compound were analyzed by XRD, SEM/FESEM, EDX and HRTEM to observe the morphological changes and to identify phase and structural modifications. The powder then were consolidated into bulk form in order to measure the density and micro hardness alterations. This process were repeated again after heat treatment were completed. Thermal analyses were performed simultaneously during the heat treatment process.

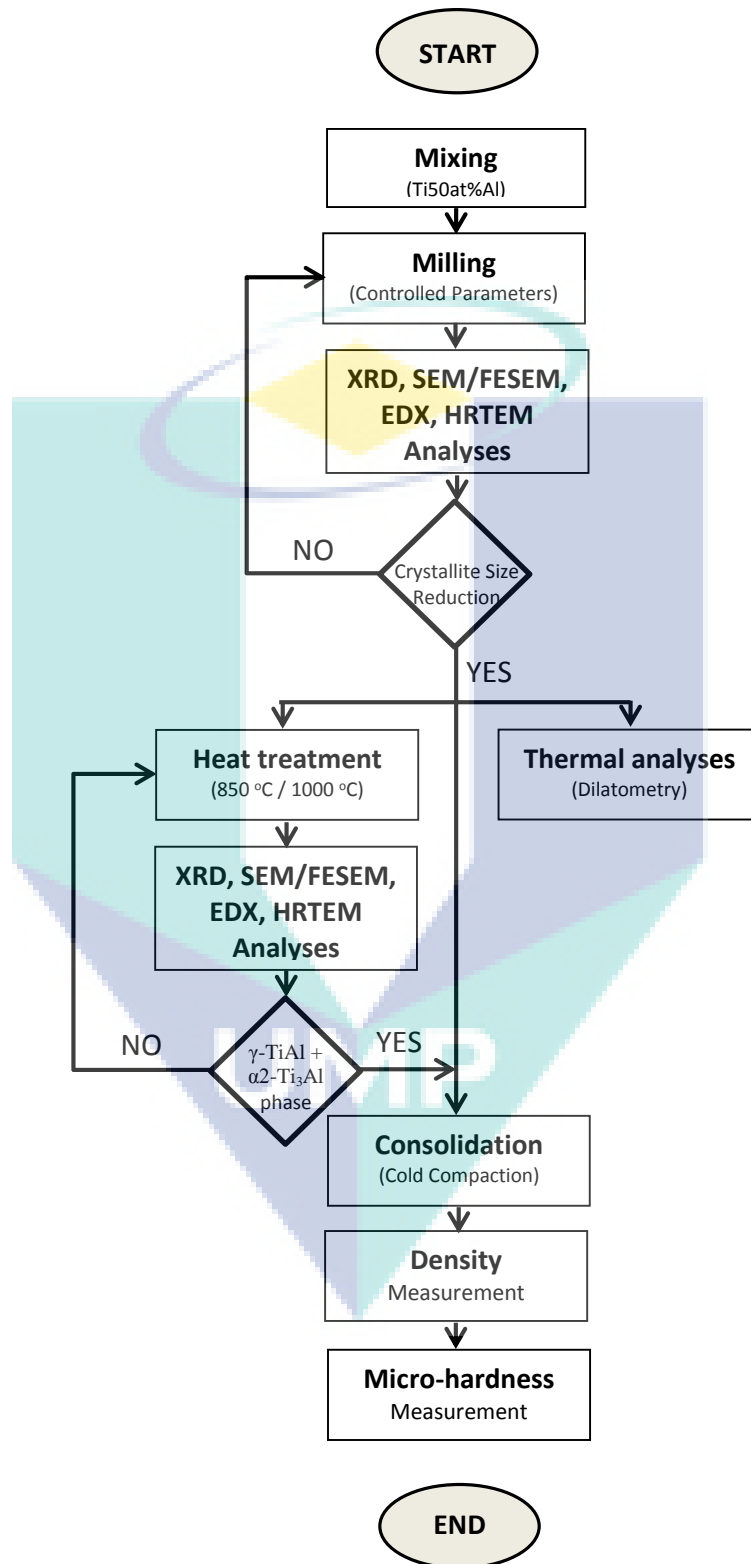


Figure 3.1: Research framework of this study.

3.2 SAMPLE PREPARATION

3.2.1 Materials

Commercial-grade elemental powders of 325 μm (100 mesh) Ti and 50 μm Al from Acros Organics, New Jersey, U.S.A. were used as starting materials with 99.5 % and 99.97 % of purity, and a molecular weight at 47.88 and 26.98 respectively (Figure 3.2). Since the primary focus of this study is to produce dual phase $\gamma\text{-TiAl} + \alpha\text{-Ti}_3\text{Al}$ phase which have more engineering significance, a composition of Ti50%Al of atomic percentage were use as the feed powder mixture. For each batch, the elemental powders were weighted in a ceramic vial on an electronic scale with an initial weight of 3.197 g for Ti powder and 1.803 g for Al powders to obtain a 5 g of powder mixture with Ti50%Al atomic percentages. The powder mixtures then were hand blended by using a spatula for a while to ensure the homogenous distribution between Ti and Al powder particles prior MA process.



Figure 3.2: Elemental titanium and aluminum powder used as a feed materials.

3.2.2 Mechanical Alloying

The MA processes were carried out using a Retsch PM 100 planetary ball mill (Figure 3.3). One of the major issues associated with MA is the contamination of the powders from the milling tools. Therefore, throughout this research work, tungsten

carbide jar and balls as a milling media were used to minimize this problem as this material is the hardest metal available for the specific tools. The powder mixtures were poured into the jar before the balls were added. The ball-to-powder weight ratio was carefully set at approximately between 10:1 to 20:1. In order to prevent excessive agglomeration and the sticking of elemental powders to the milling tools, Hexane as process control agent (PCA) was added for selected samples. The jar were back-filled with pure Argon (99.9 %) to minimize any reaction of the powder with environmental air during milling, and the pressure in the jar was kept at 0.1 MPa. Different rotation speeds were chosen between 200 rpm, 300 rpm and 400 rpm with interval time at every 5 minutes for the MA processes. The processes was interrupted at selected times and a small amount of powder were removed for characterizations and study. The milling duration, were varies between 2 hours up to 120 hours. The MA processes parameters and conditions as shown in Table 3.1. Samples were milled with seven different set of parameters for different milling durations to investigate the effect of milling parameters and conditions, to the powder products by optimizing the production factors as listed in Table 3.2.

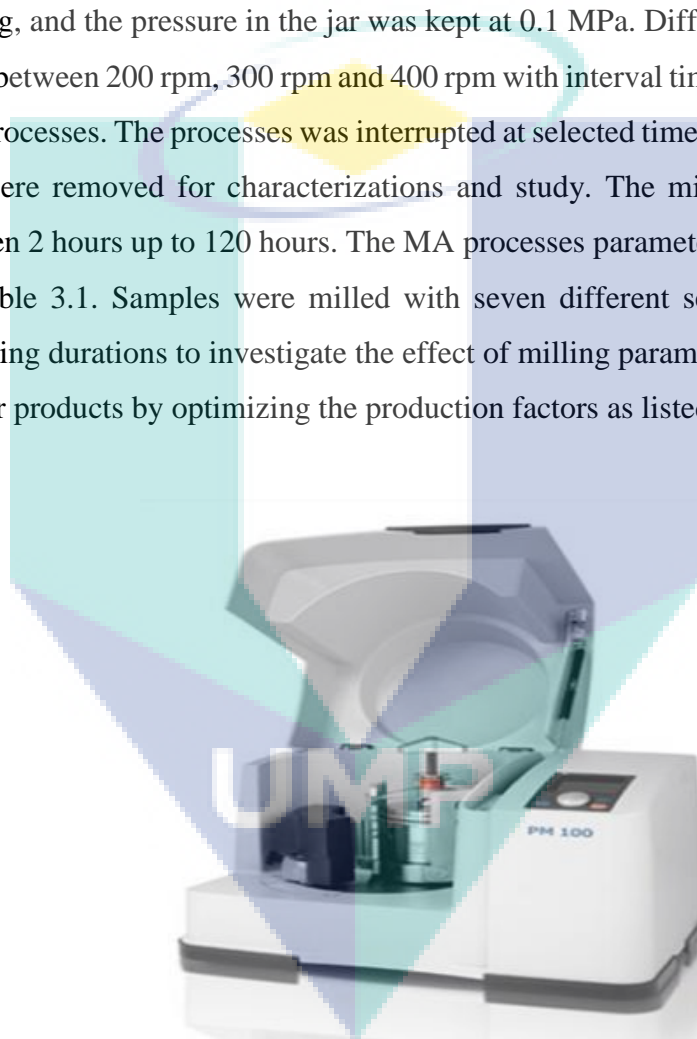


Figure 3.3: Restch PM 100 planetary ball milling machine.

Table 3.1: MA parameters and conditions

Parameters	Conditions
Milling jar	Tungsten Carbide, WC (250ml)
Grinding balls	Tungsten Carbide, WC (ϕ 10mm)
Starting powder	Ti , 100 mesh (99.5% purity), Al (99.97% purity)
Rotation speed	200, 300 and 400 rpm
Milling duration	Up to 120 hours
Ball-to-powder mass ratio	10:1 and 20:1
Process control agent	Hexane
Environment	Ar (99.9% purity)

Table 3.2: MA experimental set

Parameter	Rotation Energy (rpm)	PCA's	Ball to Powder Mass Ratio	Milling Duration (Hours)
<i>A</i>	300	Hexane (5 % wt)	10:1	4, 6, 8, 10, 15
<i>B</i>	400	Hexane (5 % wt)	10:1	4, 6
<i>C</i>	300	Hexane (5 % wt)	20:1	8, 10, 12, 15
<i>D</i>	300	Hexane (2.5 % wt)	20:1	5, 10, 15, 20, 25, 30, 35, 40, 45, 50
<i>E</i>	200	nil	10:1	2, 4, 6
<i>F</i>	300	nil	20:1	10, 20, 40, 60, 80, 100, 120
<i>G</i>	400	nil	20:1	10, 20, 30, 40

3.2.3 Powder Consolidation

Materials produced in MA process were in powder form, which have to be consolidated to obtain dense material for potential use. Choice of pressures for consolidation compromised between good inter-particle or inter-crystalline bonding and minimum porosity. The pre-alloyed powders obtained from the MA processes were pressed mechanically in a tool die by using a hydraulic press to produce a compacted Ti-Al disc as shown in Figure 3.4(a). About 1.0 g of pre-alloyed powder was poured into a tool die with a cylindrical cavity of 12 mm in diameter. The powder in the die then was pressed using a hydraulic press for a certain period. It was found that, the pressure applied and holding time was very vital during powder compaction as excessive pressure and longer holding time resulting in the difficulties to pull out the shaft and the samples from

the mould. In this experimental stage, a pressure of about 100 psi was applied and held for 10 seconds as it was enough to produce a regular compacted disc as shown in Figure 3.4(b).

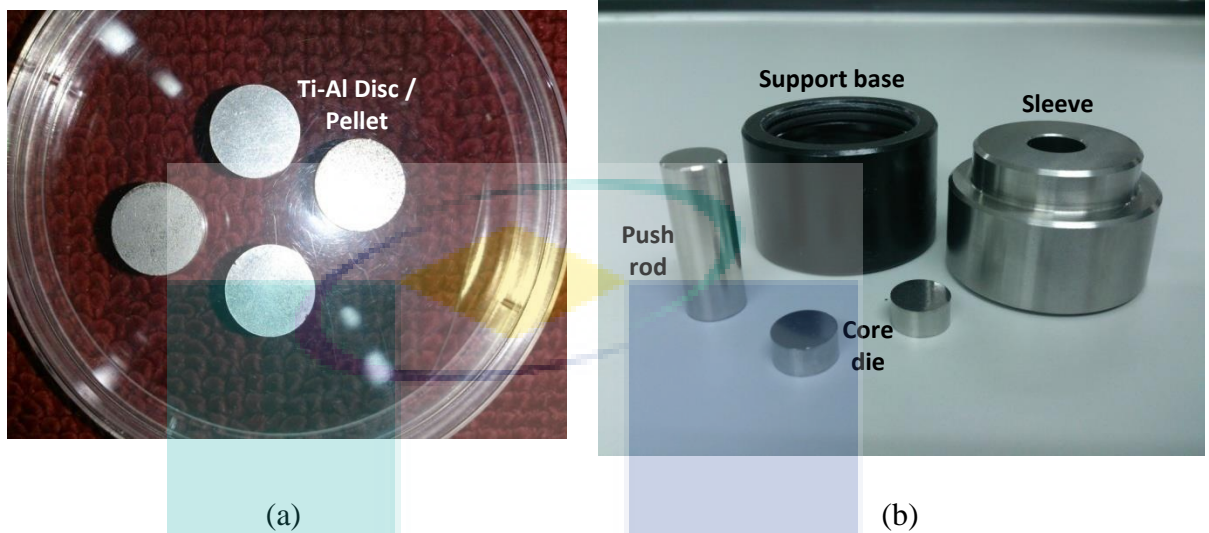


Figure 3.4: (a) Consolidated powder product. (b) custom made tool die used for the powder compaction processes

3.2.4 Heat Treatment

The choice of temperatures for the heat treatment are depending on the thermal stability of the Ti-Al powder to minimize a significant effect against grain growth, which consequently result in the loss of some of the unique properties of nano-crystalline materials. In this work, the heat treatments were carried out in two different procedures using a Linseis P75 Platinum Series dilatometer during thermal analysis. In the first procedure, the powder samples were heated up to 850 °C in a dynamic vacuum atmosphere at a pressure of 0.1 MPa at a rate of 10 °C/min and the furnace was cooled gradually to room temperature. In the second procedure, the final temperature was increased up to 1000 °C with a heating rate of 10 °C/min and maintained at this temperature for up to 4 hours for aging. The furnace then was cooled at a rate of 10°C/min down to room temperature. Prior heating, the pressure inside the furnace was reduced to 10^{-3} barr into vacuum. Then an Argon (Ar) gas was back filled into the furnace at a pressure of 30 kPa to prevent excessive oxidation of the samples during heating. The specific real time temperature of the furnace and samples were monitored by the

thermocouple equipped inside the furnace of the dilatometer employed for the heat treatment processes.

3.3 TEST AND ANALYSES

3.3.1 X-ray Diffraction Analyses

The phase evolution of the powder samples were investigated by X-ray diffraction (XRD) method to identify the powder component, phase transformation and their crystal structure changes throughout the MA process and after heat treatment. Prior measurement, the powder samples were spread as a thin layer on the glass slide. The glass slide was mounted inside the Rigaku Miniflex XRD machine using the CuK_α ($\lambda = 1.540562 \text{ \AA}$) radiation at 30 kV and 15 mA (Figure 3.5). Step-scanning were carried out from 20 to 80° with a counting time of 5s every 0.02° per minute. The data acquisition recorded the intensity, size, full width high maximum (FWHM), d-spacing and phase name of each diffraction peak. The results were interpreted using PDXL software in comparison with ICDD database, while the unidentified peaks are identified manually using the d-spacing of the corresponding element.

The crystallite sizes of the milled powders were determined from X-ray line broadening of the FWHM by using the Scherrer equation below (Scherrer, 1918);

$$D = \frac{K\lambda}{\beta \cos \theta} \quad (3.1)$$

where, D is the mean crystallite size, K is the shape factor (0.9), λ is the CuK_α radiation, θ is the diffraction angles and β is the full width at half maximum (FWHM) of the XRD peaks.

The β values were corrected by using the equation below (Mote et al., 2012);

$$\beta = (\beta M^2 - \beta I^2)^{1/2} \quad (3.2)$$

where, β_M is the full width at half maximum obtained from measurement and β_I is the correction factor for instrument broadening. In this case, the correction factor was obtained by measuring pure Silicon (Si) by using the XRD equipment. Since Si is a single crystalline material, broadening of the XRD peak from the measurement is considered as instrumental broadening and this case is 0.12367 degree.



Figure 3.5: Rigaku Miniflex X-ray diffraction equipment.

3.3.2 Scanning Electron Microscopy and Field Emission Scanning Electron Microscopy

The morphological changes of the powder samples were followed by several methods including visual observation, scanning electron microscopy (SEM) and field emission scanning electron microscopy (FESEM). This is was perform throughout MA processes to investigate the morphological and microstructure evolution of the powder samples. SEM and FESEM produce an image of a sample by scanning it with a focused beam of high energy electrons. The electrons interact with the atoms of the sample, producing various signals detected and that contain information about the sample surface topography. Prior measurement, the powder samples were coated with an ultrathin coating of electrically conducting material (Pt) deposited on the sample by using low-vacuum sputter coating. The samples then were mounted rigidly on a specimen holder before inserted into the machine. Zeiss Evo 50 SEM was employed at an

accelerating voltage of 10 kV for different samples and Joel JSM 7800F field emission scanning electron microscopy FESEM (Figure 3.6) were employed to study the morphological and microstructure evolution of selected powder throughout MA processes and after the heat treatment.



Figure 3.6: (a) Zeiss Evo 50 SEM. (b) Joel JSM 7800F FESEM.

3.3.3 Energy Dispersion X-ray Analyses

Energy dispersive X-ray spectrometer (EDX) measurements were performed to identify the powder component to investigate phase changes after MA process as well as after the heat treatment for selected powder samples. This measurement is performed using an Oxford X-Max device coupled with Joel JSM 7800F field emission scanning electron microscopy (FESEM) at an accelerating voltage of 10 kV (Figure 3.7). During the measurement, a high-energy beam of electrons is focused into the samples. The electron interacted with the samples atoms and X-ray energy released. The number and energy of the X-rays emitted measured by an energy-dispersive spectrometer that allows identifying the elemental composition of the samples. The number of ions calculation based on 8.00 anions per formula, with Manganese used as the element for optimization. Pulse pile up correction was performed for each measurement and the number of iterations was set at 2. The results were interpreted using standard database software.

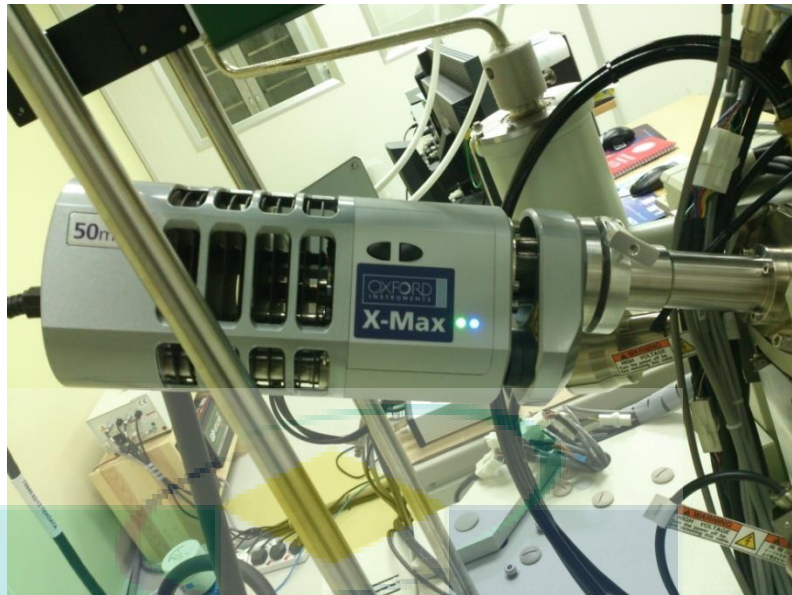


Figure 3.7: Oxford X-Max EDX device coupled with FESEM.

3.3.4 High Resolution Transmission Electron Microscope (HRTEM)

High Resolution Transmission Electron Microscope (HRTEM) analyses were performed to get a closer view of selected powder samples in order to investigate the crystallite structure changes after MA process as well as after the heat treatment for selected powder samples. This measurement is performed using an FEI TeCNai J20 at an accelerating voltage of 200kV. The sample is placed onto the inner meshed (Cu) TEM grid with a diameter of approximately 2.5 mm. This grid is placed into the sample holder, which is paired with the specimen stage before inserted into TEM. Once inserted into a TEM, the samples were manipulated to the region of interest to the beam, up to single grain diffraction. The SAED technique in TEM measurement was also performed for the identification of the materials and determination of the crystal structure including the unit cell parameters. Every spot in the SAED patterns are corresponds to lattice planes of a certain miller index. To analyze the SAED patterns, the d-spacing for the spots were calculated by Equation (3.3).

$$d = \frac{D}{(\lambda L)} \quad (3.3)$$

where, d is spacing between planes, λ is the wavelength of the electron beam ($\lambda = 2d \sin\theta$, Bragg's law), θ is the diffraction angle, D is the distance between spots on the SAED pattern, L is camera length for the TEM machine. The results were interpreted manually by comparison with the standard XRD PDF Card as the diffraction pattern could be regarded as a finger print for a specific crystal.

3.3.5 Thermal Analysis

The thermal analysis was conducted in a Linseis P75 Platinum Series dilatometer utilized a standard resistance furnace and a single alumina pushrod for the determination of coefficient of thermal expansion (CTE) and differential thermal analysis (DTA) evaluation feature of the pre-alloyed Ti-Al powders under thermal load. Dilatometry is a technique which measures the dimensional change of samples as a function of temperature while the samples were subjected to a controlled temperature. The DTA measurement is a mathematical routine based on the sample temperature. Exothermic and endothermic effects influence the change of the sample temperature during the dynamic heating or cooling cycle. In the first procedure, about 0.5g of the powder samples were hand-compacted in alumina (Al_2O_3) sample holder (adapter) and placed in the alumina pushrod tube for the test to final temperatures up to 850 °C. In the second procedure, the powder samples were made into bulk 6 mm x 6 mm cylindrical specimen. Prior heating, the furnace was vacuum for about 1 hour to reach a pressure around 10^{-3} barr. A flowing argon (Ar) gas then was back filled into the furnace to prevent excessive oxidation of the samples during heating at a pressure of 30 kPa. The powder samples then were heated uniformly at a constant rate of 10 °C/min from room temperature to final temperatures up to 1000 °C. The data acquisition recorded running time, furnace temperature, control temperature, and change in length of the sample relative to the alumina reference material. The data obtained were interpreted using Linseis standard software. The experimental set up for the thermal analyses are shown in Figure 3.8.



Figure 3.8: Linseis P75 Platinum Series dilatometer.

3.3.6 Density Measurement

The density of consolidated samples were measured using Archimedes principle using distilled water as immersing liquid. The experimental set up for the density measurement are shown in Figure 3.9. At first the samples were weighted in air by hanged it freely. Then, the samples were submerged in distilled water and weighted again. Equations (3.5) and (3.6) were used to calculate the measured density and relative density of the samples respectively. The theoretical density of titanium aluminide used for comparison is 3.9 g/cm³.

$$D_m = \frac{W_a}{W_a - W_w} \quad (3.4)$$

$$D_r = \frac{D_m}{W_a - W_w} \quad (3.5)$$

where, D_m is the density measured, D_r is the relative density, W_a is the weight of the sample in air, and W_w is the weight of the sample in water.

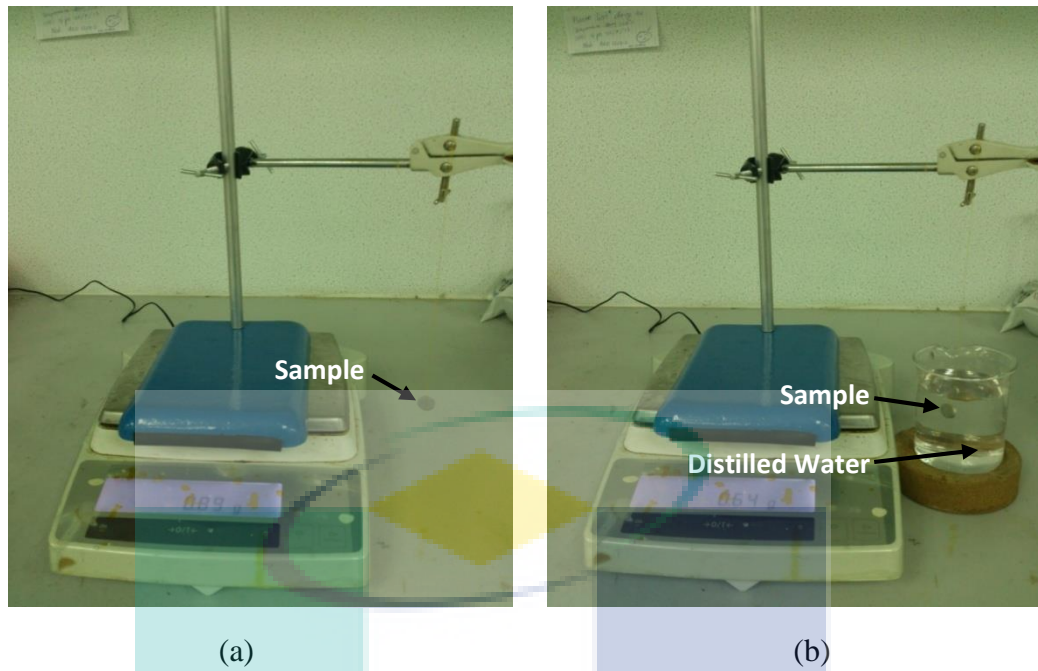


Figure 3.9: Experimental set up for the density measurement by using Archimedes method. Sample measurement in air. (b) Sample measurement in distilled water.

3.3.7 Micro-Hardness Measurement

The Vickers hardness test method consists of indenting the test material with a diamond indenter, in the form of a pyramid with a square base and an angle of 136 degrees between opposite faces subjected to a test force. The two diagonals of the indentation left in the surface of the material after removal of the load are measured using a microscope and their average calculated. The area of the sloping surfaces of the indentation is calculated. The Vickers hardness is the quotient obtained by dividing the kgf load by the square mm area of indentation. When the mean diagonal of the indentation has been determined the Vickers hardness may be calculated from the formula below.

$$HV = \frac{2P \sin \theta \left(\frac{\alpha}{2} \right)}{d^2} = \frac{1.8544P}{d^2} \quad (3.6)$$

where, HV is the Vickers hardness, P is the force (kgf), d is the mean diagonal of impression (mm), and α is the face angle of diamond ($=136^\circ$).

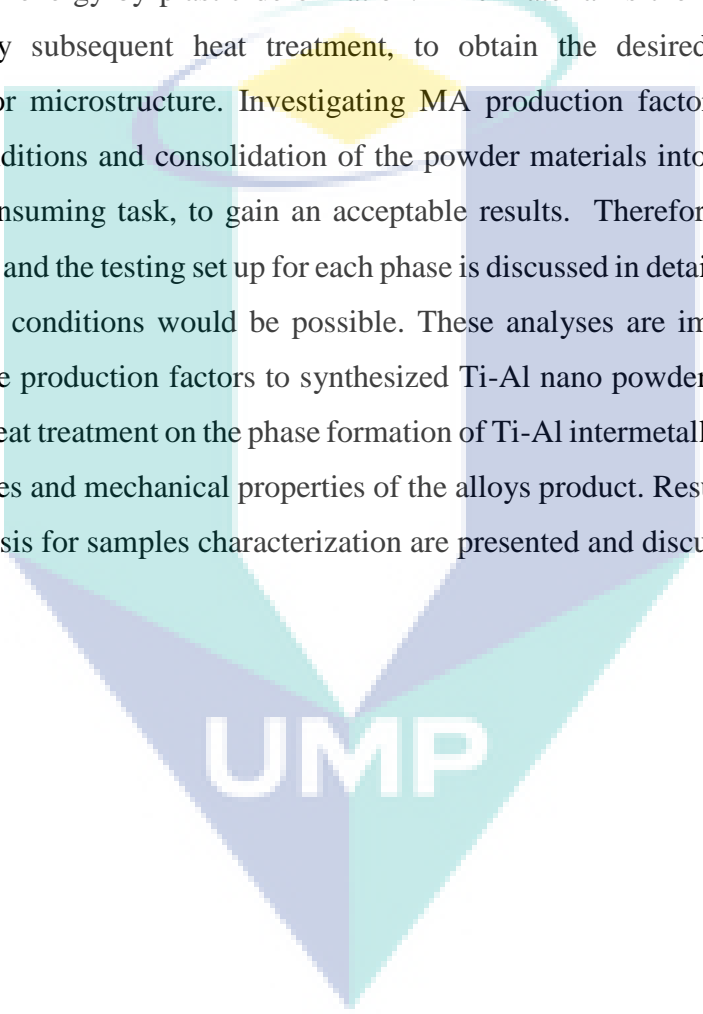
Vickers micro hardness measurements were performed using a digital Tukon 1200 Wilson Hardness micro hardness test machine (Figure 3.10). Each measurement was performed according to ASTM E 92-82 Standard Method under a load of 0.02 kg for 10 s. The hardness measurements were performed in an orientation perpendicular to the direction of compaction. The diamond indenter is pressed onto the samples surface and then the horizontal size of the impression is measured and computed to a hardness number. The test result for each sample is the average value of at least 10 successive indentations. Prior micro-hardness testing, the compacted powder samples were hot mounted in epoxy resin at 4200 Psi for 3 minutes. The mounted samples then were cured for 8 days in a humidifier before grinding using a series of emery papers (320, 400, 1200, 2000 and 4000). The samples were subjected to a successive grinding process on a manual polishing wheel, running at a slow wheel speed < 100 rpm. Tap water continuously flooded the papers to provide lubrication and clear the residual particles. The final polishing was done using a cloth and diamond particle suspension as lubricant to obtain scratch free polished samples.



Figure 3.10: Tukon 1200 Wilson Hardness testing machine.

3.4 SUMMARY

In this study, elemental Ti-Al powder were use as precursor material mechanically alloyed in planetary ball mill under specific parameters and controlled conditions to produce nano-crystalline Ti-Al powders. The central underlying approach is to break down the microstructure of the Ti-Al elemental powder into a nanostructure range, while energize the precursor material into a highly meta-stable state by external dynamic forces of mechanical energy by plastic deformation. The material is then transformed into a final state by subsequent heat treatment, to obtain the desired phases, chemical constitution or microstructure. Investigating MA production factors, developing heat treatment conditions and consolidation of the powder materials into bulk form was the most time consuming task, to gain an acceptable results. Therefore, the experimental methods used and the testing set up for each phase is discussed in detail, so that replication of the testing conditions would be possible. These analyses are important in order to investigate the production factors to synthesized Ti-Al nano powders, the effect of MA process and heat treatment on the phase formation of Ti-Al intermetallics and its influence on the densities and mechanical properties of the alloys product. Results from laboratory test and analysis for samples characterization are presented and discussed in detail in the next chapter.

The logo for UMP (Universitas Muhammadiyah Purwokerto) is a large, downward-pointing triangle composed of four smaller triangles meeting at the center. The top-left triangle is light blue, the top-right is light purple, the bottom-left is light green, and the bottom-right is light blue. The letters 'UMP' are written in white, bold, sans-serif font across the center of the triangle.

UMP

CHAPTER 4

RESULTS AND DISCUSSION

4.1 INTRODUCTION

This chapter discussed the results from laboratory test and analysis for samples characterization. It comprises of morphological observation, and the effect MA and heat treatment on phase formation, crystallite size evolution and thermal stability of mechanically alloyed Ti-Al powders. The latter section will also discussed the effect of MA and heat treatment on the density and micro hardness values of the alloys product. These analyses are important in order to investigate the relationship between phase formation and its influence on the physical and mechanical properties of the alloys product.

4.2 MORPHOLOGICAL OBSERVATION

The surface morphology of the mechanically alloyed Ti-Al powders at different milling parameters and durations were investigated by visual observation, optical microscopy, SEM and FESEM. As shown in Figure 4.1(a), the initial powder mixtures show a distinctive features of each elemental powder as Ti and Al particle. It is appear from Figure 4.1(b), that Ti particles are in irregular shapes and various sizes, and Al particles are mainly in much smaller size, Figure 4.1(c). Throughout the MA process, the powders particles experienced a characteristic change in particle shape, size and morphology as ball milling causes repeated welding, fracturing, re-welding and re-fracturing as proposed by Benjamin (1992). Investigation on morphological changes were made on *D* samples which milled with least addition of Hexane as a process control agent (PCA) for longer duration (Figure 4.2). It was found that after 10 h of milling, mainly

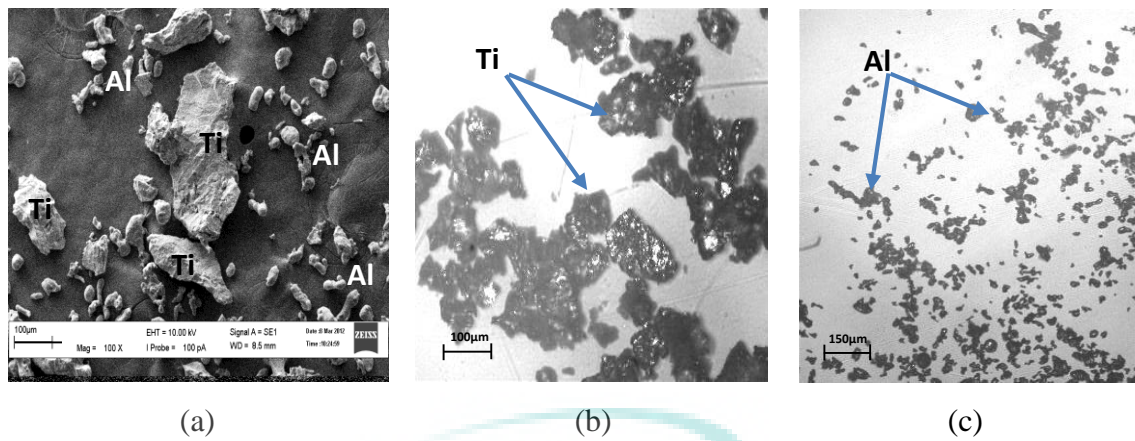


Figure 4.1: (a) SEM micrographs of the initial Ti-Al powder mixture (b) Optical microscopy pictograph of Ti powder (c) Optical microscopy pictograph of Al powder

oval-shaped particles emerged in various sizes. At this stage, no deformation were observed yet. As high energy ball milling proceeded to 50 h, increased number of particles fractured and refined, these oval-shaped particles disintegrate more to a uniform smaller size with equiaxed shape. At this stage, cold welding and plastic deformation of the powder particles, were observed and layered structure of Ti-Al mixture were produced as the powder turn into finer and relatively smaller particles. It is more visible that the particles surfaces were heavily deformed and the particle surfaces were quite rough.

Ti-Al powder samples were dry milled without any addition of PCA under *E*, *F* and *G* parameters (Table 3.2). Powders milled under *E* parameter shows the most remarkable changes in particles morphologies (Figure 4.3). During the first 2 h of milling process, as both Ti and Al particles are ductile, they are subjected to heavy deformation and are welded together forming large rounded-shape beads and particles. The formation of these beads and large particles is due to the agglomeration of large amount of small powder particles. Severe sticking of the powder particles to the balls and milling jar were observed. On further milling up to 4 h, repeated collision between the particles to the balls and milling jar causes the beads to be flattened and turn into large size particles. At this stage, the amount of the sticking powder to the balls and milling jar were also reduced. On continues milling to 6 h, these flaky particles disintegrate more to a uniform smaller size flakes with finer and flattened surface particles as a result of increased numbers of re-welding and re-fracturing.

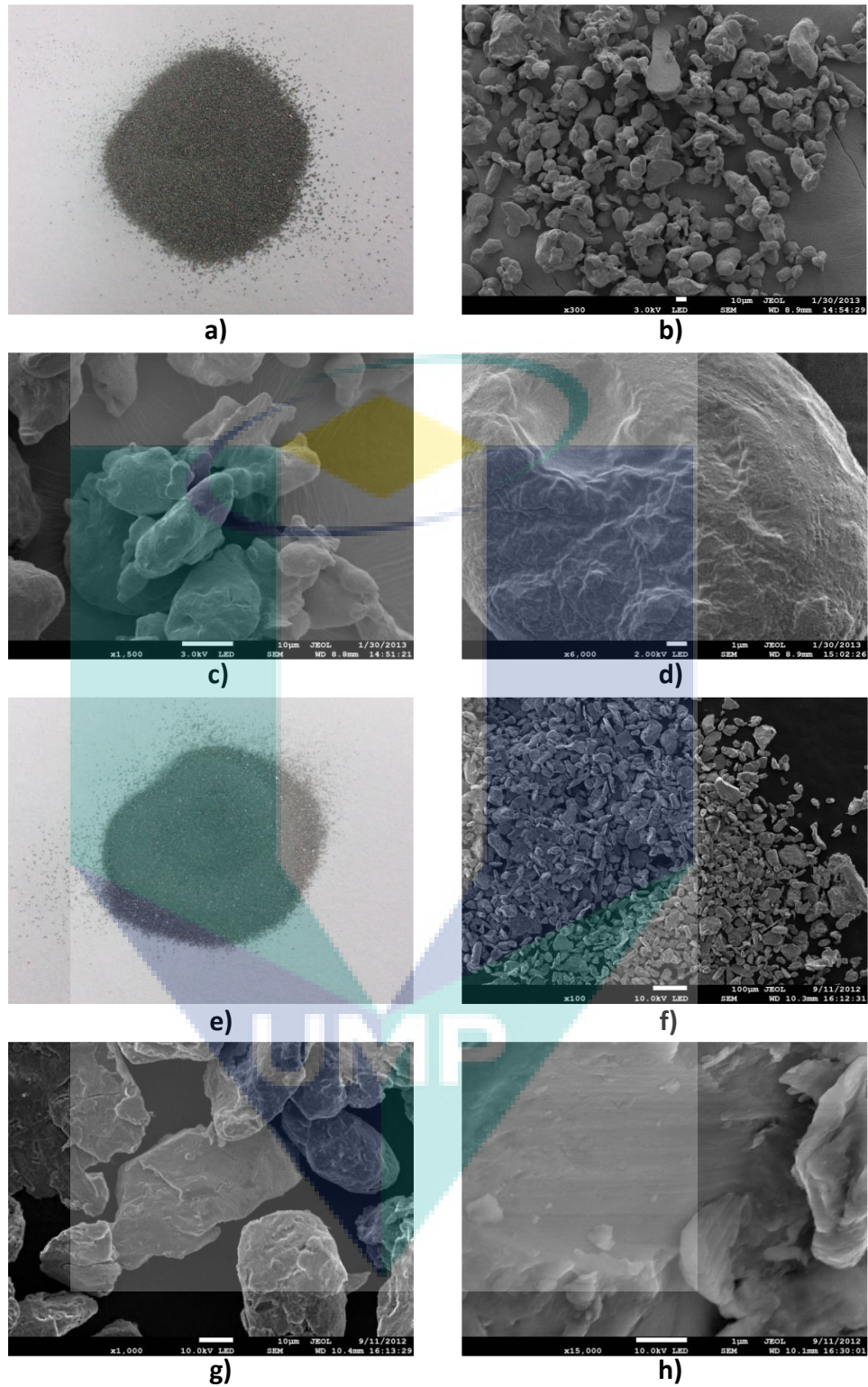


Figure 4.2: FESEM micrographs and visual observation of Ti-Al powders milled under D parameter (300rpm, 2.5% wt Hexane, 20:1 bpr). 10 h milled (a), (b), (c) and (d). 50 h milled (e), (f), (g) and (h).

This phenomenon has also been observed by several researchers including Lu, et al. (2002) and Szweczek and Wyrzykowski (1999) as a result from repeated welding, fracturing and re-welding during milling as proposed by Benjamin (1992). Fadeeva et al. (1998) reported that during the first 3 h of milling the powder coated the balls and inner wall of the jar, but after 6 h of milling the powder was easily detachable. However, in this current work it was difficult to remove the sticking powder from the milling balls and jar, leading to a very low milling yield. Therefore milling under this parameter was not further explored in this research work.

Further investigations were made through higher rotation speeds of 300 rpm and 400 rpm respectively under F and G parameters. In these groups of samples, even though agglomerations were observed at the initial stage of milling, the sticking of powders to the balls and milling jar was almost negligible resulting in high milling yield. After prolonged milling up to 40 h, the size and shape of the powder particles were much smaller compared to powder at the initial stage (Figure 4.4). At this stage, cold welding and plastic deformation of the powder particles, essentially mixed by means of solid-state diffusion between titanium and aluminum atoms, produced a multilayered and fairly homogeneous composite structure of Ti-Al powder particles. On continued milling up to 100 h, the particle size of powders milled under F parameter are very fine in size and structure. As shown in Figure 4.5, it is more visible that a large amount of different defects were developed in these Ti-Al powder particles. These defects are due to the deformation caused by ball to powder collisions during MA which produced a high density of dislocations.

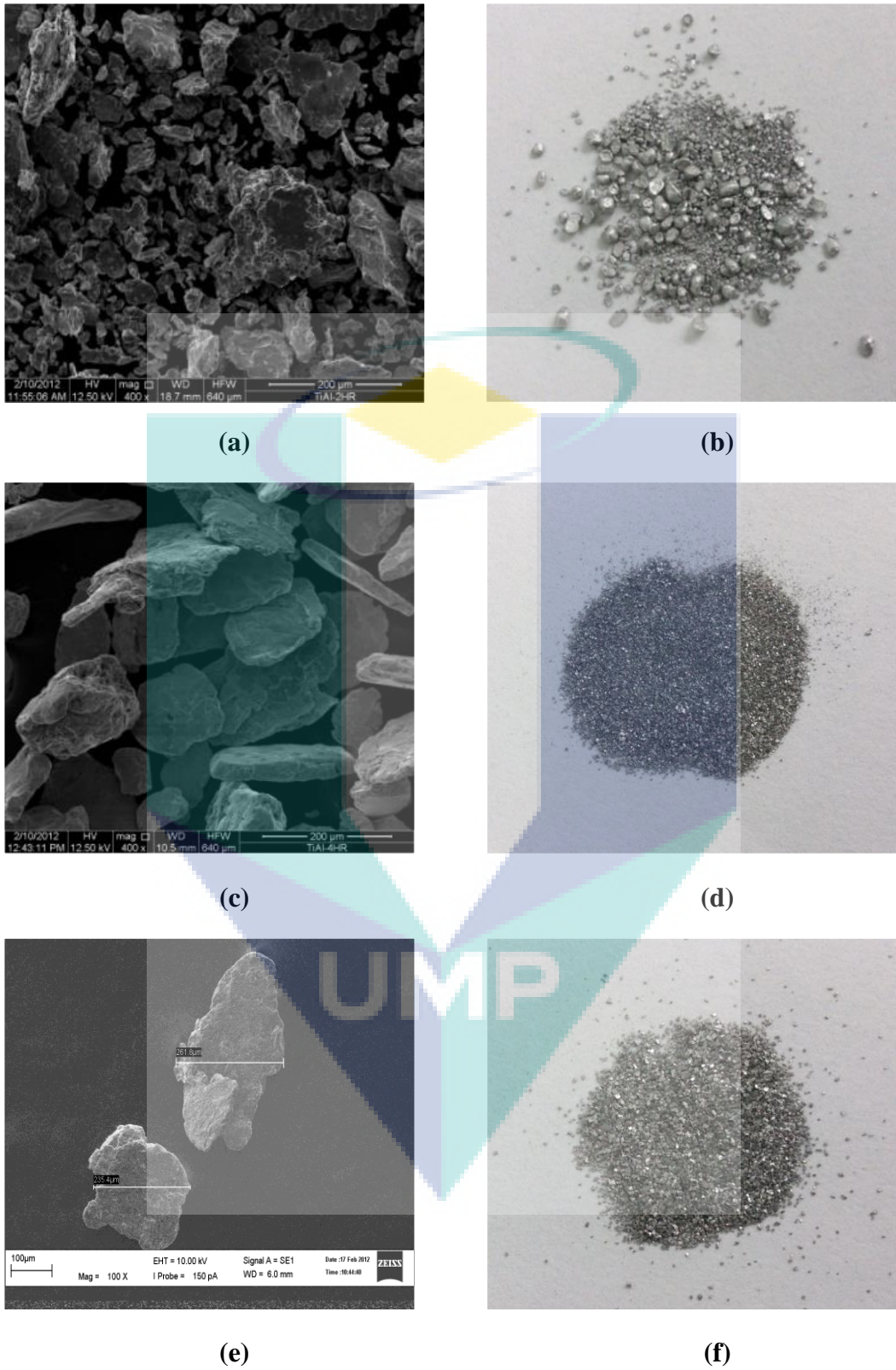


Figure 4.3: SEM micrographs and visual observation of Ti-Al powders milled under E parameter (200rpm, without PCA's, 10:1 bpr). 2 h milled (a) and (b). 4 h milled (c) and (d). 6 h milled (e) and (f).

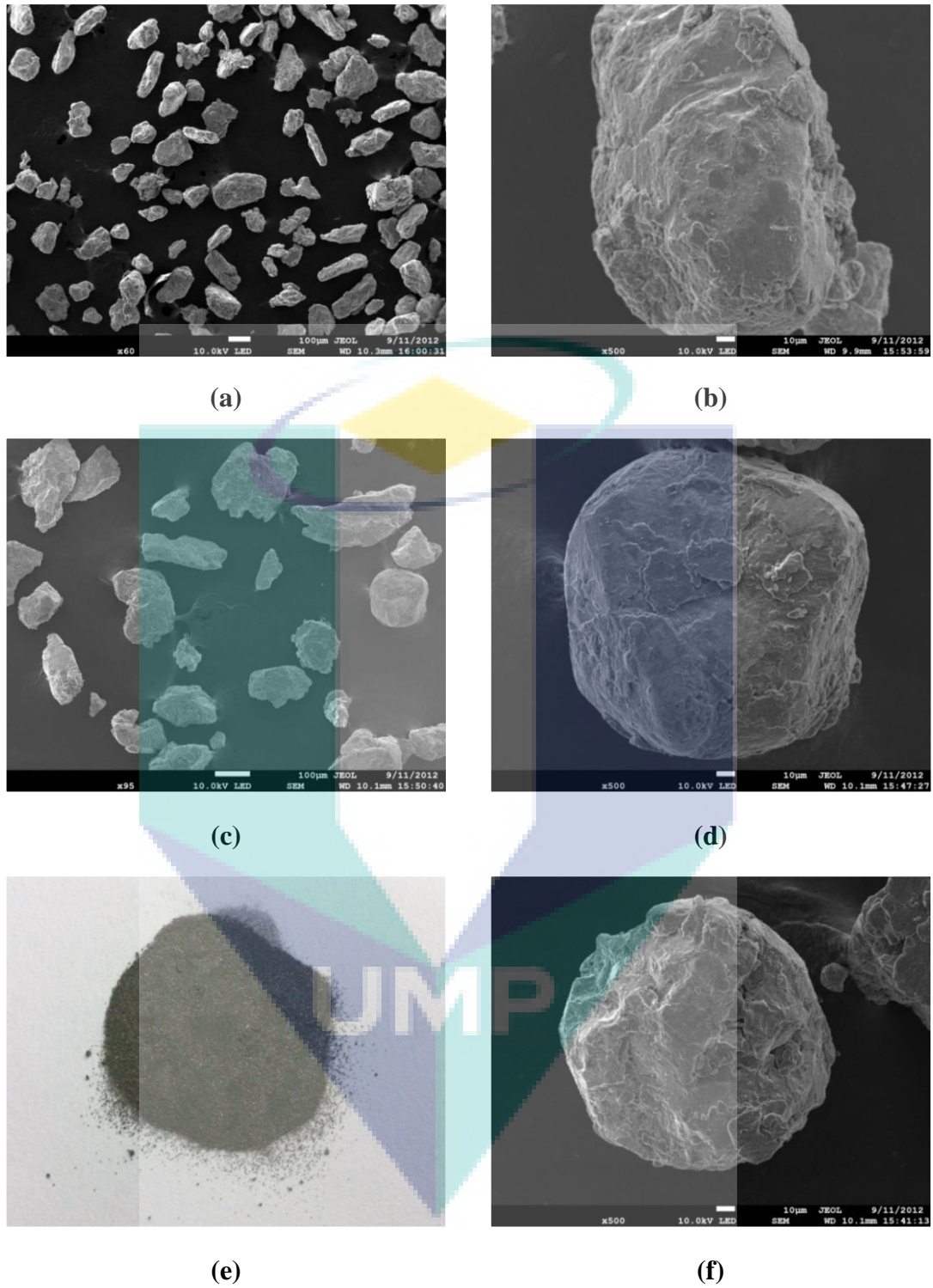


Figure 4.4: SEM/FESEM micrographs and visual observation of Ti-Al milled powders. *F* parameter – 40 h milled (a) and (b). *G* parameter – 40 h milled (c) and (d). *F* parameter – 100 h milled (e) and (f).

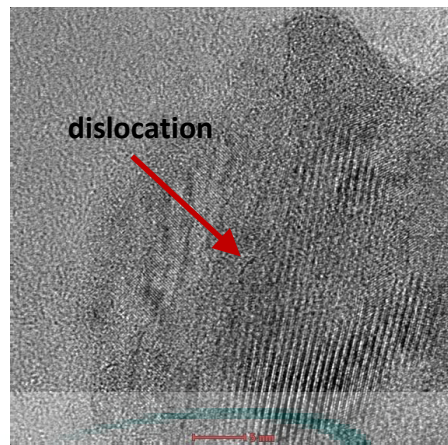


Figure 4.5: HRTEM images of high density of dislocation on Ti-Al powders powder milled under F parameter (300rpm, without PCA's, 20:1 bpr) for 100h.

4.3 CHARACTERIZATION OF MECHANICALLY ALLOYED POWDERS

4.3.1 Effect of MA on Phase Formation

Phase analyses were performed by XRD, EDX and TEM measurement according to the procedure described in previous chapter. The analyses were performed to investigate the phase evolution throughout the MA processes. XRD measurements were performed to Ti-Al powder at selected stage to investigate the phase formation throughout the MA processes. The XRD spectrums of individual Ti and Al powders along with the initial Ti-Al powder mixture are shown in Figure 4.6. In the initial powder mixture (0h), a sharp Bragg diffraction peaks of Ti (hcp) and Al (fcc) are displayed with a principal peak of Ti and Al appears at 2θ of 40.31° and 38.46° respectively.

X-ray diffraction patterns from mechanically alloyed Ti-Al powders are presented in Figure 4.7 – 4.13. In this present investigation, there are no evidence of formation of any titanium aluminide intermetallic phases as the XRD pattern shows only Ti and Al peaks individually. However, milling resulted in the changes of XRD patterns with gradual broadening, intensities decreasing and an apparent shift of the principal diffraction peaks to higher angle side. Ti and Al peaks gradually becoming broader and the intensity decreased by milling duration. The gradual broadening of Ti and Al peaks,

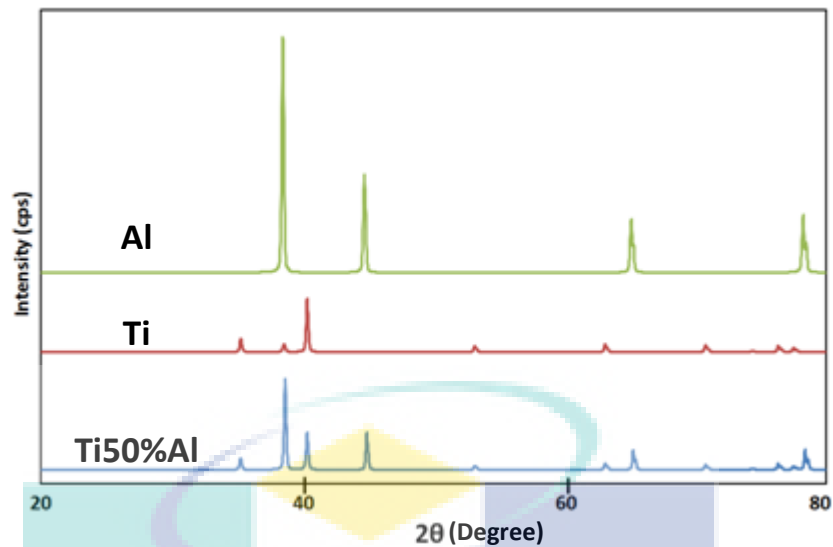


Figure 4.6: X-ray diffractogram for Ti, Al and initial Ti-Al powder mixture

suggests an increase of strain in the internal crystallite or a decrease in the effective crystallite size, or both. Furthermore, comparison of the principal α -Ti (1 0 1) and Al (1 1 1) peaks in the XRD patterns obtained indicate a gradual shift of the principal peaks towards higher angle. It is known that, MA of pure metal powders alone can only produce a broadening of XRD peaks, that fore, the shifting of these peaks was due to the diffusion of Al into Ti matrix which attribute to a reduction of Ti lattice parameter, promoting the formation of Ti(Al) solid solution as proposed by Vyas (2009). In addition, by assuming the structure between the phase obtained and α -Ti structure are similar, it was found that the lattice parameters up to $a = 0.29315$ nm and $c = 0.4644$ nm was obtained. These values are considerably lower than α -Ti parameters with $a = 0.2944$ nm and $c = 0.4678$ nm, indicate that MA process has enhanced the solubility of Al into Ti and substantially form supersaturated Ti(Al) solid solution. Guo et al. (1991) also observed the shrinkage of the α -Ti lattice and they concluded that it was due to the diffusion of Al into Ti, which promotes the formation of h.c.p. Ti(Al) solid solution. So as expected, Al diffuses into Ti predominantly during MA and considerable solid solubility extensions were achieved by MA alone. The XRD analysis revealed that the obtained homogeneous microstructure was comprised of bcc Ti-Al solid solution and deformed hcp Ti particles which in good agreement with findings of Li et al., 2011.

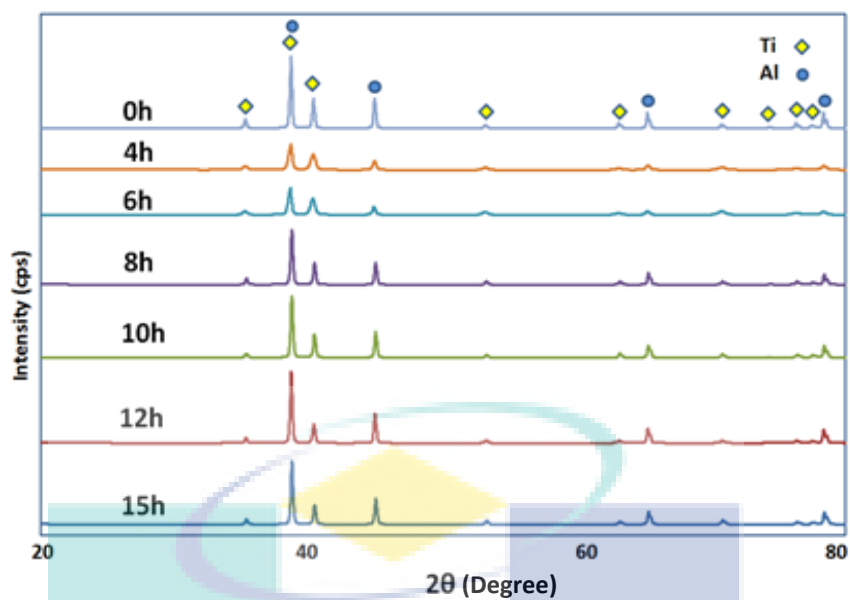


Figure 4.7: X-ray diffractogram for Ti-Al powders milled under *A* parameter (300rpm, 5.0% wt Hexane, 10:1 bpr).

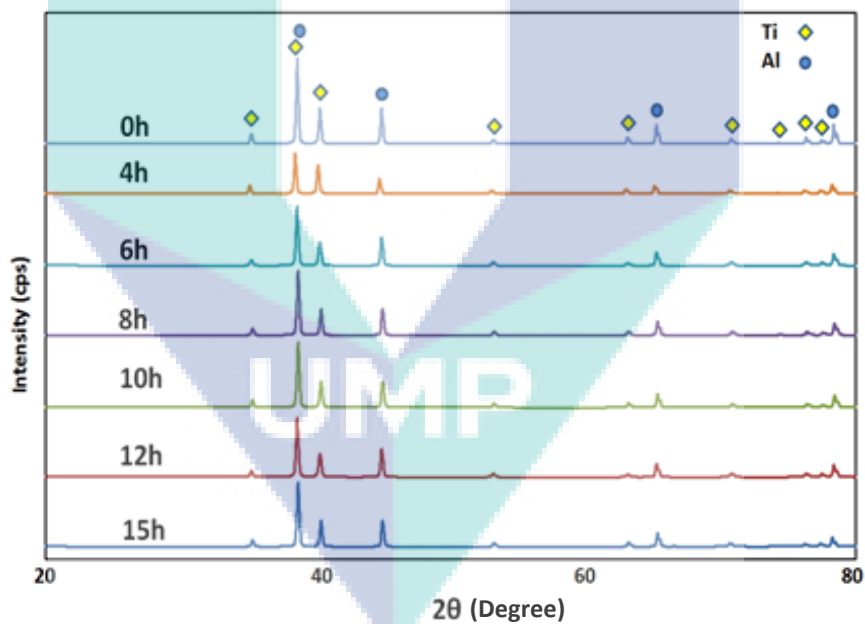


Figure 4.8: X-ray diffractogram for Ti-Al powders milled under *B* parameter (400rpm, 5% wt Hexane, 10:1 bpr).

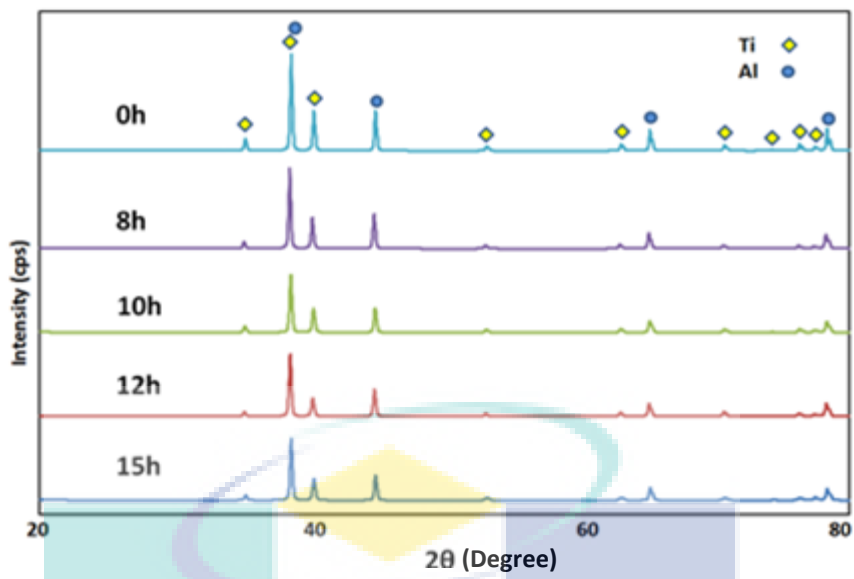


Figure 4.9: X-ray diffractogram for Ti-Al powders milled under *C* parameter (300rpm, 5% wt Hexane, 20:1 bpr).

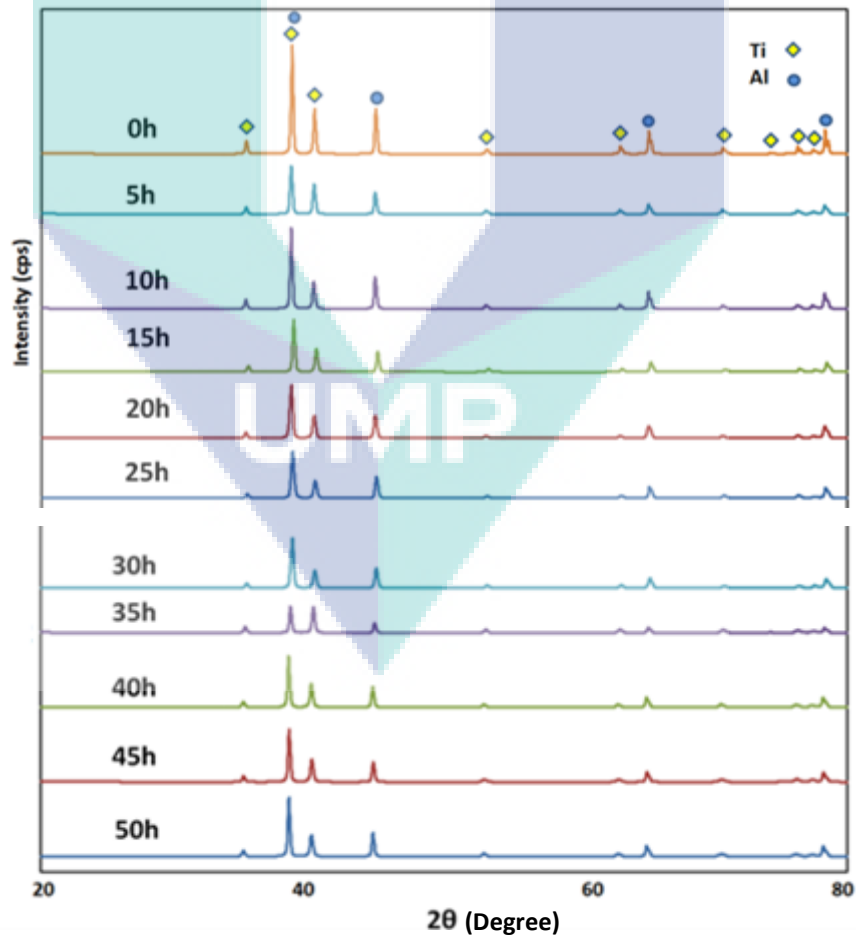


Figure 4.10: X-ray diffractogram for Ti-Al powders milled under *D* parameter (300rpm, 2.5% wt Hexane, 20:1 bpr).

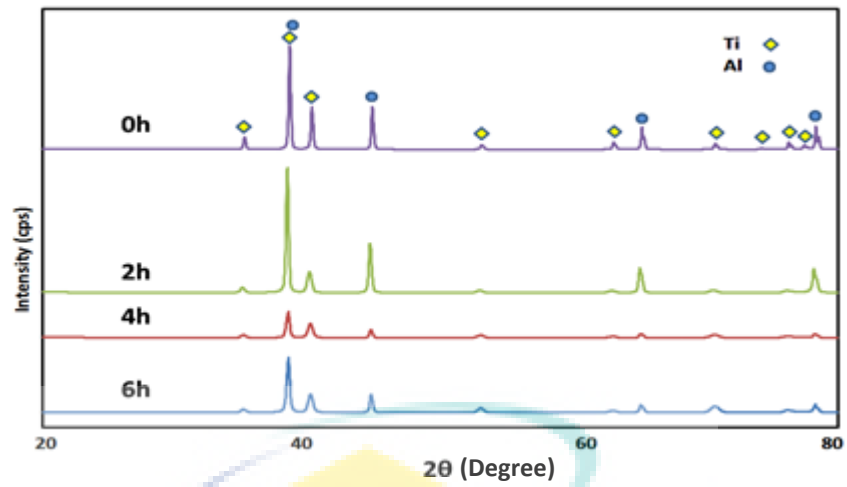


Figure 4.11: X-ray diffractogram for Ti-Al powders milled under *E* parameter (200rpm, without PCA's, 10:1 bpr)

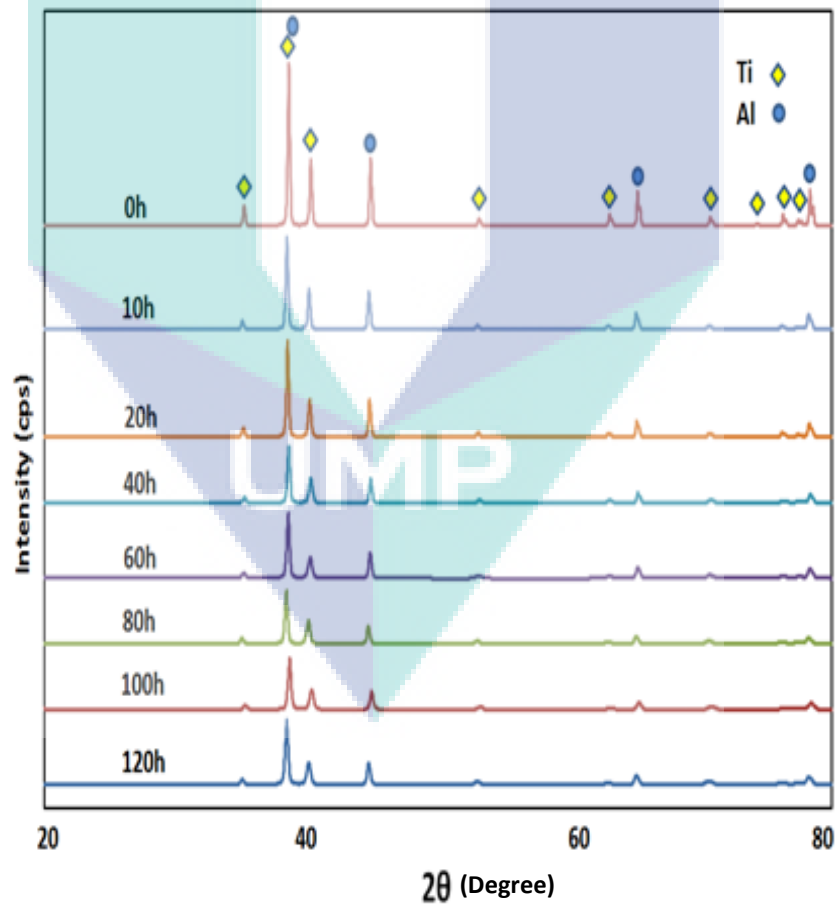


Figure 4.12: X-ray diffractogram for Ti-Al powders milled under *F* parameter (300rpm, without PCA's, 20:1 bpr).

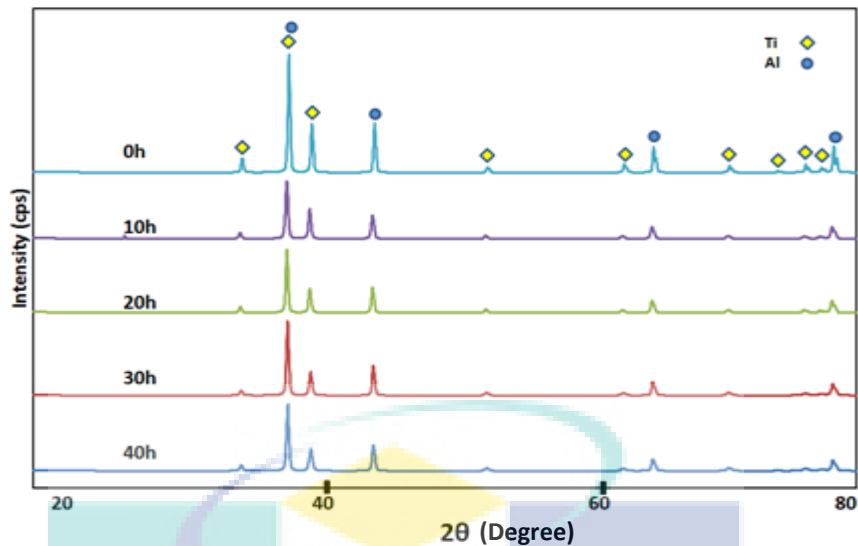


Figure 4.13: X-ray diffractogram for Ti-Al powders milled under *G* parameter (400rpm, without PCA's, 20:1 bpr).

The formation of Ti(Al) solid solution after MA were supported by the result from EDX analysis for selected samples. Figure 4.14 shows the EDX results for Ti-Al powder milled under *D* parameter for 10 h. As shown the images of a distinctive Ti and Al powder particle individually with 100% composition respectively. These indicate that, at this point, inter diffusion reaction between Ti and Al particles were restricted. However, when the milling processes were prolonged to 50 h a particle with a composition of 82.82% of Ti and 17.18% of Al was identified. This result suggested that inter diffusion reaction between Ti and Al particles only occurs after prolonged milling and confirms that alloying of Ti and Al was realized in each particles. Even though free un-react Ti and Al particles still at large, the results can be attribute to formation of Ti(Al) solid solution.

The progressive dissolution due to inter-diffusion between the Ti and Al elements in Ti-Al powder milled under *F* parameter, after prolonged milling was also supported by Energy Dispersive X-ray (EDX) analyses. The perimeter area of the micrograph given in Figure 4.14 indicated that with prolonged milling, the contents of Al and Ti in particles were close to the composition of Ti-Al phases respectively. From the results obtained, particles with a likely phase of TiAl were found in powders milled for 40 h and 100 h under *F* parameter. On the other hand, particles with likely phases of TiAl and Ti₃Al were obtained in powder milled for 40 h under *G* parameter (Figure 4.15). The formation of

Ti(Al) solid solution during milling was further supported by TEM analysis for powder milled for 100 h under F parameter. Comparisons on the lattice parameter indicated that the powder constituent TiAl_3 with single crystallite structure (Figure 4.16). This results have confirmed that Ti(Al) solid solution have been formed by MA process at room temperature where its behavior is strongly depends on the parameters and durations of the MA process.

The behavior of the light elements when alloying with titanium is varies and has a high dependency on their properties. From the widely accepted Ti-Al phase diagram, Al has an extended solubility in Ti, while Ti has a limited solubility in Al at different temperatures. The maximum solid solubility of Al in Ti at the temperature of about 1500 °C is about 50at%, while at room temperature the solubility only about 0.5 at% (James and Lord, 1992). The formation of Ti(Al) from elemental Ti-Al powders by ball milling from this work was similar with findings of Li et al., 2011. Even though Farhang et al., (2010) indicated that even at room temperature, formation of Ti-Al intermetallics compound was possible during MA, it did not occurs in this current work. Despite the fact that this work shared almost the same parameter and milling condition of Farhang et al., (2010) such as feed materials composition, rotation speed, milling duration, environment and ball to powder ratio, nonetheless the equipment employed by them was different. However, a glimpse of TiAl_3 was detected in powder particles correspond to the first reaction of titanium aluminide intermetallics phase indicate that a small portion of intermetallic phase has already formed during milling. Nevertheless, results from this current work was in a good agreement with report by Suryanarayana (2001) which indicate that the formation of intermetallic compounds of $\alpha_2\text{-Ti}_3\text{Al}$ or $\gamma\text{-TiAl}$ cannot be synthesized directly through milling.

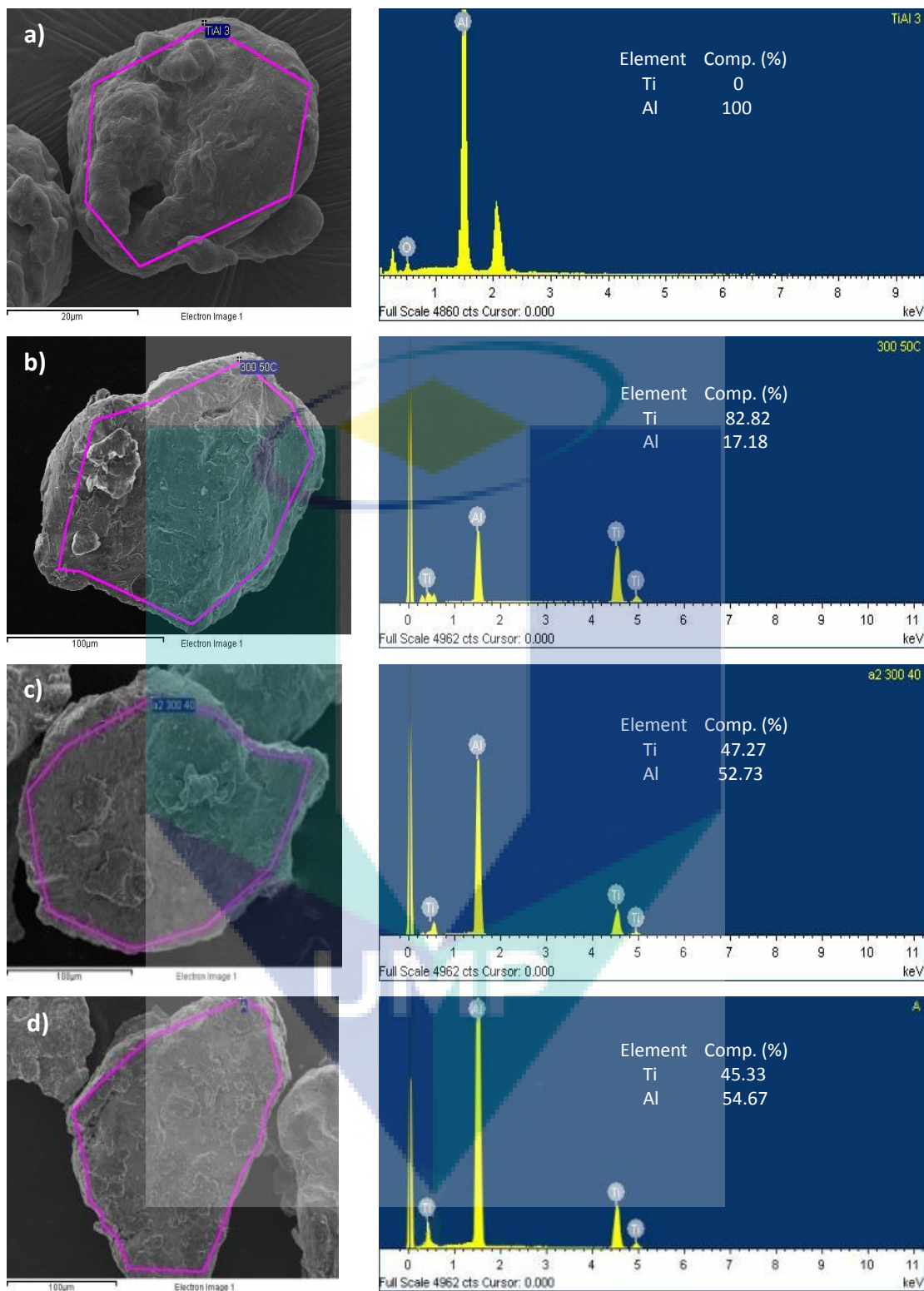


Figure 4.14: FESEM images and EDX spectrums for Ti-Al powders milled under *D* parameter (300rpm, 2.5% wt Hexane, 20:1 bpr) and *F* parameter (300rpm, without PCA's, 20:1 bpr). (a) *D* - 10 h, (b) *D* – 50, (c) *F* - 40 h, and (d) *F* - 100 h of milling.

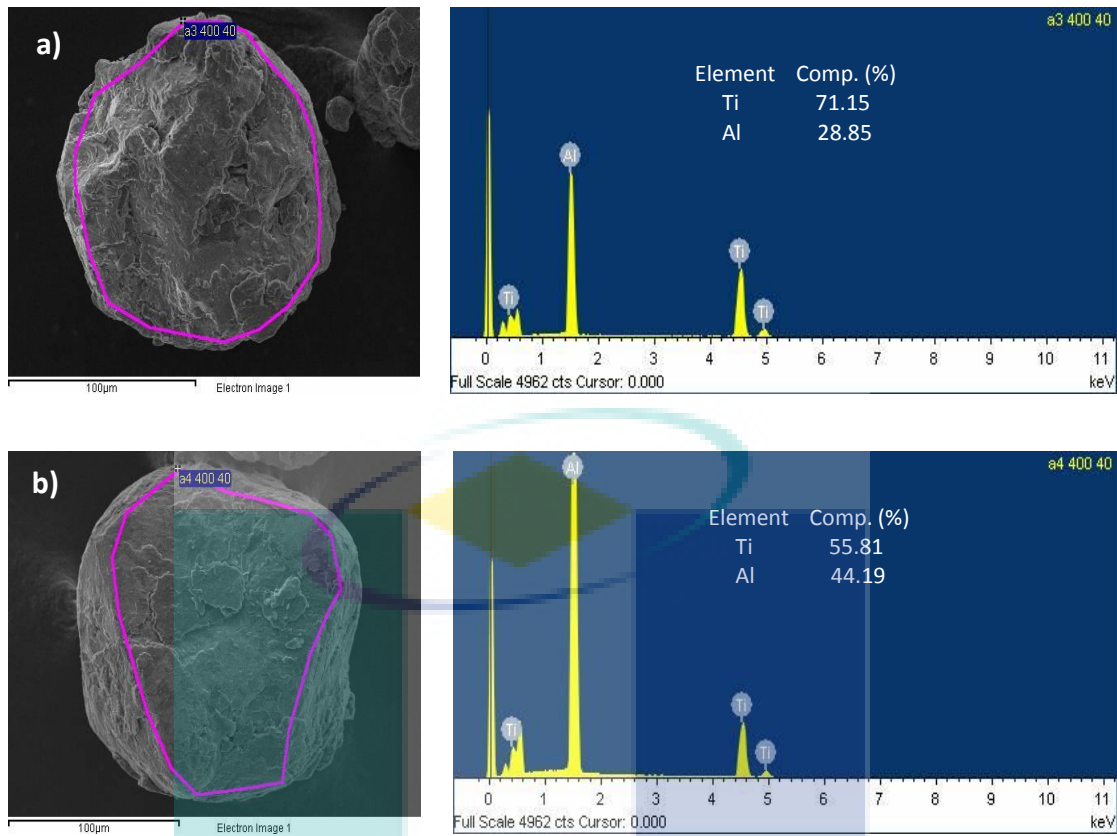


Figure 4.15: FESEM images and EDX spectrums of Ti--Al powder milled under *G* parameter (400rpm, without PCA's, 20:1 bpr) after 40 h with a likely phase of (a) Ti_3Al and (b) $TiAl$ phase.

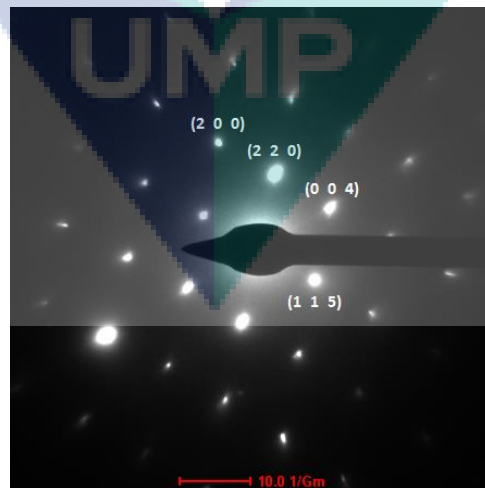


Figure 4.16: SAED pattern from TEM analysis of Ti-Al powder milled under *F* parameter (300rpm, without PCA's, 20:1 bpr) for 100 h with $TiAl_3$ phase.

4.3.2 Effect of Heat Treatment on Phase Formation

In the initial stage of this study, Ti-Al powder samples were annealed in dynamic vacuum under control heating up to 850°C. The XRD results exhibit a major difference as heating has transformed the powder mixture into equilibrium Ti-Al intermetallics phases (Figure 4.17 to 4.20). In most cases, a formation of dominant TiAl_3 along with γ -TiAl and minor reflection of α_2 - Ti_3Al phase and residual Ti were occurred. In some cases, almost single phase TiAl_3 were obtained along with residual Ti. The phase identified in all samples is listed in Table 4.1.

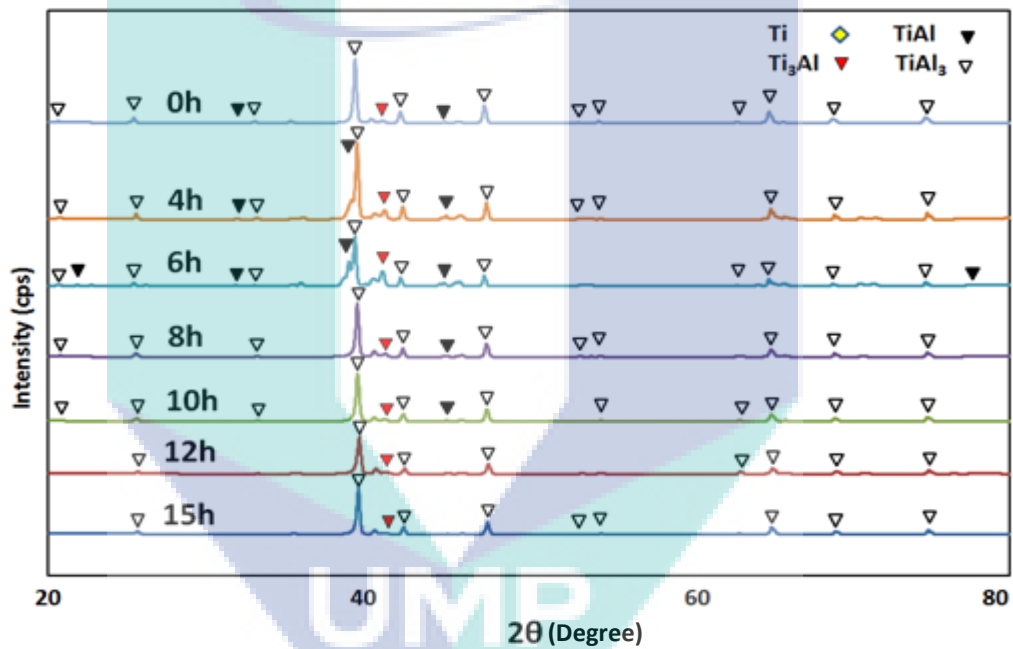


Figure 4.17: X-ray diffractogram of Ti-Al powders milled under A parameter (300rpm, 5% wt Hexane, 10:1 bpr) after heating up to 850 °C.

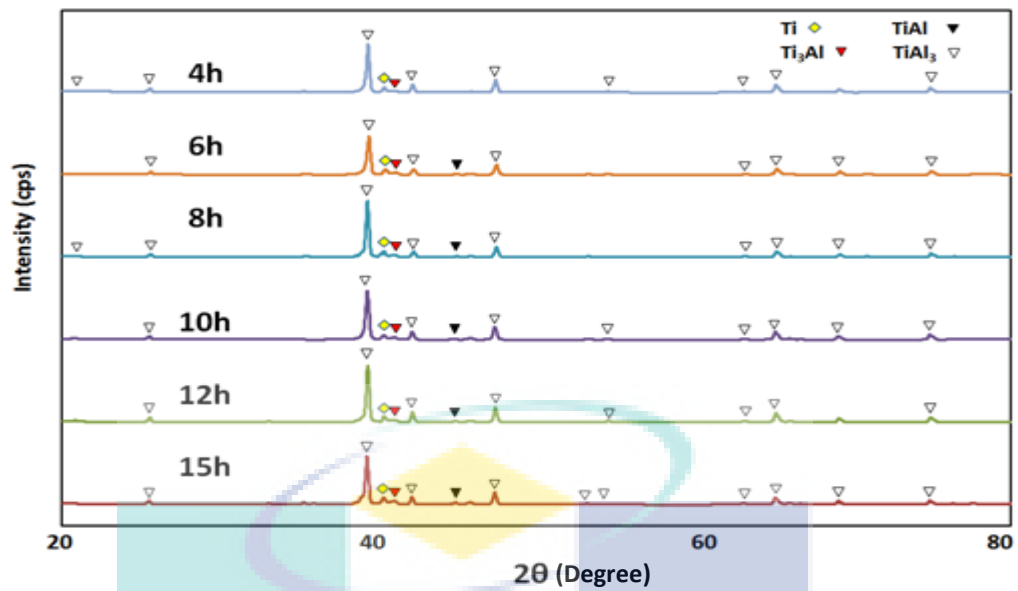


Figure 4.18: X-ray diffractogram for Ti-Al powders milled under *B* (400rpm, 5% wt Hexane, 10:1 bpr) parameter after heating up to 850 °C.

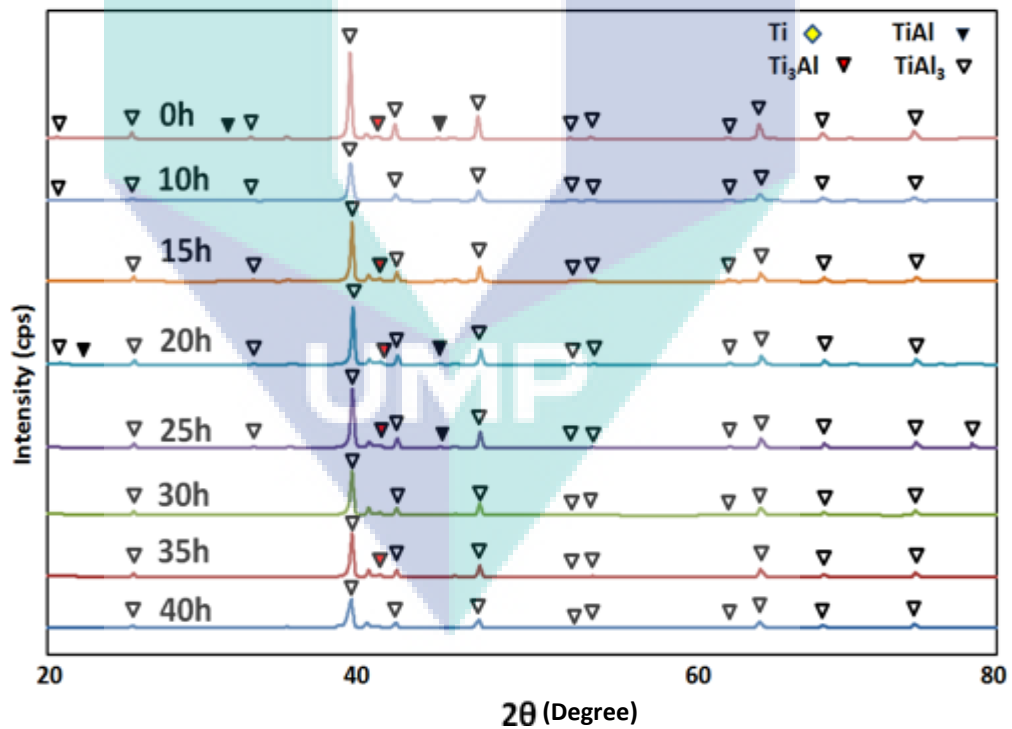


Figure 4.19: X-ray diffractogram for Ti-Al powders milled under *D* parameter (300rpm, 2.5% wt Hexane, 20:1 bpr) after heating up to 850 °C.

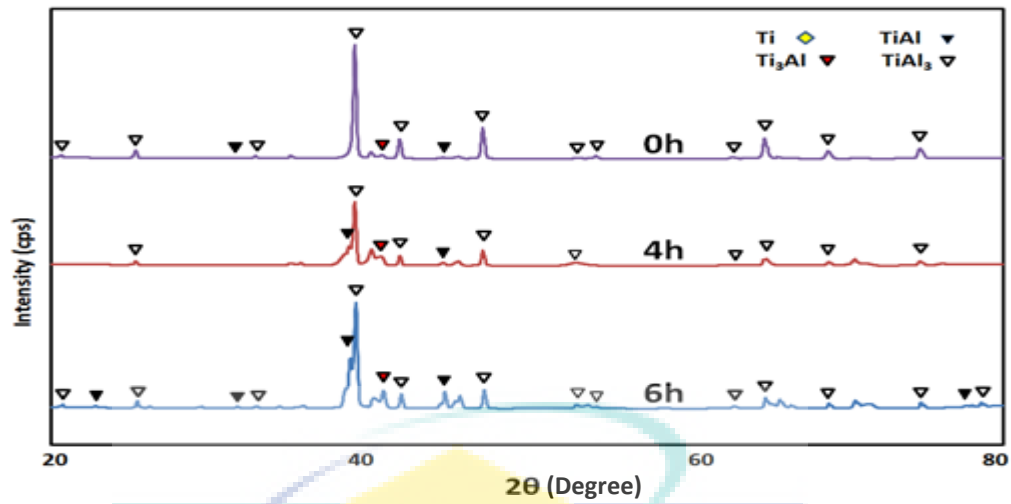


Figure 4.20: X-ray diffractogram for Ti-Al powders milled under *E* parameter (200rpm, without PCA's, 10:1 bpr) after heating up to 850 °C.

Table 4.1: Phase identified in Ti-Al powders after subsequent heat treatment at 850 °C.

Parameters	Milling Duration (h)	Identified Phases
A	4	Major TiAl ₃ + minor TiAl + minor Ti ₃ Al + Ti
	6	Major TiAl ₃ + minor TiAl + minor Ti ₃ Al + Ti
	8	Major TiAl ₃ + minor TiAl + minor Ti ₃ Al + Ti
	10	Major TiAl ₃ + minor TiAl + minor Ti ₃ Al + Ti
	12	Major TiAl ₃ + minor Ti ₃ Al + Ti
	15	Major TiAl ₃ + minor Ti ₃ Al + Ti
B	4	Major TiAl ₃ + minor Ti ₃ Al + Ti
	6	Major TiAl ₃ + minor TiAl + minor Ti ₃ Al + Ti
	8	Major TiAl ₃ + minor TiAl + minor Ti ₃ Al + Ti
	10	Major TiAl ₃ + minor TiAl + minor Ti ₃ Al + Ti
	12	Major TiAl ₃ + minor TiAl + minor Ti ₃ Al + Ti
	15	Major TiAl ₃ + minor TiAl + minor Ti ₃ Al + Ti
D	5	Mixture of TiAl ₃ +Ti ₃ Al
	10	Single phase TiAl ₃ + Ti
	15	Major TiAl ₃ + minor Ti ₃ Al + Ti
	20	Major TiAl ₃ + minor TiAl + minor Ti ₃ Al + Ti
	25	Major TiAl ₃ + minor TiAl + minor Ti ₃ Al + Ti
	30	Single phase TiAl ₃ + Ti
	35	Major TiAl ₃ + minor Ti ₃ Al + Ti
40	Single phase TiAl ₃ + Ti	
E	2	Major TiAl ₃ + minor TiAl + minor Ti ₃ Al + Ti
	4	Major TiAl ₃ + minor TiAl + minor Ti ₃ Al + Ti
	6	Major TiAl ₃ + minor TiAl + minor Ti ₃ Al + Ti

It has been well established that the formation of TiAl_3 or supersaturated $\text{Ti}(\text{Al})$ solid solution, depending on the scale of the Ti-Al diffusion couples and is attributed by the first reaction between Ti and Al in Ti-Al powders (Forouzanmehr et al., 2009). On continuous heating, the reaction between TiAl_3 or $\text{Ti}(\text{Al})$ solid solution and Ti, developed the formation of $\gamma\text{-TiAl}$. On continuous heating, if Ti is still not fully consumed, $\gamma\text{-TiAl}$ will react with Ti to form $\alpha_2\text{-Ti}_3\text{Al}$ (Kim et al., 1991). It was found that under the first heat treatment procedure at $850\text{ }^\circ\text{C}$, the dominant phase obtained from all of the processed samples was TiAl_3 along with residual Ti. This is in a good agreement with the findings of Lagos and Agote (2013). They reported that a treatment at $600\text{ }^\circ\text{C}$ was unable to produce Ti-Al intermetallics as the temperature was below the melting point of Al ($660\text{ }^\circ\text{C}$). However the formation of TiAl_3 are possible under a treatment at $700\text{ }^\circ\text{C}$ with a formation of a balanced mixture between TiAl_3 and residual Ti which is the first reaction of Ti-Al transformation phase. According to them, diffusion of the Al in the Ti particles was very limited and the reaction occurs only in the surface of the Ti particles. This phenomenon is due to the temperature use for the process, which when heated at lower temperature, the elements do not have enough energy for long-range diffusions (Oehring et al., 1993). Sujata et al., 1997 has also reported that TiAl_3 is the first phase to form during reactive sintering between Ti and Al and that by using elemental powders of Ti and Al, leads only to the formation of TiAl_3 phase. Comparing with results from this current research, instead of a formation of TiAl_3 , minor reflection of $\gamma\text{-TiAl}$ and $\alpha_2\text{-Ti}_3\text{Al}$ phase obtained. This is due to the influence of enhanced inter-diffusion between Al and Ti during MA process that lowered the free energy resulted for the early formation of both phases, and higher treatment temperature at $850\text{ }^\circ\text{C}$. According to, Lee et al., 1998 the formation of $\gamma\text{-TiAl}$ and $\alpha_2\text{-Ti}_3\text{Al}$ instead of TiAl_3 are possible by increasing the heating rates above $50\text{ }^\circ\text{C}/\text{min}$. As the heating rate increases, the amount of $\gamma\text{-TiAl}$ and $\alpha_2\text{-Ti}_3\text{Al}$ phases increases too. However, the heating rate in this present study was kept at $10\text{ }^\circ\text{C}/\text{min}$, leaving the enhanced inter-diffusion between Al and Ti during milling, and higher temperature as the reason for the formation of $\gamma\text{-TiAl} + \alpha_2\text{-Ti}_3\text{Al}$ phase.

Generally, titanium aluminide used for structural applications consists of two phases, with $\gamma\text{-TiAl}$ as the base alloys and $\alpha_2\text{-Ti}_3\text{Al}$ distributed in different ways depending on the type of microstructure obtained. As it was unable to obtain the dual phase alloys under 850°C temperature, in the second stage of this study, Ti-Al powder

milled under F and G parameters were annealed under control heating up to 1000°C in Argon condition. The phase identified of the Ti-Al powder after controlled heating at $10^{\circ}\text{C}/\text{min}$ and aging at 1000°C in Argon atmosphere are presented in Table 4.2. The formation of new phases after this 2 h heat treatment scheme shows a huge different and somehow are more complex. The results for Ti-Al powders milled under F parameter shows that during the heat treatment, formation of different phases strongly depended on the duration of milling consist of equilibrium γ -TiAl, $\alpha 2$ -Ti₃Al, TiAl₃ and TiAl₂ phases (Figure 4.21). In the early and intermediate stage of 10 h, 40 h and 60 h, TiAl₂ has dominantly occurred in the powder compound. When the milling process was prolonged to 80 and 100 h the compositions in the powders became more homogeneous and after the exothermic reaction in the thermal process, the powder becomes a dual phase of γ -TiAl and $\alpha 2$ -Ti₃Al phase. On further milling to 120 h, γ -TiAl becomes more dominant than $\alpha 2$ -Ti₃Al with minor reflection of TiAl₃ phase. In the case of TiAl powder milled under G parameters, the heating duration was amplified to 3h. As seen in Figure 4.22, after the thermal annealing, powder milled for 10h exhibits a formation of a dominant TiAl₃ phase, while powder milled for 20 h and 30 h exhibit a formation of a mixture between γ -TiAl, $\alpha 2$ -Ti₃Al and TiAl₃ phase. At longer milling after 40 h, the powder becomes a dominant γ -TiAl along with minor $\alpha 2$ -Ti₃Al phase.

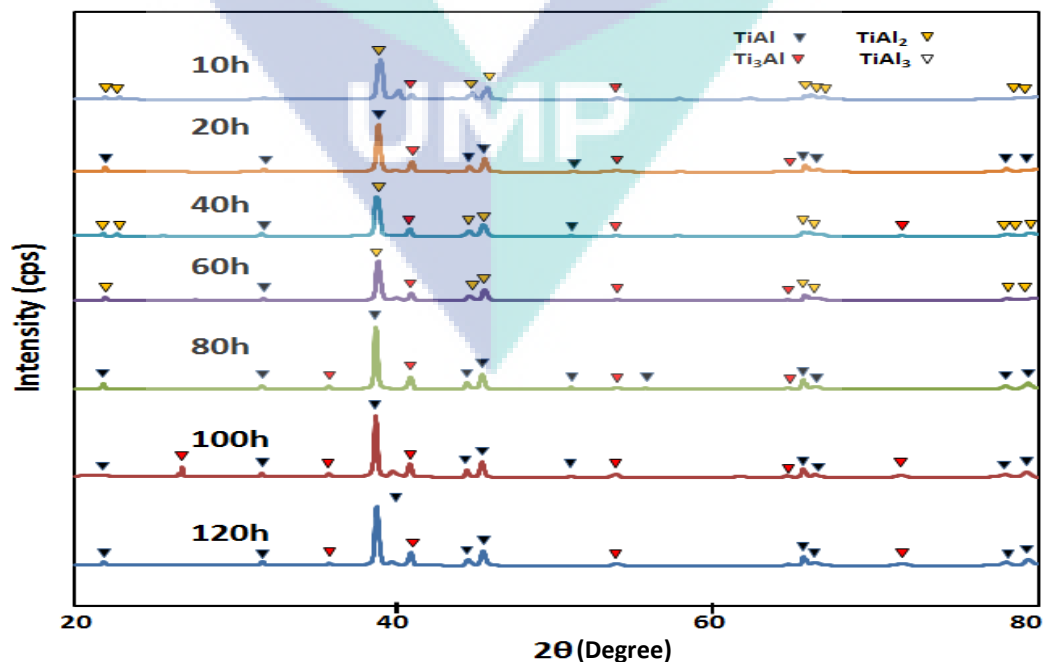


Figure 4.21: X-ray diffractogram for Ti-Al powders milled under F parameter (300rpm, without PCA's, 20:1 bpr) after heating up to 1000°C for 2 h.

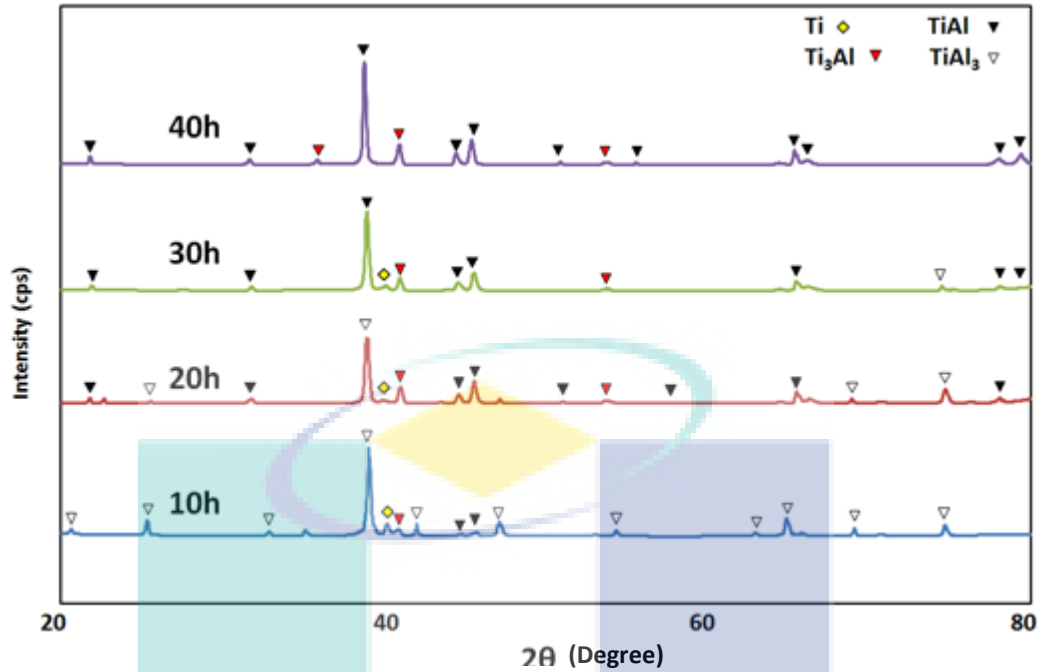


Figure 4.22: X-ray diffractogram for Ti-Al powders milled under *G* parameter (400rpm, without PCA's, 20:1 bpr) after heating up to 1000 °C for 3 h.

Table 4.2: Phase identified in Ti-Al powders after subsequent heat treatment at 1000 °C.

Parameter	Milling Durations (h)	Phase Identified
<i>F</i>	10	Major TiAl ₂ + Ti ₃ Al
	20	Major TiAl + Ti ₃ Al
	40	Major TiAl ₂ + TiAl + Ti ₃ Al
	60	Major TiAl ₂ + TiAl + Ti ₃ Al
	80	Mixture of TiAl + Ti ₃ Al
	100	Mixture of TiAl + Ti ₃ Al
	120	Mixture of TiAl + Ti ₃ Al
<i>G</i>	10	Major TiAl ₃ + TiAl
	20	Mixture of TiAl + TiAl ₃
	30	Mixture of TiAl + TiAl ₃
	40	Major TiAl + Ti ₃ Al

The transformation of Ti-Al powder into Ti-Al inter-metallic phases after the heat treatment was further demonstrate by Energy Dispersive X-ray (EDX) analyses. The perimeter area of the micrograph given in Figure 4.23 indicated that the atomic ratio of

Ti and Al is 1:1, which further confirms the existence of the γ -TiAl grains in the 100 h powder product, which is in a good agreement with the XRD results. Selected area diffraction (SAED) pattern from TEM analysis of this particle is shown in Figure 4.24. It consisted of the spots in lined arrangement, which indicate the formation of single crystallite structure. Comparisons on the lattice parameter indicate that the powder constituent is α 2-Ti₃Al phase which is in good agreement with the phase obtained in XRD result.

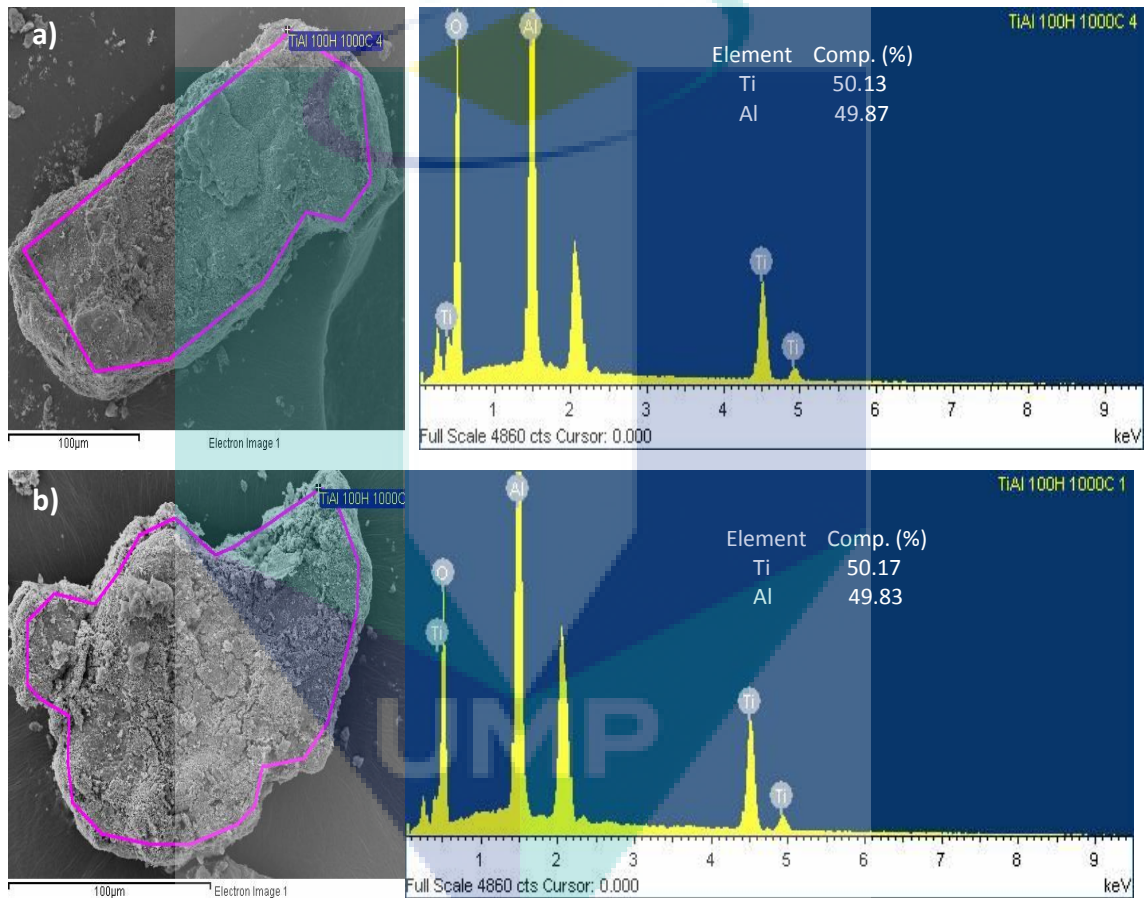


Figure 4.23: FESEM images and EDX spectra of Ti-Al powder milled under F parameter after 100 h of milling

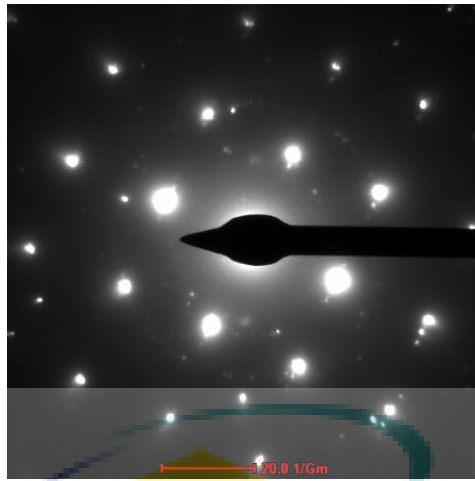


Figure 4.24: SAED pattern from TEM analysis of Ti-Al powder milled under F parameter for 100 h.

The phase formation of mechanically alloyed Ti-Al powders after the heat treatments were strongly dependent on the treatment temperature and MA which resulted in the formation of multiple Ti-Al equilibrium phases. When heated at higher temperature, the elements possessed enough energy for long-range diffusions. It increased the Ti-Al diffusion couples for the second reaction for the formation of γ -TiAl and the third reaction for the formation of α_2 -Ti₃Al. Under a higher treatment temperature of 1100 °C and 1300 °C, Lagos and Agote (2013) reported a formation of a balanced mixture between γ -TiAl and α_2 -Ti₃Al. There were no other phases observed by them. The same findings were reported by Hasegawa and Fukutomi (2009) with a treatment temperature around 1000 °C. Taking into account the fact that the Ti(Al) solid solution is supersaturated and that it is heavily deformed by prolonged milling as shown in Figure 4.5, one can presume that the Ti(Al) lattice is highly distorted due to the presence of dislocations (Suryanarayana, 1995). Therefore, after the thermal process at 1000 °C in this work, variation in powder product obtained consists of multiple equilibrium γ -TiAl, α_2 -Ti₃Al, TiAl₃ and TiAl₂ phases. The formation of TiAl₃ phase is well explained because of the first reaction for the formation of Ti-Al intermetallic phase. However, the formation of dominant TiAl₂ phases is quite unusual. According to Al-Doshan (2005), although TiAl₂ has the lowest free energy of formation, it requires the presence of γ -TiAl as a starting phase, where Al forms oriented precipitates within the γ -TiAl matrix to form TiAl₂. However, from the results obtained, the formation of TiAl₂ occurs at some point of milling under the same heat treatment procedure of this work follows a similar formation of various phase

reaction as proposed by Gupta et al. (2010), from Al-end towards Ti-end of the Ti-Al phase-diagram progresses. In addition, comparing the phase obtained between *F* and *G* samples, with the formation of TiAl_3 and TiAl_2 respectively for both samples, one can presume that the influence of Ti-Al diffusion and deformation during milling are more dominant than the effect of treatment temperature and duration.

4.3.3 Effect of MA on the Crystallite Size

In this work, the modification of micro-structural features is done by refinement of the crystallite size to produce Ti-Al powder in a nano-range size by MA. The crystallite sizes of the milled powders were estimated from X-ray line broadening of the FWHM by using the Scherrer equation. The experimental variables involved are the rotation speed, ball to powder mass ratios, amount of PCAs and milling durations. As the aimed of this study is to produce nano crystallite alloys, comparison were made between those specific factors to the crystallite size refinement. In the preliminary stage of this study, several finding can be drawn in a perspective of the effect of milling parameters by comparing the crystallite size of the powder product before optimal parameter were chosen and further explore in order to obtain the finest size of crystallite. Figure.4.25 shows the relations between the crystallite size and milling duration under different parameters and conditions of MA.

In general, MA has resulted in refinement of crystallite size which is varies depending on the milling parameters and durations. With an addition of Hexane for Ti-Al powders milled under *A*, *B*, *C* and *D* parameters (Table 3.2), the refinement process appears to be progressive in the first 4 h of milling where the crystallite size was reduced from 70.79 nm to around 40 nm. Prolonged milling up to 15 h was found to be ineffective for crystallite refinement where the size only reduced with an average around 33 nm to 38 nm. It is worth to note that, powders milled under *D* parameter with the least addition of Hexane amongst all, exhibit an increase in crystallite size from the minimum size at 32.63 nm after 35h to 44.51 nm after 50 h of milling. Because of the use of PCA, this increased of size could be explained due to the formation of contaminant phases from the reaction between Ti-Al powders and Hexane during milling. According to Bhattacharya et al., 2004, whose studied the effect of PCA on the production of titanium aluminide by

ball milling, it is clear that milling of Ti-Al elemental powders with an addition of PCA led to a significant increase in O concentration, and possibly also to small increases in H, N, and C with a trace of undesirable phase such as TiH_2 , TiC and Ti_2O .

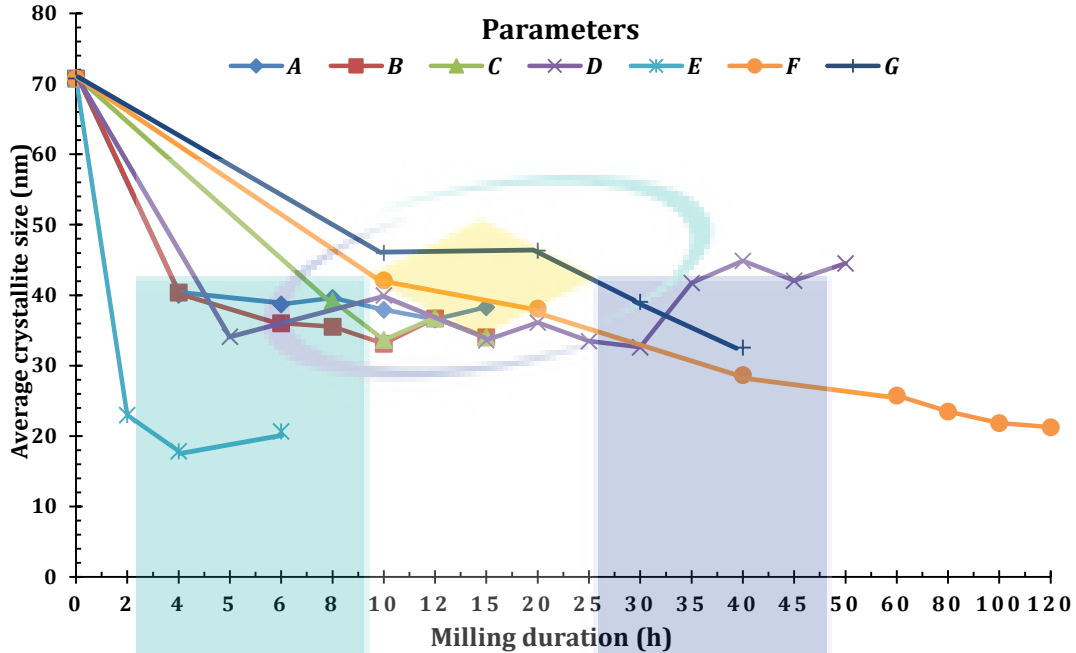


Figure 4.25: Crystallite size evolution of Ti-Al powder milled under different parameters.

Dry milling of Ti-Al powders under *E* parameter shows the most remarkable reduction in crystallite sizes. As shown in Figure 4.24, even after just 2 h of milling, the crystallite size was reduced remarkably from 70.79 nm down to 17.84 nm. This findings are comparable to Bhattacharya et al., (2004) who reported that milling of Ti-Al elemental for 12.5 h resulted in decreased of crystallite size to 7.5 nm. Somehow, as milling under this parameter was problematic with severe sticking of powder to the milling tools, the process was not continued further. This agglomeration problem were also observed by Bhattacharya et al., (2004) which resulted in unproductive result because of very low milling yield. However, dry milling under higher rotation energy which reduced the sticking and agglomeration problem not resulted in the expected crystallite size reduction. After 10 h of milling at 300 rpm and 400 rpm under *F* and *G* parameters respectively, the size only reduced to 42.10 nm and 46.03 nm respectively, which is higher than the powder milled with an addition of Hexane. Because of the crystallite size for powder milled under 300 rpm was slightly smaller than the powder milled under 400 rpm, the milling processes

were continued further until 120 h. At this point, the refinement processes was able to produce crystallite size at 21.29 nm in powder milled under F parameter. As shown in Figure 4.21, the bright-field TEM images of the powder indicate that the particles were cold welded to each other where many small grains can be seen. The sample exhibited an equiaxed microstructure with crystallite sizes typically in the range of 20 - 40 nm which is in a good agreement with the estimation by Schearer equation from XRD results.

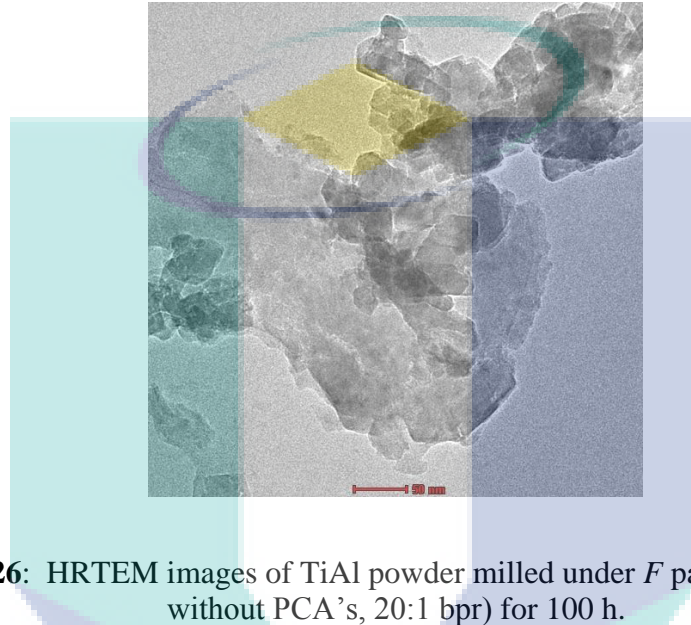


Figure 4.26: HRTEM images of TiAl powder milled under F parameter (300rpm, without PCA's, 20:1 bpr) for 100 h.

Generally, results from this current research concluded that milling parameter plays a vital roles in MA of Ti-Al powders. The use of PCA has retarded the refinement process as partial of the kinetic energy of the impact during milling were absorbed by PCA instead of the powder particles, or the formation of contaminant phase has increased the size of crystallite as propose by Bhattacharya et al., (2004). In addition, milling with higher rotation speed at 400 rpm, leads to a better crystallite refinement compared to milling at slower rotation speed at 300 rpm. By increasing the rotation energy, the number of impact between the ball to the powder and the milling jar was increased resulted in better refinement and smaller crystallite sizes (Suryanarayana, 2001). Observation on the ball to powder mass ratio effect has also shown that powder milled with higher ratio resulted in better refinement on crystallite size. By increasing the ratio, the crystallite size of powder milled with 20:1 ratio was reduced more compared to powder milled with 10:1 ratio. The better refinements are derived from the increased of the surface area for the

balls to powder impact, resulting in multiplication of collisions for improved crystallite refinement (Suryanarayana, 2001).

Even though the effect of rotation speed, the ball to powder mass ratio and the amount of Hexane used on the crystallite size during milling is inter-correlated, somehow the effects are less significant when comparing with the effect of the addition of PCA. Comparison of all milling parameter indicated that dry milling without an addition of PCA is the most effective means in reducing the crystallite size. Therefore, in point of refinement capability, contaminant issues from PCA and with regard of uncomplicated processing, dry milling at a rotation speed of 300 rpm is considered as the most effective condition for crystallite refinement.

4.3.4 Effect of Heat Treatment on Crystallite Size

The estimation on the crystallite sizes of the milled Ti-Al powders after subsequent heat treatment shows a variant in size thus not depending on the crystallite size before annealing. As shown in Figure 4.36 to 4.38, in most cases, considerable grain growth was occurred with an increased in crystallite size. In the initial stage of milling, the crystallite size of Ti-Al powders milled under *A* parameter after annealing at 850°C shows a grain growth with gradual increased up to 6 h milled powders with 57.33 nm in size. With increased milling duration, the size then decreased slowly up to 10 h milled powders (35.14 nm) before a slight increased afterwards up to 15h milled powders (38.53 nm). On the other hand, the crystallite size of Ti-Al powders milled under *B* parameter after similar annealing conditions shows a decreased in crystallite size after 4 h of milling. Somehow, after 6h of milling, the crystallite size shows a sign of growth with 49.11 nm in size. However, prolonged milling has resulted in significant reduction in crystallite size up to 15 h milled powders with 32.68 nm.

In the case of Ti-Al powders milled under *D* parameter, a remarkable reduction in crystallite size was observed in the initial 5 h of milling with 23.13 nm in size. On further milling, a grain growth was occurred with a gradual increase in size up to 42.73 nm milling for 20 h. However, milling for durations greater than 20 h shows a significant reduction in crystallite size with gradual decreased up to 22.45 nm after 40 h of milling which is almost half the size before annealing. Powder milled under *E* parameter also

indicated a grain growth with a crystallite size of 31.96 nm in powder milled for 4 h to a size of 58.04 nm after 6 h of milling.

Controlled aging at 1000°C under Argon atmosphere indicate a different pattern in crystallite size evolution. For powders milled under *F* parameter, a reduction in crystallite size was observed in the initial stage of milling up to 20 h with a size of 32.15 nm. However, milling for durations greater than 20h shows a gradual increased in crystallite size up to 64.52 nm after 80 h of milling. On continuous milling, a remarkable reduction in size was observed up to 30.12 nm after 120 h of milling. On the other hand, Ti-Al powders milled under *G* parameter did not shows any sign of growth. As observed, the crystallite size for this group of sample shows a gradual reduction from 33.69 nm after 10 h of milling, to 23.75 nm after 40 h of milling, which is smaller compared to the size before the heat treatment.

Grain growth of Ti-Al nano powders were reported by Forouzanmehr et al., 2009. Under a thermal load at 900 °C for 30 min, they found that powder with crystallite size of 13 nm after milling for 60 h was increased to 51 nm. Results from this research study follows a similar pattern to report of Murty et al., 2003. They reported that in almost all studies, under a thermal load, nanocrystalline materials cannot be obtained without a sharp increase in crystallite size. This occurs when recovery and recrystallisation are complete and further reduction in the internal energy can only be achieved by reducing the total area of grain boundary. In addition, nano crystalline materials produce by MA is in meta-stable state as intense cold working during milling not only resulted in decreased of crystallite size, but also leads to dramatic increase in dislocation or numbers of point and lattice defects. That fore grain growth of nanostructured Ti-Al powders in this current research was unavoidable.

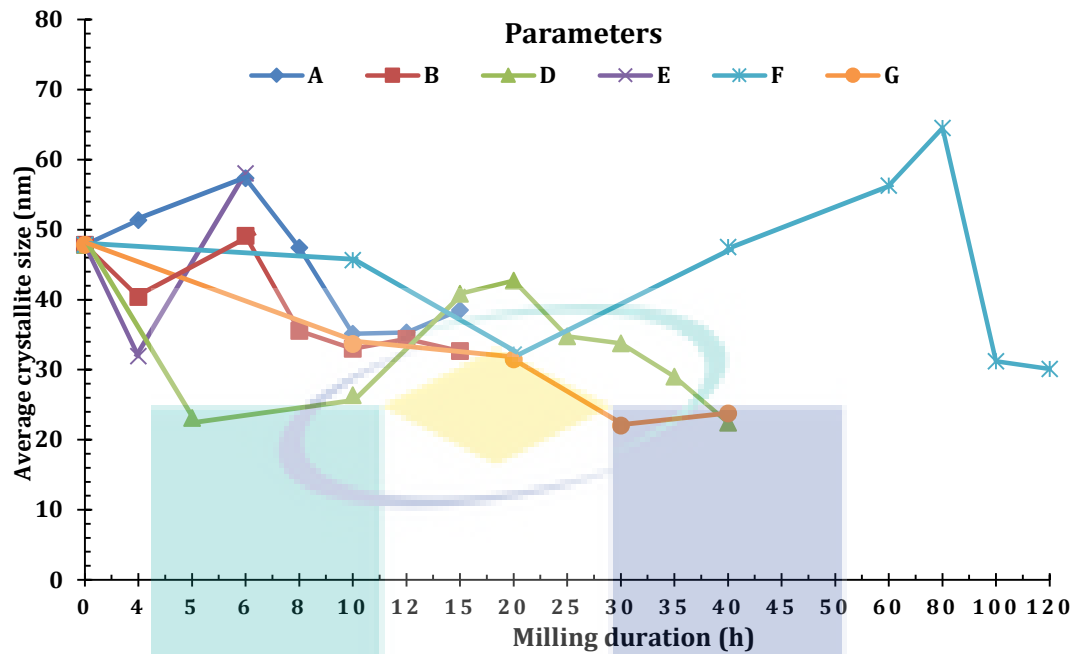


Figure 4.27: Crystallite size evolution after subsequent heat treatment of Ti-Al powder milled under different parameters.

4.3.5 Effect of MA on the Thermal Stability

The coefficient of thermal expansion describes how the size of an object changes with a change in temperature. Specifically, it measures the fractional change in size per degree change in temperature at a constant pressure. The CTE results of the Ti-Al powder sample at a heating rate of 10 °C/min under vacuum atmosphere are evaluated and plotted as a function of temperature. Almost all samples have similar CTE pattern from room temperature up to around 550 °C - 580 °C, at which point they begin to diverge before climb up to a main peak. When the reaction process has completed around 780°C – 830 °C, the CTE curve runs back to the basis line to a final temperature. In some cases, shrinkage was detected, which is due to a change in the atomic structure, known as the curie-point. Data points used for the analysis were automatically calculated by the dilatometer Linseis Data Evaluation software with linear interpolation between them correspond with the average measured CTE values between room temperature to the point where the samples begin to diverge (in this case at around 500 °C). CTE value for the Ti-Al powder is unknown because of the unavailability of literature using powder materials

for this similar method. Anyhow, the result obtained was in a range between the CTE value of Ti ($8.6-10.5 \text{ E}^{-6}/\text{k}$) and Al ($22-24 \text{ E}^{-6}/\text{k}$). As presented in Table 4.3, the CTE values are varies depending on the milling parameters. Ti-Al powders milled under *A*, *B* and *D* parameters which milled for short and intermediate duration with an addition of PCA has a significant decreased pattern of CTE value from high to lower values by milling durations. In comparison, it also shows that the CTE value of the powder product was decreased proportionally with crystallite size. However, powders milled under *E*, *F* and *G* parameters which milled for intermediate and longer duration without PCA, the CTE values were varies and did not shows any significant pattern. Even though the refinement outcomes in these group of samples are more significant, there is no clear inter-correlation between the CTE and crystallite size. The reason is because the degree of diffusion between Ti and Al obtained in these group of samples are higher as discussed in para 4.3.2.

Table 4.3: CTE value (RT to 500 °C) of mechanically alloyed Ti-Al powders.

Milling Duration (h)	CTE (E^{-6}/k) Parameters					
	<i>A</i>	<i>B</i>	<i>D</i>	<i>E</i>	<i>F</i>	<i>G</i>
0			15.3733			
2	-	-	-	-4.186	-	-
4	15.3352	13.4422	-	9.3382	-	-
5	-	-	-	-	-	-
6	15.0575	11.2097	-	8.5545	-	-
8	14.8592	-	-	-	-	-
10	10.5912	9.7146	18.8526	-	22.7724	7.4944
12	9.7585	9.5123	-	-	-	-
15	9.5649	6.5524	18.3375	-	-	-
20	-	-	9.7146	-	21.0079	12.782
25	-	-	6.911	-	-	-
30	-	-	8.0707	-	-	12.8297
35	-	-	7.9269	-	-	-
40	-	-	6.5354	-	37.6237	11.5139
45	-	-	-	-	-	-
50	-	-	-	-	-	-
60	-	-	-	-	26.0462	-
80	-	-	-	-	22.3454	-
100	-	-	-	-	12.2634	-
120	-	-	-	-	20.7688	-

The calculated DTA feature enables in depth view of the thermal behavior of Ti-Al powders product during the dynamic heating. The DTA measurement was generated from the dilatometer results of mathematical routine based on the sample expansion upon heating under specific temperature. However, during the experimental test, more than half of the samples measured were unable to generate DTA data by the software. The DTA peaks appear in all of powders milled under F parameter as presented in Figure 4.41. In the initial to intermediate stage of the heating process, between 70 °C –500 °C temperature ranges, the DTA spectrums indicate an occurrence of gas releases. From that point, the spectrum curve runs back to the basis line before an exothermic peak appeared at a temperature around 670 °C -715 °C. The DTA profile for F samples are presented in Table 4.4.

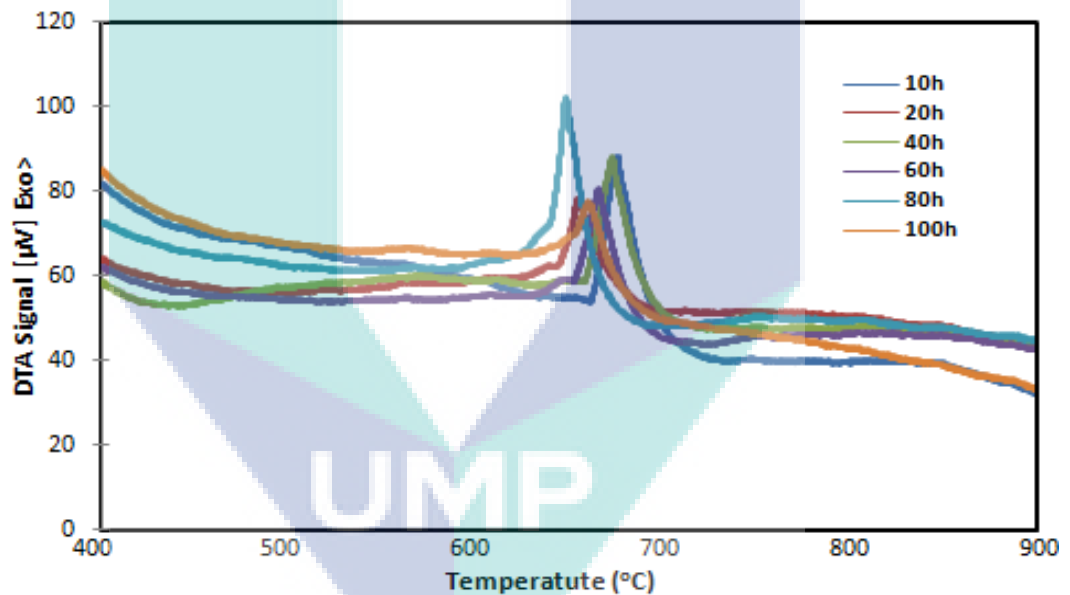


Figure 4.28: Calculated DTA peak thermogram of Ti-Al powders milled under F parameters (300rpm, without PCA's, 20:1 bpr)

The 'onset' temperature corresponds to the melting of the Al phase, where the starting point of diffusion reaction begins, whilst the 'offset' temperature is the point where the diffusion reaction is completed. In addition, the 'point of reaction' temperatures are correlated with the transformation into the equilibrium Ti-Al phases. The reaction temperature decreased significantly below the Al melting point (660°C) after prolonged milling. It has been well established that the formation of $TiAl_3$ or supersaturated Ti(Al)

solid solution depending on the scale of the Ti-Al diffusion couples and was attributed by the first reaction between Ti and Al in Ti-Al powders (Li et al., 2011). From the XRD result, it can be concluded that this exothermic reaction is due to the formation of $TiAl_3$. Since considerable amount of Ti(Al) solid solution achieved during milling, the diffusion barrier between Al and Ti decreased resulting in lower reaction temperature. In addition, the non-existence of endothermic peak indicates that the percentage of pure Al is less at its melting point and can be taken as evidence that it was consumed by the inter diffusion reactions occurring in the course of milling. On the other hand, intense cold working during milling leads to a dramatic increase in the number of point and lattice defects. This also leads to decreasing of the thermodynamic stability of the starting materials (Froes and Suryanarayana, 1989). Apart from that, prolonged milling from this work reduced the crystallite size gradually by milling duration. As reported by Li et al., 2011, mechanical milling of the powders significantly lowered the ignition temperature of the reaction by refining its Ti-Al structure. Therefore it can be concluded that the thermal behavior of Ti-Al powders is highly influenced by crystallite refinement.

Table 4.4: DTA peak data profile for mechanically alloyed Ti-Al powder under F parameter.

Milling Duration	Onset	Offset	Point of Reaction	Max / Min
	Temperature ($^{\circ}C$)			
0	675.80	697.10	678.50	705.2
10	664.60	687.20	669.30	678.70
20	647.50	668.50	652.80	656.60
40	656.80	678.30	665.10	671.00
60	656.10	678.60	663.70	667.80
80	638.90	658.60	648.90	650.20
100	651.30	674.10	657.90	660.50
120	641.50	662.30	647.90	652.80

4.4 PHYSICAL AND MECHANICAL ANALYSES

4.4.1 Effect of MA and heat treatment on density

The density of Ti-Al powder samples was another characteristic measured in this research work. The powder samples were made into a disc and the density were measured

by using Archimedes method in distilled water as displacement medium. The test result for each sample is the average value of at least 5 measurements. In the beginning, density measurement was performed to the initial Ti-Al powder mixture as a control sample. As detailed in Table 4.5, the density value at room temperature were varies, but generally decreased to a lower value than the density of initial powder mixture at 4.09 g/cm^3 and in between the density value of Ti (4.56 g/cm^3) and Al (2.8 g/cm^3). However in the case of powder milled under F parameters, the density values were decreased gradually to 3.5640 g/cm^3 after 120 h of milling. The difference in the density values may attribute by the crystallite size changes estimated from XRD results as the size gradually reduced by milling duration. The relation can clearly be seen in as shown in Figure 4.29. Other factor may also influence the decreased in density is the size of the powder particles. As discussed earlier in Section 4.2, finer and finer particles were obtained by prolonged milling. Such differences in fineness may affected the quality of the consolidated disc samples, as more dense discs were produced from finer powder particles. In turn, the density were decreased too.

F parameter was considered as the optimized parameter for the preparation Ti-Al nano powders; therefore, density measurement was performed to investigate the effect of heat treatment on the density of the powder products. Figure 4.30 shows the differences in densities value of powder milled under F parameter before and after heat treatment. The density of the consolidated specimens was found to be in the range of $3.75\text{--}3.91 \text{ g/cm}^3$. As discussed earlier (Section 4.3.2), the powder compound after the thermal process consists of multiple Ti-Al phases comprises of γ -TiAl, α_2 -Ti₃Al and TiAl₂. Since the density value of γ -TiAl phase is $3.7\text{--}3.9 \text{ g/cm}^3$, α_2 -Ti₃Al phase is $4.1\text{--}4.7 \text{ g/cm}^3$ (Liu et al., 1990) and TiAl₂ have a value in between those other two phases, the density values of the consolidated samples were between the densities of the phases obtained in the powder product as identified in XRD results. It also explained the highest density of powder milled for for 80 and 100 h because of that α_2 -Ti₃Al rich powder. These results is comparable with the findings of Al-Doshan, 2005, where he reported a values of $3.8\text{--}4.0 \text{ g/cm}^3$ for specimen heated at different temperature range between $900\text{--}1200 \text{ }^\circ\text{C}$. Hence, as discussed earlier (Section 4.3.4), grain growth occurs after the thermal processes. However, such increased of crystallite size doesn't seem to have any direct

correlation to the density values. Therefore, the density values after heat treatment are highly influence by the phases obtained.

Table 4.5: Density values of mechanically alloyed Ti-Al powders.

Milling Duration (h)	Density (g/cm ³) Parameters				
	A	C	D	F	F, Heat Treated
0	4.091	4.091	4.091	4.091	3.8333
4	3.7515	-	-	-	-
5	-	-	3.6188	-	-
6	3.7028	-	-	-	-
8	3.7209	3.7064	-	-	-
10	3.7096	3.6038	3.7103	3.8972	3.8195
12	3.7012	3.7097	-	-	-
15	3.7222	3.6551	3.593	-	-
20	-	-	3.6718	3.8512	3.7729
25	-	-	3.6953	-	-
30	-	-	3.5492	-	-
35	-	-	3.7096	-	-
40	-	-	3.7507	3.7749	3.7564
45	-	-	3.7038	-	-
50	-	-	3.7865	-	-
60	-	-	-	3.6617	3.7660
80	-	-	-	3.6321	3.8749
100	-	-	-	3.5952	3.9195
120	-	-	-	3.5640	3.8195

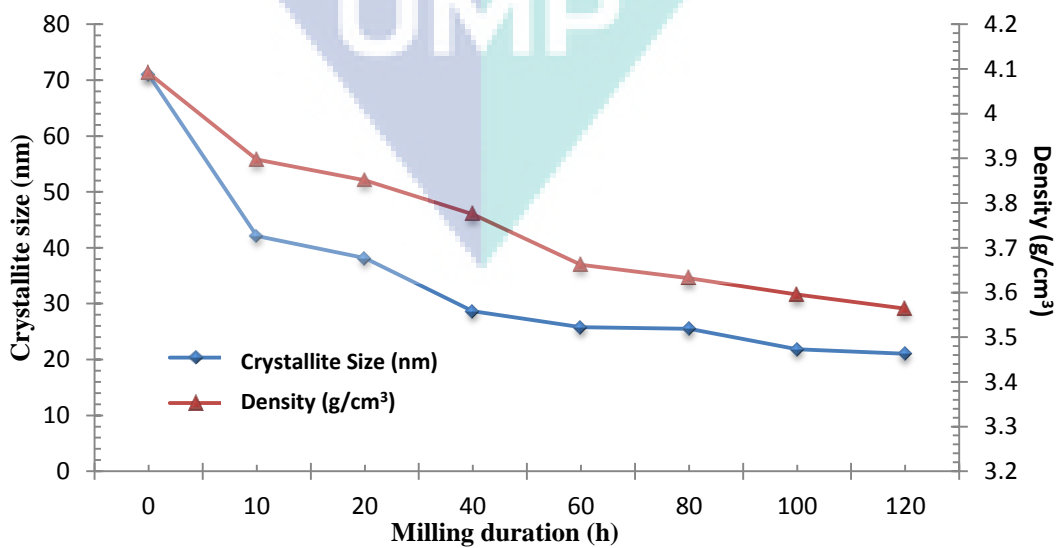


Figure 4.29: Comparison between density value and crystallite size of Ti-Al powders milled under *F* parameter

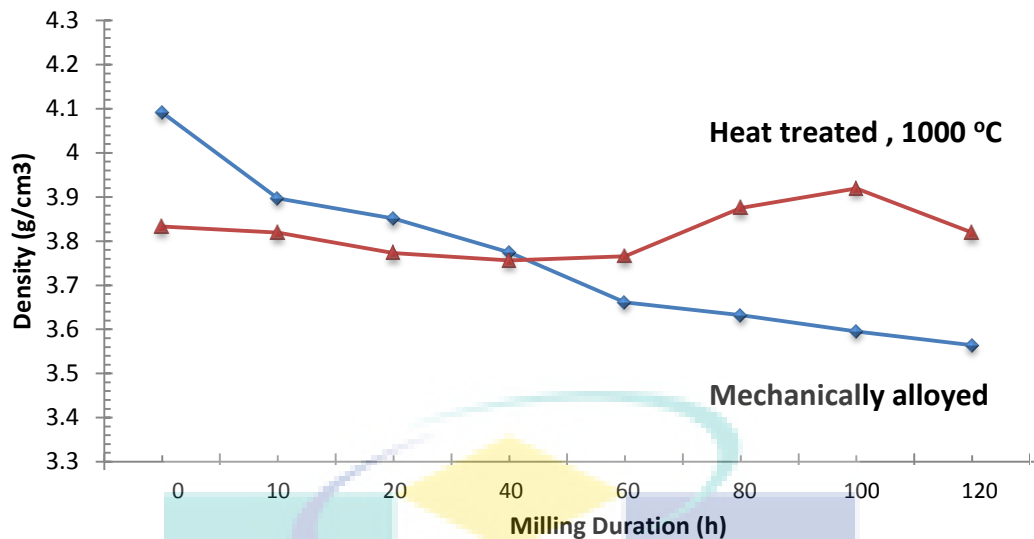


Figure 4.30: Density value for Ti-Al of powders milled under F parameter (300rpm, without PCA's, 20:1 bpr) before and after subsequent heat treatment.

4.4.2 Effect of MA on Micro Hardness

The mechanical properties of metallic materials are influenced by grain boundaries, solute atoms, dislocations, second-phase particles and etc. Dimiduk et al. (1998) has found that the relationship between micro-hardness and yield stress of titanium aluminide alloys is linear, which allows the mechanical properties of titanium aluminide to be envisage from the values of Vickers micro-hardness. Therefore, Vickers micro-hardness test were performed to investigate the effect of MA on the hardness of Ti-Al powder samples from various milling conditions. Vickers micro hardness measurements were performed on selected disc samples of the Ti-Al powders. The test result for each sample is the average value of at least 10 successive indentations.

Hardness measurements were performed to the initial Ti-Al compacted powder as a control sample shows a value of 43.16 HV. As shown in Figure 4.31 the hardness values are plotted as a function of milling durations under specific parameter. It was found that prolonged milling of the Ti-Al powder produces a rapid, almost linear increased in Vickers micro hardness for all samples over that of the starting Ti-Al powder. At the final stage (120 h) of milling under F parameter, the HV value almost 3 times (117.09 HV) higher than the control sample. As predicted, the hardness value was increased with refinement of Ti-Al powders crystallite size. This results is in good agreement with Hall-

Petch law where the yield strength of nano-crystalline materials inversely proportional to its crystallite size. The value obtained from this research work follows a similar trend of findings by Cuevas et al. (2004). Using an attritor-type ball mill with higher composition of Ti of 90%, they found that, by increasing the milling duration, the hardness was also increased and at the final stage, the value is 10 times higher than at the beginning of processing. Since this current work was using lower composition of Ti at 50%, the results obtained are comparable with an increase in hardness 3 times higher than at the beginning of processing. The primary reason for the hardness increase is influenced by grain boundaries as a result of crystallite size refinement after MA. This phenomenon occurs from the crystallite size strengthening mechanism. The average number of dislocations per crystallite decreases with average crystallite size. A lower number of dislocations per crystallite results in a lower dislocation pressure building up at grain boundaries. Since the crystallites were refined by MA, it has a greater total grain boundary area to impede dislocation motion that made it harder.

As discussed earlier in Section 4.3.2, prolonged milling resulted in an increase in the inter-diffusion between Ti and Al atoms to form a Ti(Al) solid solution. This is the other reason which also contributed to the increase in hardness which is due to changes in Ti-Al internal structure or alloying hardening brought about by Ti in metastable Ti(Al) solid solution. According to Cuevas et al., (2004), the dissolution of Al in Ti has a linear correlation with micro-hardness values. For this strengthening mechanism, solute atoms of Al are added to Ti, resulting in either substitutional or interstitial point defects in the crystal. The presence of solute atoms imparts stresses to the lattice, which interfere with nearby dislocations, causing the solute atoms to act as potential barriers. This causes lattice distortions that impede dislocation motion and increase the yield stress that resulted in an increase in hardness. As can be seen in the FESEM images in Section 4.2, the evolution of particle size as repeated fracturing and re-fracturing of particles during milling resulted in refining of the powder particles. Since high-energy milling of Ti-Al particles promotes a dynamic recovery, the full cold worked structure is most likely not retained. This could give rise to repeated sub-grain formation and a final refined structure. This may contribute to the increase in hardness because refinement of the powder particles is associated with a decrease in the mean intermetallic inter-particle distance which always resulted in an increase in hardness. However, Cuevas et al., (2004), indicated that the

evolution of particles size was not proportional to hardness values, leaving the primarily attribute of the increased in hardness by the refinement of Ti-Al powders crystallite size and increased in the inter-diffusion between Ti and Al atoms.

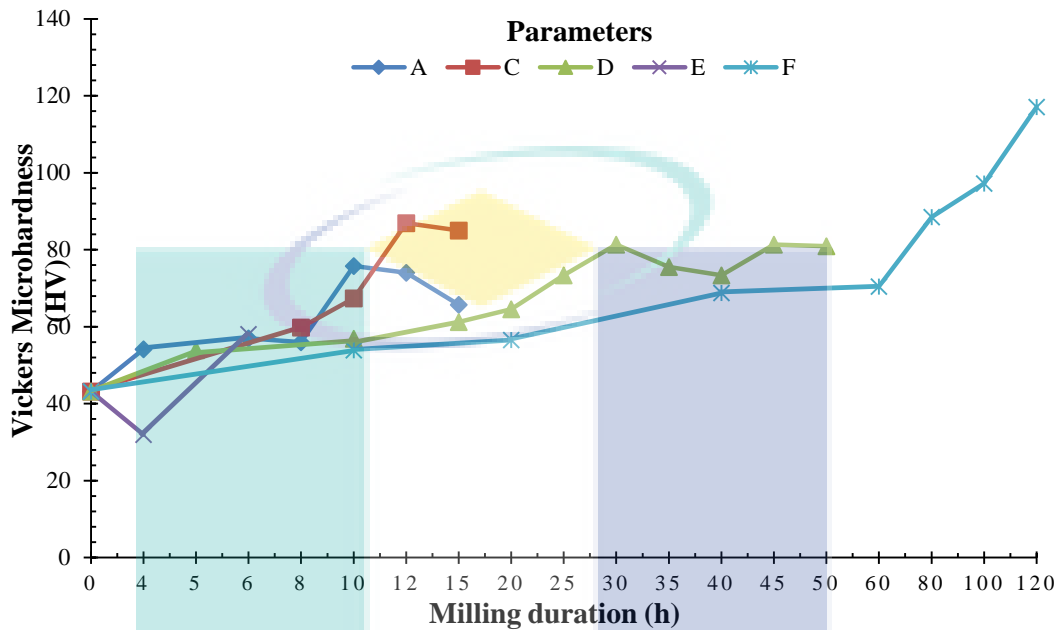


Figure 4.31: Micro-hardness values by milling duration of Ti-Al powders milled under different parameters.

4.5.2 Effect of Heat Treatment on Micro Hardness

From all the previous findings, the Ti-Al powder milled under *F* parameter was considered as the optimized parameter for the preparation Ti-Al nano powders. For that particular reason, Vickers micro hardness test was further explored to investigate the effect of heat treatment on the mechanical properties of the powder product. Figure 4.32 shows the relation between HV values and milling durations for powder milled under *F* parameters before and after annealing process at 1000°C for 2 h. It was observed that, the hardness shows a remarkable increase ranging between 480.3 HV and 622.1 HV. These values are 5 times higher than the values observed for the un-heat treated samples with powder milled for 40 h has the highest value whilst powder milled for 10 h has the lowest value. This nano-crystalline powder exhibits a considerable average hardness value of 544.84 HV which is higher than titanium aluminide samples fabricated using spark plasma sintering (SPS) as reported by Al-Doshan (2005) with an average value of 392.6

HV and Matsugi et al. (1996) at 336-397.7 HV. As shown in the XRD results, the powder constituent after the heat treatment consists of different phases depending on milling duration and treatment. Comparison on the HV value shows that, the micro-hardness obtained after heat treatment was in good agreement and within the micro-hardness range of phases obtained in the powder compound. According to Matsugi et al. (1996) and Wang and Dahms (1992), dual phase γ -TiAl + α 2-Ti₃Al exhibited the highest micro hardness values, while γ -TiAl showed the lowest values and the micro hardness values of titanium rich phase α 2-Ti₃Al were close to the dual phase. It's explained the high hardness obtained in this research since all samples exhibits a formation of dual phase alloys as discussed in Section 4.3.2. Meanwhile the crystallite size after heat treatment shows a slight growth, leaving the primarily attribute of the increased in hardness by the formation of new phase after the thermal process. The presence of TiAl₂ phase occurs in two samples with highest microhardness values, explained the increased of hardness as high as 622.1 HV and 612.1 HV which is comparable with results obtained by Rastkar et al. (2013), whose observed a hardness value of up to 600 HV on the surface layers consisted mainly of TiAl₃ and TiAl₂ compounds. Therefore, by considering their findings, results of this current work were totally influenced by the formation of multiple phases in the powder constituent after the heat treatment processes.

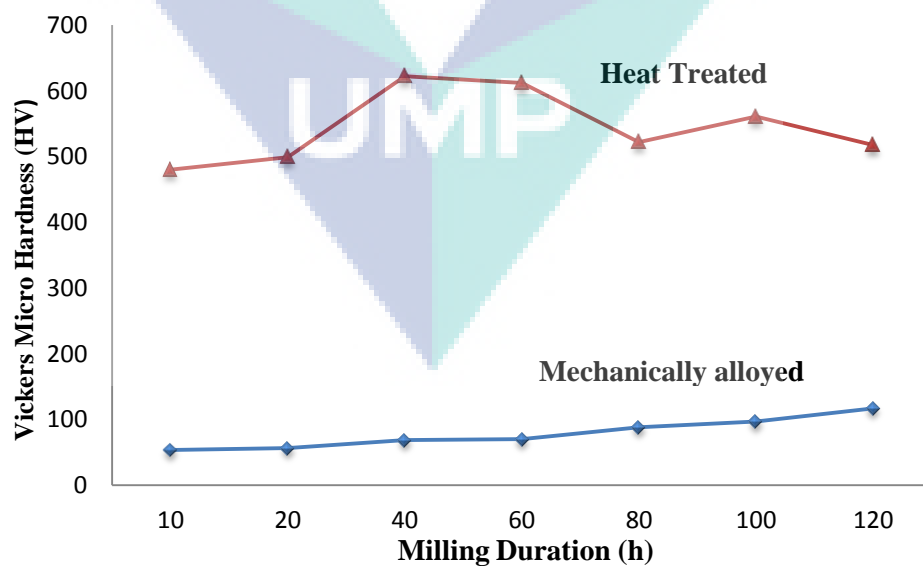
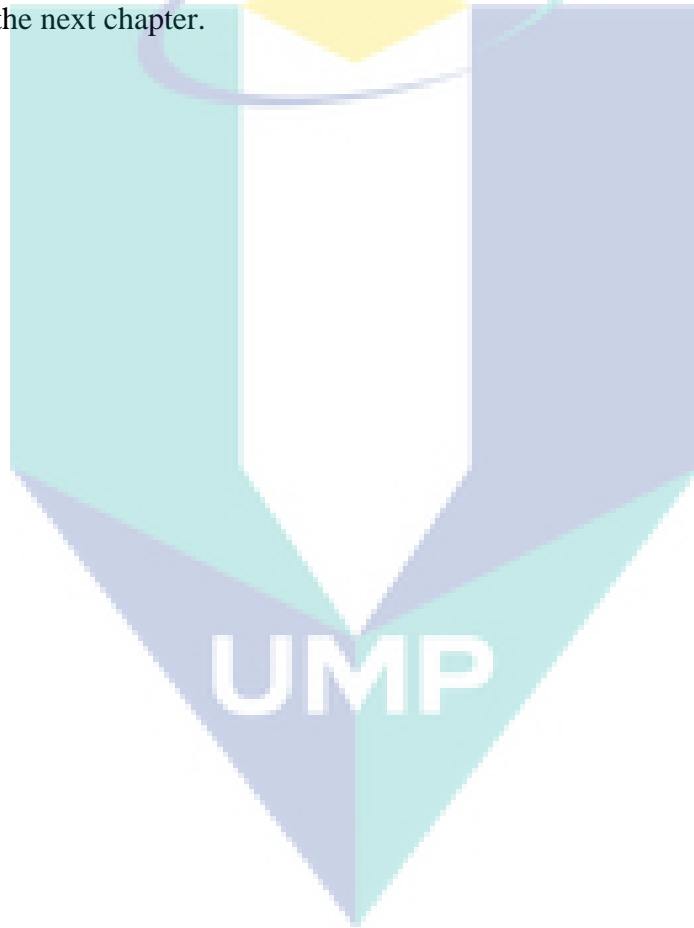


Figure 4.32: Comparison on micro hardness value of Ti-Al powders milled under F parameter (300rpm, without PCA's, 20:1 bpr) before and after heat treatment.

4.6 SUMMARY

This study demonstrated the feasibility of mechanical alloying technique to produce nanostructured Ti-Al powders at room temperature where the characteristics of final product are highly dependent on milling parameters. It is highly noted that reduced in crystallite size in turn decreased the density and hardness of the powder compact significantly. Furthermore, considerable modifications on thermal stability and phase formation alteration were achieved from Ti-Al powders processed by mechanical alloying technique. Conclusions and recommendations of this research work are presented in the next chapter.



CHAPTER 5

CONCLUSIONS AND RECOMMENDATIONS

5.1 CONCLUSIONS

Following are numbers of conclusions drawn from the research findings;

- i. Significant refinement of crystallite size of Ti-Al powder samples from MA process as low as 20 nm achieved. Dry milling at intermediate rotation speed 300 rpm with 20:1 ball to powder weight ratios is the most optimum parameter for Ti-Al powder crystallite refinement that produced Ti(Al) solid solutions.
- ii. MA is a viable technique to alter the phase formation of Ti-Al with the formation of four different Ti-Al phases namely as γ -TiAl, α_2 -Ti₃Al, TiAl₃ and TiAl₂ after the heat treatment process. Regardless of milling parameters, all samples produced a dominant phase of TiAl₃ after subsequent heat treatment at 850°C under vacuum conditions. While controlled heating at 1000°C under Argon atmosphere for 2 to 3h duration resulted in the formation of dominant γ -TiAl, TiAl₂, or a mixture of γ -TiAl + α_2 -Ti₃Al or TiAl₃ phases depending on the milling parameters and durations.
- iii. The thermal stability of mechanically alloyed Ti-Al at a short milling duration resulted in an increased of reaction temperature. On the other hand, the reaction temperature decreased significantly below the Al melting point (660°C) after prolonged milling. The CTE value of the powder product at short milling and intermediate duration decreased proportionally with crystallite size. Somehow at longer milling duration, the value are high and varies.

- iv. The densities of mechanically alloyed Ti-Al powder samples are found to have strong dependence on the crystallite size. The relation between the densities and crystallite size is proportional where the densities values were decreased by refinement of crystallite size. However, after heat treatment, the densities are found to be as low as 3.75g/cm^3 which are determined by the new phases of the powder product obtained.
- v. The mechanical properties of mechanically alloyed Ti-Al powder samples are also regulated by the crystallite size and phases obtained. The micro hardness was found to be inversely proportional to crystallite size throughout the MA process. Somehow, the micro hardness after heat treatment, strongly depend on the phases of the powder product. Hence, its mechanical properties were found as high as 622.17 HV.

5.2 CONTRIBUTION OF THE STUDY

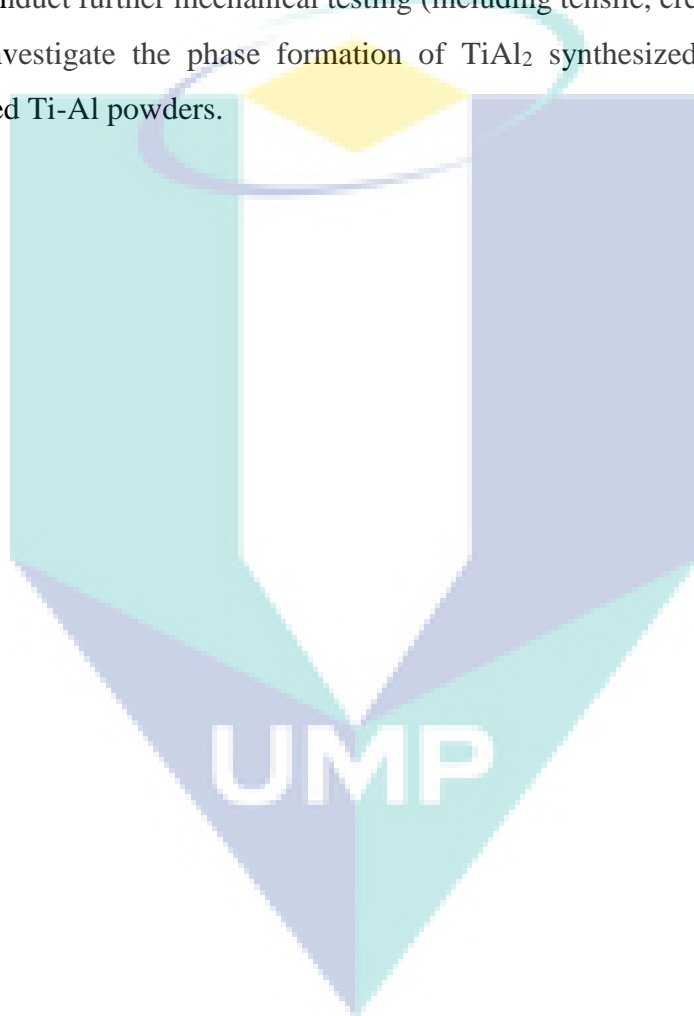
The future of titanium aluminide intermetallics developed from Ti-Al powder metallurgy by MA possess a unique ability in modifying the phase and in turn on the properties of the alloys product. The major contribution of the present study are the findings on the optimization of milling parameter for producing Ti-Al powders to produce nanostructured materials by using Restch PM 100 ball milling equipment. Optimization of milling parameter, not only succeeded in producing nano-structured dual phase of γ -TiAl + α_2 -Ti₃Al alloys, but also the formation of metastable TiAl₂ phase in powder constituent resulted in enhanced mechanical performance of the alloys product.

5.3 RECOMMENDATIONS FOR FUTURE WORK

In the present study, a powder metallurgy has been used to produce titanium aluminide intermetallics. The mechanical properties were found to be significantly dependent on phase and crystallite size. In order to have a broad understanding of the relationship between mechanical alloying processing and the properties of the alloys,

there are some findings from this research that is worth to be explore in order to identify key factors that control the behavior of the alloys;

- i. To produce bulk specimen of nano-structured titanium aluminide-based alloy into fully a dense material.
- ii. To determine the optimal heat-treatment conditions and its influence on the grain growth.
- iii. To conduct further mechanical testing (including tensile, creep and fatigue test)
- iv. To investigate the phase formation of $TiAl_2$ synthesized from mechanically alloyed Ti-Al powders.



REFERENCES

- Al-Dabbagh, J.B., Ishak, M., Tahar, R.M. and Harun, S.A. 2013. Effect of the milling parameters on the characteristics of Ti-50%al nanocrystallite synthesized by MA. *International Journal of Engineering Research and Technology*. **2**(8): 2113-2119.
- Al-Doshan A.A. 2005. *Spark plasma sintering of titanium aluminide intermetallics and its composites*. MSc. Thesis. King Saud University, Riyadh, Saudi Arabia.
- Appel, F. David, J. Paul, H. and Oehring, M. 2011. *Gamma Titanium Aluminide Alloys: Science and Technology*. Germany: Wiley-VCH Verlag GmbH.
- Appel, F. Oehring, M., Paul, J.D.H., Klinkenberg, C.H. and Carneiro, T. 2004. Physical aspects of hot-working gamma-based titanium aluminide. *Intermetallics*. **12**(7-9): 791-802.
- Appel, F. Brossmann, U. Christoph, U. Eggert, S. Janschek, P. Lorenz, U. Müllauer, J. Oehring, M. and Paul, J. D. H. 2000. Recent progress in the development of gamma titanium aluminide alloys. *Advanced Engineering Materials*. **2**(11): 699-720.
- Bartolotta, P.A. and Krause, D.A. 1999. Titanium aluminide applications in the high speed civil transport. Technical Memorandum. NASA Glenn Research Centre, Cleveland, Ohio, USA. NASA/TM 1999-209071.
- Benjamin, J.S. 1992. Fundamentals of mechanical alloying. *Materials Sciences Forum*. **88-90**: 1-18.
- Benhaddad, S., Bhan, S. and Rahmat, A. 1997. Effect of ball milling time on Ti-Al and Ni-Al powder mixtures. *Journal of Materials Science Letters*. **16**: 855-857.
- Benjamin, J.S. 1990. Mechanical alloying - A perspective. *Metal Powder Report*. **45**(2): 122-127.
- Beschliesser, M., Clemens, H., Kestler, H. and Jeglitsch, F. 2003. Phase stability of a γ -TiAl based alloy upon annealing: comparison between experiment and thermodynamic calculations. *Scripta Materialia*. **49**(4): 279-284.
- Bhattacharya, P. Bellon, P. Averback, R.S. and Hales, S.J. 2004. Nanocrystalline TiAl powders synthesized by high-energy ball milling: Effects of milling parameters on yield and contamination. *Journal of Alloys and Compounds*. **368**(1-2): 187-196
- Bird, K., Wallace, T.A. and Sankaran, N.S. 2004. Development of protective coatings for high-temperature metallic materials. *Journal of Spacecraft and Rockets*. **41**(2): 213-220.

- Cahn, R.W., Haasen, P. and Kramer, E.J. 1991. *Processing of metals and alloys*. Materials science and technology - A comprehensive treatment. **15**. Germany: Wiley-VCH.
- Chraponski, J., Szkliniarz, W., Koscielna, W. and Serek, B. 2003. Microstructure and chemical composition of phases in Ti-48Al-2Cr-2Nb intermetallic alloy. *Material Chemistry and Physics*. **81**(2-3): 438-442.
- Clemens, H. and Kestler, H. 2000. Processing and applications of intermetallic γ -titanium aluminide based alloys. *Advanced Engineering Materials*. **2**(9): 551-570.
- Courtney, T.H. and Maurice, D.R. 1989. Solid state powder processing. *Proceedings of the 9th International Symposium on Metallurgy and Materials Science*, pp. 35-40.
- Cuevas, F. G., Cintas, J., Montes, J. M. and Gallardo, J. M. 2004. Al-Ti powder produced through mechanical alloying for different times. *Journal of Materials Science*. **41**: 8339-8346.
- Dimiduk, D.M., Hazzledine, P.M., Parthasarathy, T.A., Seshagiri, S. and Mendiratta, M.G. 1998. The role of grain size and selected microstructural parameters in strengthening fully lamellar TiAl alloys. *Metallurgical and Materials Transactions A*. **29**(1): 37-47.
- Donachie, M.J. and Donachie, S.J. 2002. *Super Alloys - A Technical Guide*. 2nd ed. USA: ASM International.
- Draper, S.L., Krause, D., Lerch, B., Locci, I.E., Doehnert, B., Nigam, R., Das, G., Sickles, P., Tabernig, B., Reger, N. and Rissbacher, K. 2007. Development and evaluation of TiAl sheet structures for hypersonic applications. *Materials Science and Engineering: A*. **464**(1-2): 330-342.
- El-Eskandarany, M.S. 2013. *Mechanical Alloying: For Fabrication of Advanced Engineering Materials*. USA: Univ. Press of Mississippi.
- Fadeeva, V.I., Leonov, A.V., Szewczak, E. and Matyja, H. 1998. Structural defects and thermal stability of Ti(Al) solid solution obtained by mechanical alloying. *Materials Science and Engineering A*. **242**(1998): 230-234.
- Farhang M.R., Kamali, A.R. and Samani M.N. 2010. Effects of mechanical alloying on the characteristics of a nano-crystalline Ti-50at.%Al during hot pressing consolidation. *Materials Science and Engineering B*. **168**(1): 136-141.
- Fecht, H.J. 1995. Nanophase materials by mechanical attrition: Synthesis and characterization. *Nanophased Materials*. **260**: 125-144.
- Fecht, H.J., Hellstern, E., Fu, Z. and Johnson W.L. 1990. Nanocrystalline metals prepared by high-energy ball milling. *Metallurgical Transactions A*. **21**(9): 2333-2337.

- Forouzanmehr, N., Karimzadeh, F. and Enayati, M.H. 2009. Study on solid-state reactions of nano-crystalline TiAl synthesized by MA. *Journal of Alloys and Compounds*. **471**(1): 93-97.
- Froes, F.H. and Suryanarayana, C. 1996. *Physical metallurgy and processing of intermetallic compounds*. Stoloff, N.S. and Sikka, V.K. Titanium aluminide. New York: Chapman and Hall.
- Froes, F. H. and Suryanarayana, C. 1989. Nano-crystallines metals for structural application. *Journal of Metals*. **41**(6): 12-17.
- Gabbitas, B., Cao, P., Raynova, S. and Zhang, D. 2012. Microstructural evolution during mechanical milling of Ti/Al powder mixture and production of intermetallic TiAl cathode target. *Journal of Materials Science*. **47**(3): 1234-1242.
- Gaffet, E., Abdellaoui, M. and Malhourox-Gaffet, N. 1995. Formation of nanostructured materials induced by mechanical processing. *Materials Transaction*. **36**(2): 198-209.
- Gerasimov, K.B. and Pavlov, S.V. 1996. Metastable Ti-Al phases obtained by MA. *Journal of Alloys and Compounds*. **242**(1): 136-142
- Gleiter, H. 1989. Nanocrystalline materials. *Progress in Materials Science*. **33**(4): 223-315.
- Gonzalez, G., Sagarzazu, A., Bonyuet, D., D'Angelo, L. and Villalba, R. 2009. Solid state amorphisation in binary systems prepared by mechanical alloying. *Journal of Alloys and Compounds*. **483**(2009): 289–297.
- Guo, W., Martelli, S., Burgio, N., Magini, M., Padella, S., Paradiso, E. and Soletta, I. 1991. Mechanical alloying of Ti-Al system. *Journal of Materials Science*. **26**(22): 6190-6196.
- Gupta, R.K., Pant, B., Agarwala, V., Agarwala, R.C. and Sinha, P.P. 2010. Effect of pressure and temperature on phase transformation and properties of titanium aluminide obtained through reaction synthesis. *Journal of Materials Sciences and Technology*. **26**(8): 693-704.
- Hall E.O. 1951. The deformation and aging of mild steel: III Discussion of results. *Proceeding of Physical Society: B*. **64**(9): 747-753.
- Hao, Y.L., Yang, R., Cui, Y.Y. and Li, D. 2000. The influence of alloying on the $\alpha/\alpha+\gamma/\gamma$ phase boundaries in TiAl based systems. *Acta Materialia*. **48**(6): 1313–1324.
- Hasegawa, M. and Fukutomi, H. 2009. Lamellar orientation control in TiAl base alloy by two-step compression process at high temperatures. *Materials Science and Engineering A*. **508**(5): 106-113.

- Itsukaichi, T., Masuyama, K., Umemoto, M., Okane, I. and Cabanas-Moreno, J.G. 1993. Mechanical alloying of Ti-Al system. *Journal of Materials Research*. **8**: 1817.
- James, A.M. and Lord, M.P. 1992. *Macmillan's Chemical and Physical Data*. London: Macmillan.
- Kadkhodapour, J., Ziaei-Rad, S. and Karimzadeh, F. 2009. Finite-element modeling of rate dependent mechanical properties in nanocrystalline materials. *Computational Materials Science*. **45**(4): 1113-1124.
- Karadge, M. and Gouma, P. I. 2004. Metastable phase formation during $\alpha_2(D0_{19})$ to $\gamma(L_{10})$ transformation in as-atomized γ -TiAl alloy powders. *Applied Physics Letters*. **85**(21): 4914-4916.
- Khosroshahi, R.A, Ahmadi, N.P. and Samadzadeh, S. 2008. Effect of silicon on nanostructured TiAl(γ) formation kinetic via mechanical alloying method. *Journal of Applied Sciences*. **8**(20): 3727-3732.
- Kim, Y.W. 1995a. Gamma titanium aluminide: Their status and future. *The Journal of the Minerals, Metals & Materials Society*. **47**(7): 39-42.
- Kim, Y.W. 1995b. Effects of microstructure on the deformation and fracture of γ -TiAl alloys. *Materials Science and Engineering: A*. **192-193**(2): 519-533.
- Kim, Y.W. 1994. Ordered intermetallic alloys, Part III: Gamma titanium aluminide. *The Journal of the Minerals, Metals & Materials Society*. **46**(7): 30-39.
- Kim, Y.W. 1992. Microstructural evolution and mechanical properties of a forged gamma titanium aluminide alloy. *Acta Metallurgica et Materialia*. **40**(6): 1121-1134.
- Kim, Y.W. and Dimiduk, D.M. 1991. Progress in the understanding of gamma titanium aluminide. *The Journal of the Minerals, Metals & Materials Society*. **43**(8): 40-47.
- Kim, Y.W. 1989. Intermetallic alloys based on gamma titanium aluminide. *The Journal of the Minerals, Metals & Materials Society*. **41**(7): 24-30.
- Klaus, G. 2006. Performance, tolerance and cost of TiAl passenger car valves. *Intermetallics*. **14**(4): 355-360.
- Koch, C.C. 1997. Synthesis of nanostructured materials by mechanical milling: problems and opportunities. *Nanostructured Materials*. **9**(1-8): 13-22.
- Koch, C. C. 1993. The synthesis and structure of nanocrystalline materials produced by mechanical attrition: A review. *Nanostructured Materials*. **2**(2): 109-129.
- Kothari, K., Ramachandran, R. and Wereley, N.M. 2012. Advances in gamma TiAl and their manufacturing techniques. *Progress in Aerospace Sciences*. **55**: 1-16.

- Lagos, M.A. and Agote, I. 2013. SPS synthesis and consolidation of TiAl alloys from elemental powders: Microstructure evolution. *Intermetallics*. **36**: 51-56.
- Lee, C. H., 1998. The effect of reactive sintering rate on the reactive sintering of Ti-48%Al elemental powder mixture. *Journal of Materials Science Letters*. **17**(16): 1367-1370.
- Leyens, C. and Peters, M. 2003. *Titanium and titanium alloys*. Germany: Willey-VCH.
- Li, S., Sun, H., Fang, W. and Ding, Y. 2011. Structure and morphology of Ti-Al composite powders treated by mechanical alloying. *Trans. Nonferrous Metallic Society China*. **21**(2011): 338-341.
- Lipsitt, H.A. 1985. Titanium aluminide - An Overview. *Materials Resource Society Proceedings*, pp. **39**:351-364.
- Liu, C.T. and Stiegler, J. 2002. *Properties and Selection: Nonferrous Alloys and Special Purpose Materials*. ASM Handbook, 2. USA: ASM International.
- Liu, C.T., Stiegler, J. and Froes, F.H. 1990. *Properties and Selection: Nonferrous Alloys and Special Purpose Materials*. ASM Handbook, 2. USA: ASM International.
- Matsugi, K., Ishibashi, N., Hatayama, T. and Yanagisawa, O. 1996. Microstructure of spark sintered titanium-aluminide compacts. *Intermetallics*. **4**(6): 457-467.
- Maki, K., Ehira, A., Sayashi, M., Sasaki, T., Noda, T., Okabe, M. and Isobe, S. 1996. Development of high-performance TiAl exhaust valve. *SAE International Journal of Engines*. **8**(3):117-125.
- Meyers, M.A., Mishra, A. and Benson, D.J. 2006. Mechanical properties of nanocrystalline materials. *Progress in Materials Science*. **51**(4): 427-556.
- Moll, J.H. and McTiernan, B.J. 2000. PM TiAl alloys: the sky's the limit. *Metal Powder Report*. **55**(1): 18-22.
- Mote, V.D., Purushotham, Y. and Dole, B.N. 2012. Williamson-Hall analysis in estimation of lattice strain in nanometer-sized ZnO particles. *Journal of Theoretical and Applied Physics*. **6**(6): 1-8.
- Murty, B. S., Datta, M. K. and Pabi, S. K. 2003. Structure and thermal stability of nanocrystalline materials. *Sadhana Academy Proceeding in Engineering Sciences*, pp. 23-45.
- NASA. 2003. *PM gamma titanium aluminide and fabrication techniques*. Technical Support Package. NASA Technical Brief. LEW 17173. Ohio: USA.
- Norris, G. Power House. 2006 (online)
<http://www.flightglobal.com/news/articles/power-house-207148/.html> (13 June 2011)

- Oehring, M., Klassen, T. and Bormann, R. 1993. The formation of metastable Ti-Al solid solutions by MA and ball milling. *Journal of Material Research*. **8**(11): 2819-2829
- Petch, N.J. 1953. The cleavage strength of polycrystals. *Journal of Iron Steel Institute*. **174**: 25-28.
- Ramanujan, R.V. 2000. Phase transformations in gamma based titanium aluminide. *International Materials Reviews*. **45**(6): 217-240.
- Rastkar, A.R., Parseh, P., Darvishnia, N. and Hadavi, S.M.M. 2013. Microstructural evolution and hardness of TiAl₃ and TiAl₂ phases on Ti-45Al-2Nb-2Mn-1B by plasma pack aluminizing. *Applied Surface Science*. **276**: 112-119.
- Recina, V. 2000. *Mechanical properties of gamma titanium aluminide*. Ph.D. Thesis. Chalmers University of Technology, Sweden.
- Roco, M.C. 2011. The long view of nanotechnology development: the National Nanotechnology Initiative at 10 years. *Journal of Nano-particles Research*. **13**(2):427-445.
- Sarkar, S. Datta, S., Das, S. and Basu, D. 2009. Oxidation protection of gamma-titanium aluminide using glass-ceramic coatings. *Surface and Coatings Technology*. **203**(13): 1797-1805.
- Scherrer, P. 1918. Determination of the size and the internal structure of colloidal particles by X-ray. *News of the Society of Sciences in Mathematics and Physics Class*, pp. 98-100.
- Sujata, M., Bhargava, S. and Sangal, S. 1997. On the formation of TiAl₃ during reaction between solid Ti and liquid Al. *Journal of Materials Science Letters*. **16**(14): 1175-1178.
- Suryanarayana, C. 2012. Mechanical behavior of emerging materials. *Materials Today*. **15**(11): 486-498.
- Suryanarayana, C. 2008. Recent developments in mechanical alloying. *Rev. Advanced Materials Sciences*. **18**(3): 203-211.
- Suryanarayana, C. 2001. Mechanical alloying and milling. *Progress in Materials Science*. **46**(1-2): 1-184.
- Suryanarayana, C. and Koch, C.C. 2000. Nanocrystalline materials – Current research and future directions. *Hyperfine Interactions*. **130**(1-4): 5-44.
- Suryanarayana, C. 1995. Does a disordered γ -Titanium aluminide phase exist in mechanically alloyed Ti-Al powders?. *Intermetallics*. **3**(2): 153-160.
- Suryanarayana, C., Sundaresan, R. and Froes, F.H. 1992. TiAl formation by mechanical alloying. *Materials Science and Engineering: A*. **150**(1): 117-121.

- Suzuki, T. and Nagumo, M. 1992. Mechanochemical reaction of TiAl with hydrocarbon during mechanical alloying. *Scripta Metallurgica et Materialia*. **27**(10): 1413-1418.
- Szewczak, E. and Wyrzykowski, J.W. 1999. Influence of the MA parameters on crystallite size of Ti–Al powders. *Nanostructured Materials*. **12**(1-4): 171-174.
- Takasaki, A. and Furuya, Y. 1999. Mechanical alloying of the ti-al system in atmosphere of hydrogen and argon. *NanoStructured Materials*. **11**(8). 1205–1217.
- Tetsui, T. 1999. Gamma Ti aluminide for non-aerospace applications. *Current Opinion in Solid State and Materials Science*. **4**(3): 243-248
- Voice, W.E., Henderson, M., Shelton, E. and Wu, X. 2005. Gamma titanium aluminide, TNB. *Intermetallics*. **13**(9): 959-964.
- Vyas, A., Rao, K.P. and Prasad, Y.V.R.K. 2009. Mechanical alloying characteristics and thermal stability of Ti–Al–Si and Ti–Al–Si–C powders. *Journal of Alloys and Compounds*. **475**(1-2): 252-260.
- Wendler, B.G. and Kaczmarek, L. 2005. Oxidation resistance of nano-crystalline microalloyed TiAl coatings under isothermal conditions and thermal fatigue. *Journal of Materials Processing Technology*. **164-165**: 947-953.
- Wang, G. and Dahms, M. 1992. Influence of heat treatment on microstructure of Ti-35wt.%Al prepared by elemental powder metallurgy. *Scripta Metallurgica et Materialia*. **26**(5): 717–722.
- Wu, X. 2006. Review of alloys and process development of Titanium aluminide Alloys. *Intermetallics*. **14**(10-11): 1114-1122.
- Xiao, S., Tian, J., Xu, L., Chen, Y., Yu, H. and Han, J. 2009. Microstructures and mechanical properties of TiAl alloy prepared by spark plasma sintering. *Transactions of Nonferrous Metals Society of China*. **19**(6): 1423-1427.
- Yamaguchi, M., Inui, H. and Ito, K. 2000. High-temperature structural intermetallics. *Acta Materilia*. **48**(1): 307-322.
- Yu, H.B., Zhang, D.L., Chen, Y.Y., Cao, P. and Gabbitas, B. 2009. Synthesis of an ultrafine grained TiAl based alloy by subzero temperature milling and HIP, its microstructure and mechanical properties. *Journal of Alloys and Compounds*. **474** (2009): 105–112.
- Zhao, L., Beddoes, J., Au, P. and Wallace, W. 1997. Evaluations of P/M gamma titanium aluminide. *Advanced Performance Materials*. **4**(4): 421-434.

APPENDIX A

LIST OF PUBLICATIONS

- Al-Dabbagh, J.B., Tahar, R.M., Ishak, M. and Harun, S.A. 2015. Structural and phase formation of TiAl alloys synthesized by mechanical alloying and heat treatment. *International Journal of Nanoelectronics and Materials*. **8**(1): 23-32.
- Al-Dabbagh, J.B., Ishak, M., Tahar, R.M. and Harun, S.A. 2014. Synthesis and characterization of nano Ti-50%Al by mechanical alloying. *Design and Computation of Modern Engineering Materials*. Switzerland: Springer International Publishing.
- Al-Dabbagh, J.B., Tahar, R.M., Ishak, M. and Harun, S.A. 2013. Effect of the milling parameters on the characteristics of Ti-50%Al nanocrystallite synthesized by MA. *International Journal of Engineering Research and Technology*. **2**(8): 2113-2119.

LIST OF PROCEEDINGS

- Al-Dabbagh, J.B., Tahar, R.M., Ishak, M. and Harun, S.A. 2014. Effect of the milling parameters on the characteristics of Ti-50%Al nanocrystallite synthesized by mechanical alloying. *International Conference on Materials Science and Engineering*. Dubai, UAE: 30-31 January.
- Al-Dabbagh, J.B., Ishak, M., Tahar, R.M. and Harun, S.A. 2013. Synthesis and characterization of nano Ti-50%Al by MA. *7th International Conference on Advanced Computational Engineering and Experimenting, (ACE-X)*. Madrid, Spain. 01-04 July.
- Al-Dabbagh, J.B., Tahar, R.M., Ishak, M. and Harun, S.A. 2013. Structural and phase formation of titanium aluminide alloys synthesized by MA and heat treatment. *Joint International Conference on Nanoscience, Engineering and Management (BOND 21)*. Penang, Malaysia: 19-21 August.
- Al-Dabbagh, J.B., Ishak, M., Tahar, R.M. and Harun, S.A. 2013. Phase Formation and Thermal Properties of TiAl Alloys Synthesized by Mechanical Alloying. 2013. *Joint International Conference on Nanoscience, Engineering and Management (BOND 21)*. Penang, Malaysia: 19-21 August.

Al-Dabbagh, J.B., Ishak, M., Tahar, R.M. and Harun, S.A. 2013. Synthesis and Characterization of Nano Ti-50%Al by Mechanical Alloying (MA) for Advanced Technology Application. *Creation, Innovation, Technology and Research Exposition Competition (CITREX 2013)*. Universiti Malaysia Pahang: 28 March.

Al-Dabbagh, J.B., Ishak, M., Tahar, R.M. and Harun, S.A. 2012. Effect of the Milling Parameters on the Characteristics of Ti-50%Al Nanocrystallite Synthesized by MA. *4th International Conference on Solid State Science and Technology (ICSSST)*. Malacca, Malaysia: 18-20 December.

